Identification and Characterization of the IMC Protein Family in Toxoplasma gondii

Author: Brooke R. Anderson-White

Boston College

The Graduate School of Arts and Sciences

Department of Biology

IDENTIFICATION AND CHARACTERIZATION OF THE IMC PROTEIN FAMILY IN *TOXOPLASMA GONDII*

a dissertation

by

BROOKE R. ANDERSON-WHITE

submitted in partial fulfillment of the requirements

for the degree of

Doctor of Philosophy

December 2011

Abstract

Identification and Characterization of the IMC Protein Family in *Toxoplasma gondii*

Brooke R. Anderson-White

Thesis advisor: Dr. Marc-Jan Gubbels

The apicomplexan parasite *Toxoplasma gondii* divides rapidly and asexually through a unique process of internal daughter budding. The physical infrastructure for this process is the cytoskeleton, which is composed of subpellicular microtubules, flattened vesicles (alveoli), and a meshwork of intermediate filament-like proteins. This meshwork is composed of a family of 14 inner membrane complex (IMC) proteins that were identified based on the presence of a repeat sequence shared across the Alveolata, the alveolin-repeat. All 14 proteins were cloned as YFP fusions to study their subcellular localization and antibodies were generated against several representative IMC proteins. Each IMC displays unique spatio-temporal dynamics throughout development, but four physically distinct localizations were identified: eight IMCs localize to the alveoli, four IMCs localize to a structure known as the basal complex, IMC11 localizes to the apical cap in mature parasites, and IMC15 localizes primarily to the centrosomes and early buds. IMC15 is of particular interest because its appearance before membrane occupation and recognition nexus 1 (MORN1) in the early bud suggests that it is the first cytoskeletal component to associate with the buds. A conditional knockdown of this protein using the destabilization domain (DD) reveals IMC15 has a strong affinity for the centrosomes that overcomes targeting of the DD fusion protein to the proteasome and the presence of

IMC15 in the early bud may not be necessary for the division process. Conditional knockdowns using a tetracycline repressible promoter reveal that a minimal amount of IMC15 is sufficient for parasite survival. In order to further characterize IMC15, dominant negative constructs based on mutating putative palmitoylation sites or overexpression of deletion constructs are being pursued. Collectively, the IMC family is being incorporated into the temporal and spatial dynamics of cytoskeletal development through the creation of a comprehensive timeline of daughter bud assembly. These findings are contributing unprecedented detail to the cell division process.

Dedication

To my parents, Marjorie and Dennis, who gave me everything I needed to be successful (including a microscope and chemistry set). To my sister, Julie, who is always there to listen and give an honest opinion (especially on my wardrobe). And to my husband, BJ, who supports and encourages me and challenges me to be my best (particularly at Scrabble). I love you all.

Acknowledgements

I would like to thank my committee members, Dr. Junona Moroianu, Dr. David Burgess, and Dr. Anthony Annunziato for all their help and guidance from my first rotation through deciding my next step after graduate school. I also appreciate Dr. John Samuelson for taking the time to provide insightful comments on this dissertation. Peter Marino of the Higgins Business Office deserves acknowledgement as well for his dedication to the graduate program and his cheerful willingness to help with anything.

Dr. Marc-Jan Gubbels was vital to my success at Boston College. He provides everyone in the lab with the mentoring, opportunities, and tools necessary to develop as scientists. I would also like to thank Seth Robertson for training me at the bench and Dr. Joshua Rosenberg for training me at the microscope. Three remarkable undergraduates assisted with this work as well: Katherine Cheng, Aziz Kosber, and Lauren Jammallo. Thank you to them for exhibiting devotion to the lab despite their hectic schedules. Thank you to Dr. Tomasz Szatanek, Dr. Douglas Ivey, and Alexander Lorestani as well for their assistance with the work presented in this dissertation. I would also like to thank Rashmi Dubey for agreeing to continue this work and the rest of the Gubbels lab, past and present, for all their support and guidance.

The friendships I developed during graduate school have been as important as the scientific skills. Without Megan Farrell, Heather McKay Gudejko, and Kathleen Moorhouse, Boston would have been a cold and lonely place. I will miss the lively lunch conversations with Andrew Denninger, Jeremy Eberhard, and Veniamin Slavitskiy.

Tristan and Cathy Lubinski are always ready for anything at anytime and you can't help but be happy around this couple.

Finally the support of my family has been unwavering over the last five years. My parents, Marjorie and Dennis; my sister, Julie; and my brother-in-law, Meason, have patiently endured my ups and downs through graduate school and always been there with words of encouragement. My husband, BJ, worked grueling hours throughout the years that we were in graduate school and I am both impressed with his accomplishments and appreciative for his support.

Thank you all.

Table of Contents

List of Tables

List of Figures

List of Abbreviations

ALP – actin-like protein
AMA1 – apical membrane antigen 1
ATc – anhydrous tetracycline
BIC – basal inner collar
BIR – basal inner ring
DD – destabilization domain
DLC – dynein light chain
DOC - deoxycholic acid
ER – endoplasmic reticulum
FRAP – fluorescence recovery after photobleaching
FUDR – 5-fluorodeoxyuridine
GAP – gliding-associated protein
hTERT – human telomerase reverse transcriptase
HFF – human foreskin fibroblasts
HR – homologous recombination
Hsp – heat shock protein
IF – intermediate filament
IMC – inner membrane complex
IMP – intramembranous particle
ISP – IMC sub-compartment protein
KD - knockdown
KI - knockin
KO – knockout
LIC – ligation independent cloning
MAP – microtubule-associated protein
MLC1 – myosin light chain 1
MORN – membrane occupation and recognition nexus
MT – microtubule
MTOC – microtubule organizing center
MyoA – myosin A
NHEJ – non-homologous end-joining
PAT – palmitoyl acyltransferase
PhIL1 - Photosensitized INA-labeled protein 1
p*T7S1* – minimal SAG1 promoter preceded by seven tetracycline operator repeats
p*T7S4* – minimal SAG4 promoter preceded by seven tetracycline operator repeats
p*tub* – tubulin promoter
QDO – quadruple drop out media
RB – resuspension buffer
RNG-1 – ring-1 protein
SAG1 – surface antigen 1
SAG4 – surface antigen 4
SDS - sodium dodecyl sulfate

Shld1 – morpholine- containing ligand Shield-1
TATi – tetracycline transactivator
tet – tetracycline
TIES – third irrelevant enzyme site
TX-100 – Triton X-100
UM – unit membrane
UPRT – uracil phosphoribosyltransferase
WFA – withaferin A

Chapter 1. Cytoskeletal development in *Toxoplasma gondii*

1.1. Introduction

Toxoplasma gondii is the obligate intracellular apicomplexan parasite responsible for toxoplasmosis-associated encephalitis and birth defects (1). Other medically significant members of the Apicomplexa phylum include the causative agent of malaria [*Plasmodium* species (spp.)] (2), opportunistic infections that cause acute gastroenteritis (*Cryptosporidium* spp.) (3), and several costly veterinary scourges (*Eimeria*, *Theileria*, and *Babesia* spp.) (4-6). The virulence of these parasites and the destruction perpetrated by these organisms is correlated to their rapid rate of replication with duplication occurring about every six hours (7-9). This rapid rate of cell division in *Toxoplasma* is predicated on proper formation of the cytoskeleton (10-16).

1.2. Division by internal daughter budding

The fast replicating *Toxoplasma* tachyzoite divides asexually by a process of internal daughter budding known as endodyogeny (17-20) (Fig. 1.1). The process begins with the duplication of the Golgi late in G1 (17, 21-23). This is followed by the duplication of the centrosome early in S phase (19, 24, 25) (Fig. 1.1B). Budding is initiated in S-phase as well when the early components of the cytoskeleton begin to assemble apically to the centrosomes (9, 13, 17, 19, 26-29) (Fig.1.1C and D). Mitosis and cytokinesis progress concurrently as the cytoskeleton grows from the apical end toward the posterior end encapsulating first the divided Golgi (25), then the apicoplast (30), (Fig. 1.1E), the nucleus (19) and endoplasmic reticulum (ER) (31) (Fig. 1.1 F), and finally the mitochondrion (25) (Fig. 1.1G and A). The secretory organelles are created *de novo*

during this process (17, 22, 25) (Fig. 1.1 G). As the daughter parasites reach maturity, the cytoskeleton of the mother breaks down and the plasma membrane of the mother is recycled on to the now emerging daughters (17) (Fig. 1.1F and G). The cell cycle takes only six hours to complete and is continuous until host cell lysis (9).

1.3. Composition of the cytoskeleton

1.3.1. Ultrastructure

The *Toxoplasma* cytoskeleton is composed of two parts: the inner subpellicular microtubules (MT) and the outer pellicle. There are 22 subpellicular MT that spiral two-thirds of the length of the parasite (Fig. 1.2F). The minus ends of the MT are anchored in the microtubule organizing center (MTOC) called the apical polar ring (Fig. 1.2E). The MT grow from the apical end of the parasite toward the posterior end, with the (+)ends remaining free in the mature parasite (32, 33). Unlike other eukaryotes, single MT in apicomplexans are extremely stable (34). Some of this stability could be attributed to the microtubule-associated proteins (MAPs) that are suspected to connect the MT to the pellicle (34, 35). This MT stability is necessary as *Toxoplasma* lacks an actin cytoskeleton. The majority of actin remains in the globular form in *Toxoplasma* (36), transiently forming filaments to act during gliding and host cell invasion as part of the motility apparatus known as the glideosome (37, 38). Inhibition of or interference with actin significantly decreases motility and invasion (38, 39). However, actin is not necessary for proper internal budding and only affects the turnover of the mother's organelles, leading to a larger than normal residual body (40). Furthermore, conventional

myosin is absent from the *Toxoplasma* cytoskeleton and only divergent Type XIV myosins (41-43) are found in the glideosome (44-46). As with actin, interruption of myosin reduces motility (47). Disruption of the MT on the other hand halts daughter budding supporting its essential cytoskeletal role (16, 40, 48).

The pellicle is comprised of an outer plasma membrane (Fig. 1.2A), the alveoli of the inner membrane complex (IMC) (Fig. 1.2 yellow), and the IMC protein mesh (Fig. 1.2 bright green), which lines the cytoplasmic side of the alveoli and overlays the subpellicular MT (17, 28, 49). The alveoli are ER-Golgi derived flattened membranous sacs that form the double membrane of the IMC (17, 50). They are arranged in three rows encircling the parasite with a single capping vesicle at the apical end (49, 51). These alveoli are the defining feature of the Alveolata, a superphylum consisting of ciliates, dinoflagellates, and apicomplexans. The IMC protein mesh is composed of 8-10 nm wide intermediate filament-like (IF-like) proteins (28). The combination of alveoli and intermediate filaments are believed to serve primarily as structural supports or armor in most alveolates, but in the Apicomplexa they also serve as support for the glideosome (28, 44). Within the double membranes of the alveoli there are double rows and single rows of intramembranous particles (IMPs) organized with a 32 nm periodicity, reflecting the periodicity of the subpellicular MT (34, 49, 51). It has been hypothesized that the double rows of IMPs anchor the MAPs that interact with the MT to further stabilize the cytoskeleton (34, 35); but the single rows of IMPs run the entire length of the parasite suggesting they may interact with the IMC IF-like proteins (28). Disruption of the MT with the dinitroaniline herbicide oryzalin does not affect the development and

organization of the IMPs, supporting the hypothesis that they interact with alternative filaments like the IMC IF-like proteins (34).

The IMC runs the entire length of the parasite with openings at the apical and posterior ends. The opening at the apical end allows for the extension of the conoid that is necessary for host cell invasion (32, 52-55). The conoid consists of two preconoidal rings at the most anterior end of the parasite (Fig. 1.2C) and the apical polar ring that organizes the subpellicular MT (Fig. 1.2E). These rings are connected by spiraling α-tubulin-only MT (17, 32, 35, 56-58) (Fig. 1.2D). In addition there are two short intraconoid MT that may serve to transport secretory proteins during invasion (32, 59) (Fig. 1.2B). The opening at the posterior end is occupied by a structure known as the posterior cup or basal complex (28) (Fig. 1.2G). The function of the basal complex in the mature parasite is unknown.

1.3.2. Sub-compartments and protein families of the mature cytoskeleton

Studies of the cell biology of *Toxoplasma* reveal a more compartmentalized cytoskeleton than described in Section 1.3.1 and a growing complexity in the number of protein components. At the most apical end of the parasite, appearing to localize to the anterior preconoidal ring, there is the EF-hand containing calcium binding protein TgCentrin2 (Fig. 1.3B). This protein is believed to drive constriction of the basal complex during division (60). Posterior to TgCentrin2 is ring-1 (RNG1), which localizes to the apical polar ring. (Fig. 1.3B). The function of RNG1 is unknown but it does assemble in the absence of MT and may be essential (15). Faintly expressed near the conoid is the

membrane occupation and recognition nexus 1 (MORN1) protein (60, 61) (Fig. 1.3B). Knockouts (KO) of MORN1 show it plays an essential role in the organization of the basal complex and is necessary for proper constriction during cytokinesis (10, 11). TgCentrin3, a homolog of TgCentrin2, is found faintly in the conoid as well along with two additional EF-hand, calcium-binding domain proteins, TgCAM1 and TgCAM2 (Fig.1.3B). The latter two proteins may play a role in conoid extrusion in response to calcium (27). The (-)end-directed MT motor dynein light chain (TgDLC) localizes to the apical end of the parasite and may transport cargo along the MT (Fig. 1.3B). It may be involved in calcium signaling as well (27). Another MT-associated protein, the intraconoid microtubule associated protein 1 (TgICMAP1), interacts exclusively with the two intraconoid MT and probably fulfills a stabilizing function (62) (Fig. 1.3C).

TgDLC also appears less intensely in a structure below the conoid region called the apical cap (27), which could correspond to the first alveolin vesicle (Fig. 1.3A). Photosensitized INA-labeled protein 1 (PhIL1) localizes to this region as well (63) (Fig. 1.3A). Though the function of PhIL1 is currently unknown, KO of PhIL1 results in shorter, wider parasites that are outcompeted by wild-type parasites in tissue culture and are less infective to mice (64). A component of the glideosome, gliding-associated protein 70 (GAP70), also localizes to the apical cap (Fig. 1.3A). This protein is closely related to GAP45, which recruits the members of the glideosome to the IMC (44, 65), and it appears to function similarly to GAP45 by recruiting the glideosome components to the apical end of the parasite. Loss of GAP70 by KO does not result in a growth defect by plaque assay suggesting that GAP45 may be compensatory (65).

In addition a member of the IMC sub-compartment protein (ISP) family, ISP1, localizes to the apical cap (Fig. 1.3A). The ISP family is a group of three highly charged, apicomplexan-specific, IMC-associated proteins that share a strongly conserved C-terminal region. These proteins are soluble, unlike other cytoskeletal elements, and are anchored to the IMC by palmitoylation (14, 28). Knockout of ISP1 leads to no obvious defects in morphology or growth. In the absence of ISP1, ISP2 and ISP3 appear to compensate for the loss. It seems ISP1 acts as a gatekeeper to limit the access of other proteins to the apical cap but the reason for this is unknown (14).

The edge of the apical cap is decorated with five to six annuli of TgCentrin2 (Fig. 1.3A). These TgCentrin2 accumulations could be at the sutures between the alveolin cap and the first row of five to six alveoli. It appears these annuli arise from an early cloud of TgCentrin2 that forms around the centrosome early in budding and may function in IMC organization. Furthermore, these annuli may bind MT because disruption of MT with oryzalin leads to their random dispersion throughout the cell (27).

ISP2 occupies a region of the cytoskeleton that runs from the apical cap to about two-thirds the length of the parasite (Fig. 1.3A). This central compartment is not bounded by the ends of the subpellicular MT but instead appears to follow the edges of a row of IMC alveoli. A KO strain of ISP2 suffers outcompetition by wild-type parasites in tissue culture. When ISP2 is not present, about 40% of parasites experience the formation of multiple buds that are incapable of successful development (14). Currently ISP2 is the only identified protein within this mid-parasite compartment.

The final member of the ISP family coincides with the boundaries of the IMC with an apical gap for the conoid and a posterior gap for the basal complex. ISP3 is associated with the IMC but not a part of the protein meshwork (Fig. 1.3A). Knockout does not result in any gross defects, thus the function of ISP3 remains unclear (14). In addition to ISP3, GAP50, an integral membrane protein of the outer layer of the IMC alveoli, localizes to the entire IMC (44) (Fig. 1.3A). GAP50 anchors the glideosome to the IMC through GAP45, which is necessary for proper motility (65). The remaining glideosome elements, myosin light chain 1 (MLC1) and myosin A (MyoA), are associated with GAP45 (44, 66). GAP40 was identified recently as a new glideosome component potentially associated with the IMC (65) (Fig. 1.3A). Those proteins that do localize to the IMC meshwork are IMC1 (19, 28, 67), 3 (68), and 4 (27) (Fig. 1.3A).

At the posterior end of the cytoskeleton is the basal complex (28). MORN1 and TgCentrin2 appear in this structure, which could reinforce prominent roles for these components in constriction of the parasite during cytokinesis (27, 60, 61) (Fig. 1.3A). TgDLC localizes to the basal end as well; however its expression is quite faint (27) (Fig. 1.3A).

1.4. Mechanistic insights from gene and protein disruptions

As evidenced in the preceding sections, the subcellular dynamics of some components of the *Toxoplasma* cytoskeleton have been described, but little has been done to elucidate the mechanisms of development. Targeted gene KOs, protein destabilizers, dominant

negative constructs, and destructive overexpression have been applied to begin teasing out the potential functions of certain cytoskeletal elements.

Initial research into the mechanisms of daughter budding focused on the subpellicular MT. When parasites are treated with a high dose of oryzalin the subpellicular MT fail to form (16, 48). The early IMC will begin to assemble but the cytoskeleton's ability to elongate and accomplish cytokinesis is blocked (40, 48). Centrosome duplication is not affected by MT disruption (40). ISP1 and MORN1 will form several rings in parasites treated with oryzalin and ISP3 will collect at these early structures (14, 60, 61). GAP50 association with the early IMC continues as well (46). IMC1 will continue to accumulate at these early buds but will form sheets without MT (27). The appearance of RNG-1 in treated cells supports proper formation of the conoid, or at least the apical polar ring, without MT. It is somewhat unusual that the number of centrosomes and RNG-1 rings do not agree in affected parasites but the signal still remains to trigger late-stage RNG-1 formation without the MT or nuclear division (15). These data suggest MT are not involved in initiation of budding or in early bud formation but are necessary for proper IMC elongation and completion of cytokinesis. It is possible the unaffected centrosome may play a significant role in these early stages.

Rab11B is a small GTPase that traffics the alveoli of the IMC. Experiments inducing a dominant negative phenotype of Rab11B show that a lack of alveoli biogenesis halts bud formation. IMC1, MORN1, and GAP50 all fail to appear. Despite the ablation of IMC formation, the subpellicular MT still polymerize but are not properly shaped (13). In ISP2 KO parasites the MT develop as well, but again they do not appear

to be properly shaped. In these parasites, nascent IMCs, as indicated by ISP1, do not coincide with the MT structures and appear as amorphous, random accumulations (14). Therefore, IMC formation is not required for MT polymerization but is required for proper bud morphology.

Nuclear division and functional cytoskeletal development do not appear to be linked. KO of ISP2, which affects the earliest stages of daughter budding, still presents properly divided nuclei in the majority of affected cells (14). The dominant negative Rab11B phenotype that completely inhibits IMC formation does not affect nuclear division (13). Even when contraction of the daughter buds malfunctions in the MORN1 KO parasites, nuclear division is unaffected (10). Nuclear division is clearly not linked to IMC formation and it is questionable if it is linked to subpellicular MT formation. When parasites are treated with a high dose of oryzalin the nucleus fails to divide properly but this is most likely due to interference with the spindle MT (16, 48). When the concentration of oryzalin is kept low (0.5 μM), the spindle forms and the nucleus divides, but the cytoskeleton is not fully functional and the daughter parasites can no longer invade host cells (48).

Aside from addressing big questions like if IMC and subpellicular MT development are tightly linked and if nuclear division and cytoskeletal development are mutually exclusive, very little information on the detailed interactions of the cytoskeleton have come out of gene and protein disruptions to date. GAP70, PhIL1 and ISP1 KOs illustrate that there probably exists a high rate of redundancy or compensatory pathways in cytoskeletal development (14, 64, 65). Disruption of ISP2 leads to a gross defect in

budding, but not in all parasites, and its interactions with other cytoskeletal proteins are unknown (14). The MORN1 KO provides a clear role for the protein in completion of cytokinesis as all parasites are affected by its loss, but why or how formation and constriction of the basal complex fails is unknown (10).

1.5. Open questions on the *Toxoplasma* cytoskeleton

The process of internal daughter budding and specifically cytoskeletal development remains poorly defined. As the pathogenesis of *Toxoplasma* is closely linked to its rapid rate of replication and replication hinges on proper formation of its cytoskeleton this is an aspect of parasite biology that demands increased attention. Furthermore, this structure provides an optimal target for improved therapeutic treatments as it is largely constructed of proteins not found in the mammalian host cell.

In order to better define cytoskeletal development it is necessary to identify and characterize the proteins of the cytoskeleton. The sequenced genome of *Toxoplasma* eases the identification of protein families and the robust cell biological tools make their characterization possible. Once the spatial and temporal behavior of the protein is defined, deeper characterization of its functionality should follow. Gene KOs will be a useful tool in this pursuit. Post-translational modifications merit a close look as well since they play a prominent role in the mechanisms of protein targeting and organization (10, 14, 65). Finally, this information can be used to develop models of cytoskeletal development in *Toxoplasma*.

This work is focused on the identification and characterization of a family of IMC intermediate filament-like proteins. Included as well is a deeper analysis of IMC15, the member of this family believed to play a role in cytoskeletal nucleation. Furthermore, the timing of IMC15 and the rest of the IMC family has been put in perspective by establishing a molecular level timeline of early budding events.

Figure 1.1. *Toxoplasma* divides by internal daughter budding

(A) Mature parasite in G1. Red are MT (conoid, subpellicular, and spindle pole), yellow are the alveoli, bright green is the IMC meshwork, brown are secretory vesicles, dark blue line is the mitochondrion, purple is the apicoplast, blue is the centrosome, black is the Golgi, dark green is the ER, grey is the nucleus, and pink is the posterior cup or basal complex. (B) Mitosis is initiated at 1.2N with the duplication of the centrosomes following the duplication of the Golgi. (C) Budding is initiated with the appearance of early components of the cytoskeleton. (D) The spindle pole duplicates and the apicoplast moves below the centrosomes, elongating as the centrosomes separate. (E) The organelles begin to partition as the daughter buds elongate. The components of the basal complex accumulate at the leading edge of the bud. (F) The daughter buds contract and all the organelles are partitioned except for the mitochondrion. The secretory vesicles and cytoskeleton of the mother begin to degrade. (G) Daughter buds emerge and the plasma membrane from the mother is incorporated onto the daughters. The mother falls away as a residual body.

Figure 1.1. *Toxoplasma* divides by internal daughter budding

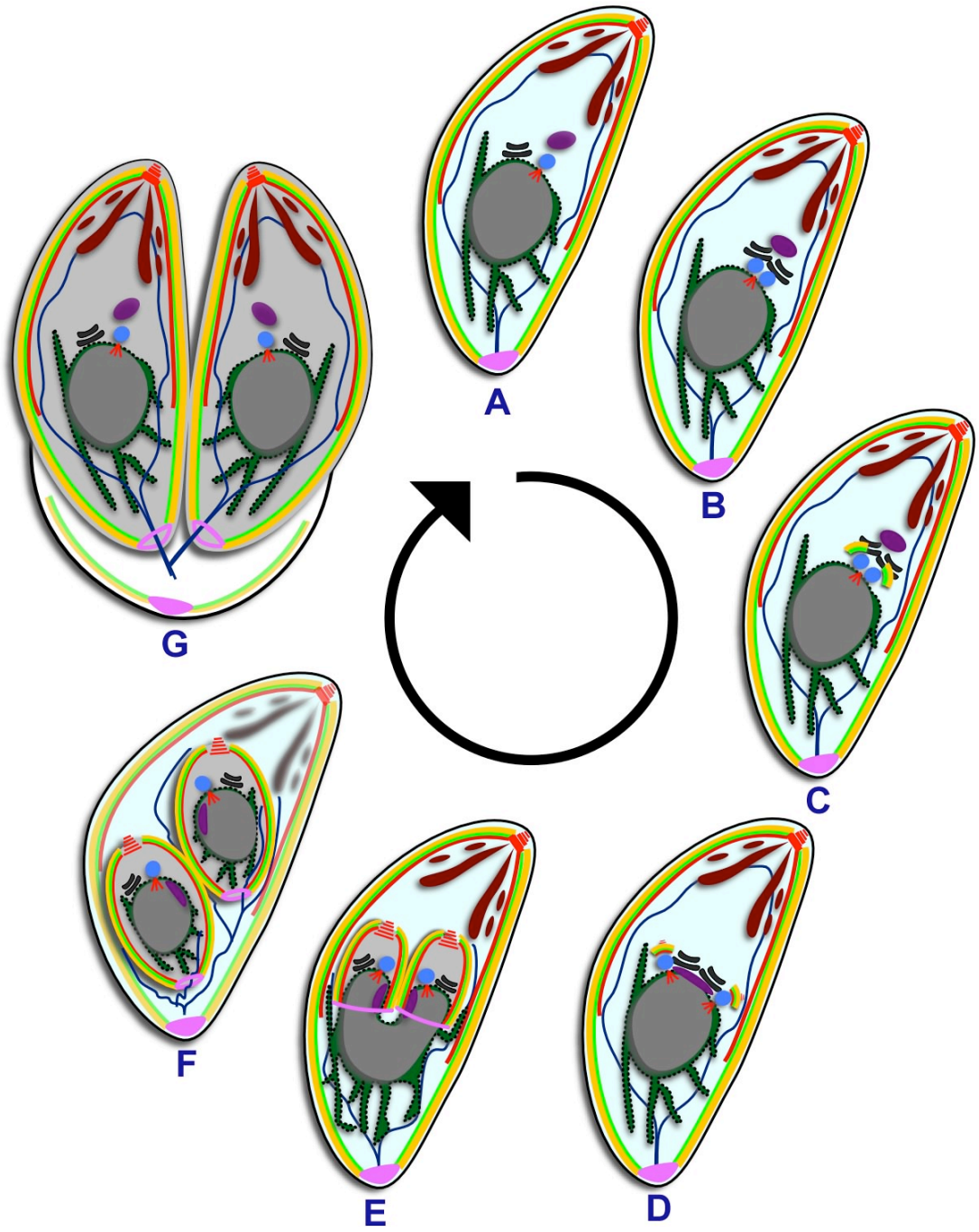

Figure 1.2. The cytoskeleton is a two part, trimembrane structure

Diagram of the layers of the cytoskeleton. The pellicle is on the left and right. The MT are in the middle. On the left is the exterior of the alveoli in yellow after removal of the plasma membrane (A) shown in grey. On the right are the IMC IF-like proteins in bright green after removal of the alveoli. The cross-sectioned bi-membranes of the alveolin vesicles are in yellow. (B-E) The conoid of the parasite is composed of two intraconoidal MT (B), two preconoidal rings (C), spiraling α-tubulin-only MT (D), and the apical polar ring (E). (F) The 22 spiraling subpellicular MT are the innermost layer of the cytoskeleton. (G) The posterior cup or basal complex is at the end of the IMC.

Figure 1.2. The cytoskeleton is a two part, trimembrane structure

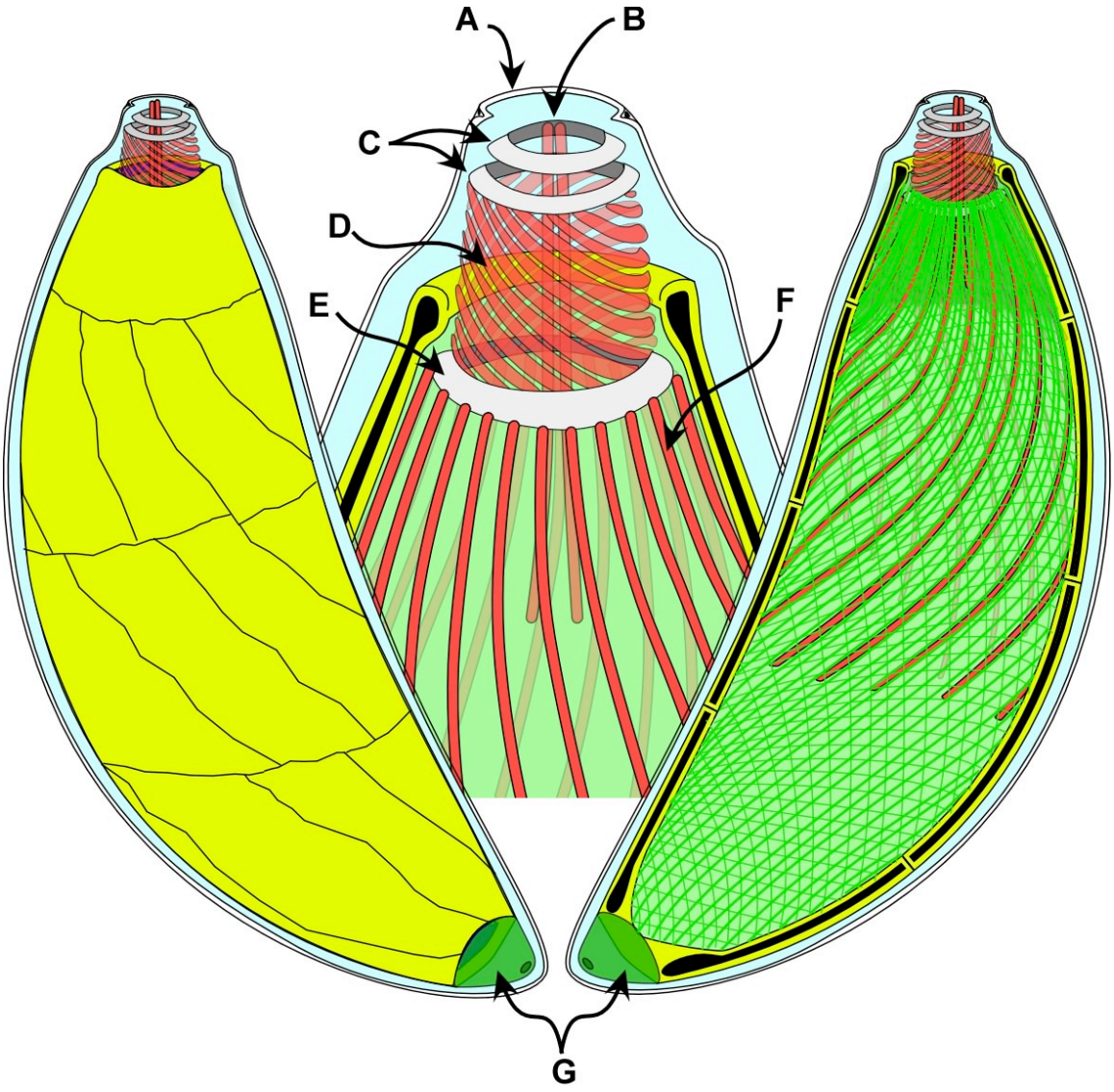

Figure 1.3. Cytoskeletal sub-compartments of *Toxoplasma*

(A) Sub-compartments are the apical cap (blue curved lines), mid-parasite region (green stripes), IMC (bright green), and posterior cup consisting of MORN1 (pink), TgDLC (blue), and TgCentrin2 (red). TgCentrin2 annuli and preconoidal localization in red as well. Names of proteins occupying each region are in corresponding colors. (B and C) Exterior and interior enlargements of the conoid, respectively.

Figure 1.3. Cytoskeletal sub-compartments of *Toxoplasma*

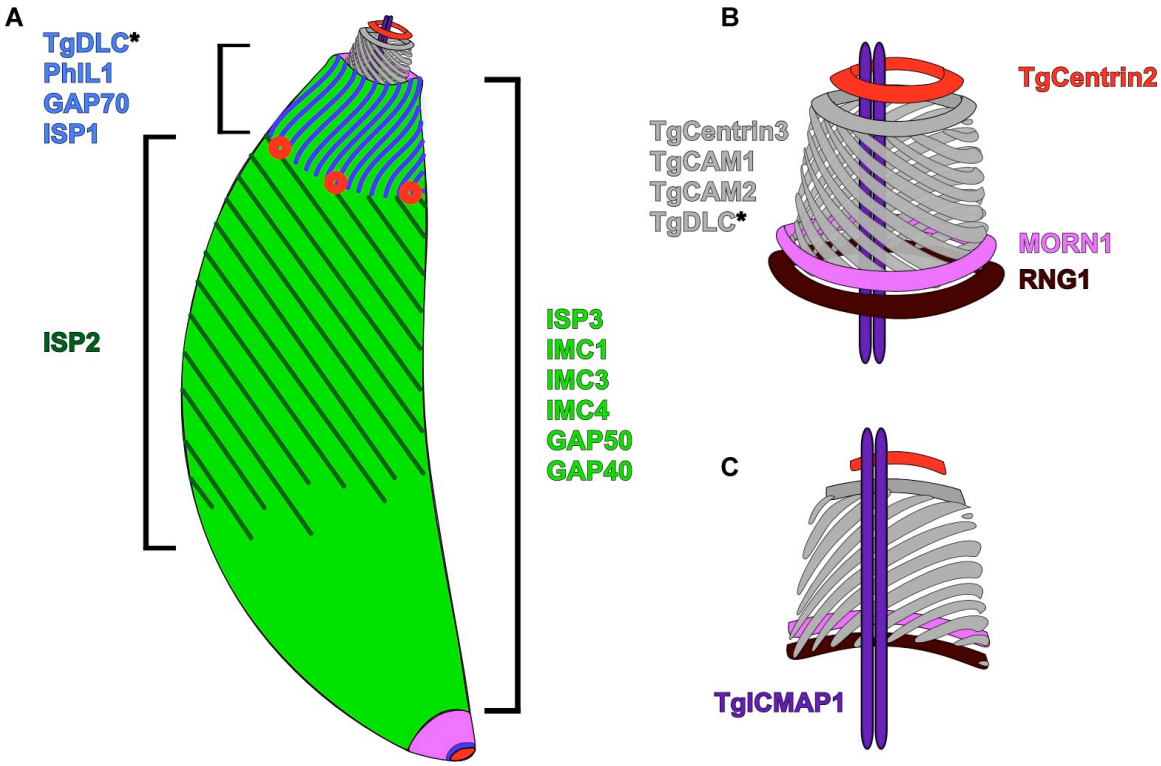

Chapter 2. A family of intermediate filament-like proteins is sequentially assembled into the cytoskeleton

2.1. Introduction

A rapid replication cycle and the resultant tissue lesions are responsible for the pathogenesis of *Toxoplasma*. Since the ability to replicate is intrinsically linked to the proper development of the cytoskeleton (10-16), the components of this structure are attractive potential therapeutic targets and comprise a growing area of research. The meshwork of 8-10 nm intermediate filament-like proteins that lines the alveoli of the IMC and overlies the MTs is particularly appealing as the IMC serves to support the actin-myosin motor apparatus that is required for host cell invasion (28, 44). Furthermore, in apicomplexans, the developing IMC functions as a scaffold for organellogenesis and organelle partitioning during division (69). Finally, the critical roles of two protein components of this meshwork in *Plasmodium berghei*, IMC1a and IMC1b, in cell stability and division were directly demonstrated through genetic knock-outs (70, 71).

In *Toxoplasma*, the first component of this meshwork, IMC1, was identified using polyclonal antibodies raised against extracted cytoskeletons (28). The second component, IMC3, arose from the use of a genomic YFP-fusion library (68). A third component, IMC4, was identified in purifications of the apical complex (27). All three localize to the cortical IMC; however, initial findings with IMC1 and IMC3 showed their dynamics to be slightly different (68, 72). As presented in Figure 2.1, IMC3 expresses strongly in the budding daughters, but its intensity decreases as the daughters mature and progress through G1, and the IMC1 signal remains constant throughout the cell cycle.

The common motif that joins these dynamically different IMC proteins together as a family emerged when Gould et al. analyzed genome sequence data for all the Alveolata (ciliates, dinoflagellates, and apicomplexans) (73) and defined a family of proteins related to IMC1, 3 and 4, which all carry a series of conserved repeats called alveolin repeats (74). The alveolin repeat motif contains conserved valine- and proline-rich domains composed of "EKIVEVP" and "EVVR" or "VPV" subrepeats (74). As the first three IMC proteins were identified in different labs and through different screening techniques there is a high probability the IMC meshwork contains more proteins that carry this repeat motif. The importance of the IMC to the parasite and the possibility that the individual IMC proteins may behave differently led us to hypothesize that these proteins could fulfill different functions within various stages of the parasite's life cycle including cytoskeletal assembly, maturation, maintenance, and disassembly.

In this chapter, 14 alveolin domain containing genes are identified in the *T. gondii* sequenced genome database. Subsequently we studied the subcellular localizations of each using YFP-tagged constructs and specific antisera. We identified a number of unique spatio-temporal patterns in addition to those previously described, such as a group of IMC proteins exclusively localizing to the basal complex, an IMC protein colocalizing with the centrosomes, and a group of IMC proteins exclusively localizing to the mature cytoskeleton. Taken together, a surprising level of diversity in the localization patterns and potential functions of the alveolin-repeat IMC proteins outlines the developmental stages of the *Toxoplasma* tachyzoite cell division at an unprecedented spatio-temporal resolution.

2.2. Results

2.2.1. Genome mining to identify the IMC family

Since the identification of IMC1, 3, and 4 was not as part of a comprehensive search for IMC proteins, we identified additional IMC genes through querying the fully sequenced *T. gondii* genome in ToxoDB using IMC1, 3, and 4 as seeds (75). This approach identified a total of 14 related IMC genes containing an alveolin domain (Table 2.1). We validated the splicing of IMC genes 7, 9, and 12-15 by RACE PCR and DNA sequencing. Only IMC14 and IMC15 varied from the predicted gene models: IMC14 has several splice variants in the Prugniaud strain, but only one in the RH strain (the RH sequence was used in this study), and IMC15 has different start and stop codons (Fig. 2.2). The remaining IMC genes have consistent gene prediction models and we were able to amplify their open reading frames from tachyzoite cDNA to confirm these annotations. The alveolin domain regions were determined using the REPRO program, which identifies repetitive sequences within a single sequence, and potential palmitoylation sites were predicted with CSS-Palm 2.0 (Fig. 2.3) (76, 77).

2.2.2. Coordinated IMC gene expression

Coordinated gene expression patterns among proteins with related functions have been observed during the erythrocytic development of the apicomplexan *Plasmodium falciparum* (78, 79). To see if this applies to the IMC proteins, the expression patterns were assembled for each of the identified IMC genes from genome-wide microarray

expression data (80). The majority of the IMC genes (IMC1, 3-6, 8-11, 13, and 15) display a highly coordinated expression profile reaching a maximum coinciding with budding, whereas IMC7 and 12 exhibit a profile opposing the majority and IMC14 trails the majority pattern by 1 hour (Fig. 2.4A). When comparing the absolute mRNA expression levels, only IMC9 and 15 stand out with maximum expression levels less than the minimum levels of almost all the other IMC genes (Fig. 2.4B). Furthermore, many mRNAs displayed up to a 10-fold dynamic range between minimum and maximum suggesting that although timing of expression is coordinated for most IMC genes, their expression levels are quite variable.

2.2.3. *Comparisons of cortical IMC proteins in budding and mature parasites*

Although IMC proteins 1, 3, and 4 had been characterized previously, it was never formally established how these three proteins localize relative to one another. When IMC1 and IMC3 are compared it is clear that more IMC3 is associated with the budding daughter cytoskeletons than with the cytoskeleton of the mother cell, as opposed to the more equal distribution that IMC1 exhibits (Fig. 2.5B, C, and D). The high intensity of IMC3 is maintained in the recently emerged daughters but then drops to lower basal levels in fully mature daughters (Fig. 2.1 and Fig. 2.5B, C, and D). Comparable results were obtained with parasites expressing YFP-tagged versions of IMC1 and IMC3 indicating that the observed differences were not due to masking of the antibody binding site (Fig. 2.5E and F). When IMC4 is compared to IMC1 and IMC3 using a parasite line expressing YFP-IMC4, it is found to localize like IMC1 with equal distribution in the

mother and daughter buds (Fig. 2.6A and B). This pattern is corroborated with a C-terminal fusion, IMC4-YFP, as well (Fig. 2.6C).

To assess the subcellular localizations of the novel IMC proteins we generated N-terminal YFP fusions for each protein and expressed them in *T. gondii*. The expressed fusion proteins were verified through western blot (Fig. 2.7). Live parasites were imaged to identify the subcellular distribution patterns of the fusion proteins and, in addition, their localization dynamics were determined in all cases relative to IMC3 with an IMC3 antibody. Among the novel IMC proteins we identified two, IMC6 and IMC10, which show a localization pattern like IMC3 (Fig. 2.8A-D and F-I). This pattern is the same with C-terminal YFP fusions (Fig. 2.8E and J). Taken together IMC3, 6, and 10 comprise a related group of cortical IMC proteins distinct from IMC1 and 4 based on their behavior during parasite development.

2.2.4. IMC7, 12, and 14 localize exclusively to the mature cytoskeleton

In contrast to the IMC proteins described above, IMC7, 12, and 14 are excluded from the budding daughters and only found in the mature cortical IMC (Fig. 2.9B, E, G, L, O, and Q). The cortical localization of IMC7, 12, and 14 does not correspond with the emergence of mature daughters (Fig. 2.9C, H, and P) but instead occurs sometime before the initiation of budding (Fig. 2.9A and N). C-terminal fusions of IMC7 and 12 confirm these observed patterns (Fig. 2.9F and M) and this behavior is not unexpected based on the delays in the expression profiles of IMC7, 12, and 14 (Fig. 2.4A). To verify that expression of YFP-IMC7, 12, and 14 do not interfere with maturation we used a

glideosome component, GAP45, which is incorporated into the IMC upon daughter maturation (12). As shown in Figure 2.9, GAP45 did associate with the cortex of the emerging daughters expressing cytoplasmically localized YFP-IMC7, 12, and 14, while some of the respective IMC protein is still in the cortex of the disassembling mother (D, I, and R). It is important to note that IMC7 and 14 are expressed under their native promoters instead of the *α-tubulin* (p*tub*) promoter as p*tub* closely matches the expression patterns of the majority of the IMC proteins but not these (Fig. 2.4A) (80). The IMC12 expression pattern is the same under the *ptub* promoter and its native promoter, but under the native promoter it fades rapidly during imaging; therefore, p*tub* driven YFP-IMC12 is presented here (Fig. 2.9J and K).

To determine the timing of the shift of IMC7 and 12 to the cortical IMC, time-lapse movies of YFP-IMC7 and YFP-IMC12 parasite lines were collected throughout tachyzoite development (Fig. 2.10A). The movies show that the time between the end of cytokinesis and the reappearance of the cortical YFP localization is approximately two hours. Thus the transition of these IMC proteins occurs in G1 (9). Collection of a comparable IMC14 movie failed due to the rapid bleaching of the weak YFP signal.

To more accurately describe the timing of this transition we employed a temperature sensitive mutant, FV-P6, which grows normally at 35°C and then arrests near the midpoint of G1 when cultured at 40°C (24, 25, 81). When N-terminal cherryRFP fusions of IMC7 and IMC14 are expressed in this mutant and scored for cortical vs. cytoplasmic localization at 35°C in an asynchronous parasite population, both proteins are fairly evenly distributed between the two locations (Fig. 2.10B through E). When the

parasites are grown at 40°C either after 18 hrs at 35°C or immediately upon inoculation, IMC7 remains evenly distributed but IMC14 becomes nearly 100% cortical (Fig. 2.10D and E). This suggests that IMC14 transitions to the cortical IMC early in G1 and IMC7 transitions later, more towards the midpoint of G1. These findings are further supported by the expression data in Figure 2.4A.

2.2.5. IMC11 localizes to the apical cap

Expression of a YFP tagged IMC11 driven by either the p*tub* or its endogenous promoter, resulted in localization of IMC11 to the buds, weak expression of YFP in an area of the cortex known as the apical cap, and an even weaker localization to the basal end of the IMC (Fig. 2.11A and B). The localization to the apical cap was confirmed through co-expression of a cherryRFP tagged version of PhIL1, an IMC-associated protein of unknown function (63) (Fig. 2.11C). The number of parasites that could be captured with visible basal IMC11 signal was too low to make a firm observation regarding basal colocalization. Using a MORN1 antibody, which highlights the basal complex (82), the basal localization of YFP-IMC11 is supported (Fig. 2.11D), but the poor YFP signal again did not permit a firm colocalization assignment. Antiserum was raised against full-length IMC11 because IMC11 is too small to use only the non-alveolin domains. This unfortunately made it cross-reactive with the alveolin motifs in other IMC proteins preventing the confirmation of the YFP fusion.

2.2.6. Four IMCs are components of the basal complex

At the basal end of the parasite, within the posterior IMC gap, is a structure called the basal complex or posterior cup that extracts with the cytoskeleton (28). The composition of this structure is largely unknown with only three previously suggested components: MORN1, TgCentrin2, and TgDLC, that all localize to the apical and basal extremes of the mature parasite (27, 60, 61). As presented in Figure 2.11, IMC11 is another potential component of this structure that localizes to both extremes as well. Unlike these previously described basal complex members, we identified four proteins that localize exclusively to the basal end of the mature parasite: IMC5, 8, 9, and 13 (Fig. 2.12). This group expresses in the whole daughter bud in the first half of budding and then halfway through budding they shift toward the basal complex (Fig. 2.12A). IMC8 is provided as an example as all members of this group behave in the same manner. Additionally, tagging on the N- and C-termini result in the same localization patterns as demonstrated by IMC13-YFP (Fig. 2.12B). A specific antiserum against the N-terminus of IMC5 further confirms the dynamics observed with the YFP fusions (Fig. 2.12C) and the localization of IMC5 to the basal complex when co-stained with anti-IMC1 and anti-MORN1 (Fig. 2.12D and E).

With several components of the posterior end now identified we performed co-IFAs with these proteins to document subtle differences in their localization patterns that could lead to greater insight into the structure of the basal complex (Fig. 2.12F). These colocalization studies resulted in the documentation of a three tiered structure in the basal complex: the upper and outermost tier contains MORN1, IMC9, 13, and 15; the middle

tier is composed of IMC5 and 8; and the most basal and innermost tier contains TgCentrin2, which partially overlaps with the IMC5 and 8 structure. IMC15 will be discussed in Section 0. Because definitive validation of these spatial relationships is limited by the resolution of light microscopy we sought to test whether the colocalizing proteins were interacting with each other and/or with their neighbors by yeast two-hybrid analysis. Unfortunately, these results were largely inconclusive (Table 2.2).

Since these distinctive basal structures have not been described at the ultrastructural level, in collaboration with Dr. David Ferguson, University of Oxford, UK, we performed electron microscopy (EM) on the basal complex (Fig. 2.12G-J). Two distinct electron-dense structures were observed in the basal complex: one directly attached to the cytoplasmic side of the basal end of the IMC (the basal inner ring or BIR; Fig. 2.12J) and a second structure separated from the IMC and the inner ring, but extending over the same length of the basal IMC and bending toward the plasma membrane (the basal inner collar or BIC) (Fig. 2.12H-J). Though it is difficult to obtain a large number of properly sectioned parasites, among 30 parasites with properly oriented basal complexes the majority displayed this folding back of the BIC to contact the plasmalemma. Both the BIR and BIC are continuous (Fig. 2.12J) and absent from the apical end of the IMC (Fig. 2.12G).

2.2.7. *IMC15 associates with the duplicated centrosomes and additional cytoskeletal structures*

p*tub* driven YFP-IMC15 localizes strongly to the budding IMC and weakly to the mature IMC like IMC3, 6, and 10 (Fig. 2.13A and C). It localizes to the apical cap like IMC11 and the basal end like IMC5, 8, 9, and 13 (Fig. 2.13A and D). In addition IMC15 presents two novel spatial features by accumulating at the extreme apical end of the parasite and colocalizing with the centrosomes (Fig, 2.13A, D, E, F, and I). A p*tub* driven C-terminal fusion confirms its localization to the centrosomes and early buds, however its expression is faint and cortical localization is only clear in some parasites (Fig. 2.13B). When under its endogenous promoter IMC15 continues to localize to the centrosomes, budding daughters, and the extreme apical end of the parasite (Fig. 2.13H). The basal localization is greatly reduced and the cortical expression and cap expression are no longer present with the endogenous promoter. This could suggest that the latter two localization phenomena are the result of overexpression; however since the native expression level of IMC15 is extremely low (Fig. 2.4B), the lack of signal could be due to inadequate detection limits. Since expression at the extreme apical end is relatively intense, even under the native promoter, we tested if this expression corresponds to the conoid by co-expresssing YFP-IMC15 with myc2-TgCentrin2, a protein present in the preconoidal ring (83). TgCentrin2 appears to be more apical than IMC15 and to be surrounded on the bottom by IMC15 (Fig. 2.13D). This indicates that the bright apical localization of IMC15 is in or around the conoid.

The colocalization of IMC15 with the centrosomes is shown by the use of a centrin antibody (Fig. 2.13E, F, and I). It appears that IMC15 localizes to the centrosomes at the time of or immediately following their duplication. These spots become very intense before the signal transitions into the early buds, arching over the apical side of the centrosomes (Fig. 2.13E and F). Previous to this study the localization of MORN1 above the centrosomes was the earliest known marker of budding (82). However, relative to the weak MORN1 signal in very early buds, two very intense IMC15 bud structures are already visible (Fig. 2.13F). IMC15 localization to the centrosomes and early buds was confirmed with a specific antiserum raised against the N-terminus of IMC15 (Fig. 2.13G-I). The antiserum does not recognize the apical accumulation, which is possibly due to post-translational modifications or to the YFP tag blocking the antibody recognition site. Consistent with potential post-translational modification is the slower than expected migration of YFP-IMC15 fusion protein (Fig. 2.7).

2.2.8. The alveolin domain determines localization to the cortical or basal cytoskeleton

Despite their variations in spatial and temporal dynamics, all of the IMCs can be divided into two general groups: those that are restricted to the mature basal cytoskeleton and those that are cortical. The localization of canonical intermediate filament proteins is governed primarily by their N- or C-termini because the central conserved domain is usually required for filament formation (84, 85). To test if this is true for the IMC proteins, we designed a series of deletion and chimeric constructs of IMC3 and IMC8.

Neither IMC3 nor IMC8 contain a predicted palmitoylation site that could potentially overrule amino acid motifs governing their localization (Fig. 2.3). For IMC3 the expression of the alveolin domain alone showed the same localization pattern as its full-length counterpart (Fig. 2.14A). The results were the same for IMC8, except for the lack of pronounced basal localization in the buds when the alveolin domain is expressed alone (Fig. 2.14B). Additional deletion and chimeric constructs indicate that sequence is required on both ends of the alveolin domain to obtain the basal localization in the buds but the sequence does not have to be IMC8 specific (Fig. 2.14B, panels 5 and 6). These results suggest that, unlike conventional intermediate filaments, the alveolin domain is necessary for IMC3 and IMC8 localization and sufficient for IMC3 localization in a wild-type background.

2.3. Discussion

Our data show that the 14 members of the *Toxoplasma* alveolin motif containing intermediate filament-like protein family have distinct spatial and temporal dynamics throughout tachyzoite development, including several phenomena not previously described. Based on our findings we established a development timeline outlined in Figure 2.15A. Formation of the daughter cytoskeleton begins with the localization of IMC15 to the centrosomes at approximately the time of duplication. All the other IMC proteins except IMC7, 12, and 14 assemble and grow with the daughter buds, with IMC3, 6, and 10 exhibiting significant abundance in the daughter buds compared to the mature mother IMC. Halfway through daughter formation IMC5, 8, 9, and 13 shift their

localization to the basal complex and the basal complex starts to constrict (Fig. 2.12A). Completion of cytokinesis coincides with the appearance of three distinct regions within the basal complex (Fig. 2.15B). At this point IMC1, 3, 4, 6, 10, and 15 are present along the full length of the cortical cytoskeleton. IMC11 and 15 occupy the apical cap sub-compartment of the IMC, and IMC15 is additionally observed at the very apical and basal ends of the IMC. Now in G1, IMC7, 12, and 14 begin to appear at the cortical IMC of the mature parasites. This series of events completes a full development cycle.

The diverse behavior of the various IMC proteins can be accounted for with three factors: expression patterns, primary protein sequences, and post-translational modifications. The localization of IMC7, 12, and 14 exclusively to the mature cytoskeleton during G1 is supported by their expression profile, with IMC14 expression peaking about an hour after the majority of the IMCs and IMC7 and 12 peaking more toward the midpoint of G1 (Fig. 2.4B). The cortical vs. basal targeting of the proteins appears to be attributable to the primary protein sequence as we showed that the alveolin motif is a determinant for these patterns (Fig. 2.14). However, we cannot assert that variations in the alveolin domain sequences are the only factor in proper basal or cortical localization since other intermediate filament proteins first assemble into homo-dimers or -oligomers through their conserved regions before being targeted to the cytoskeleton (84, 85). We can say that the alveolin domains are sufficiently distinct to allow the alveolin domain alone to oligomerize with the correct subgroup of untagged full-length native IMCs to be carried along to the appropriate location. Until the alveolin domains alone are shown to control the spatio-temporal patterns of the IMC proteins in gene-specific

knockout backgrounds it must be considered that localization information for the IMC proteins could be contained in the N- or C-terminal domains as well. Finally, though not specifically addressed in the preceding results, much of the observed IMC behavior could be attributed to post-translational modifications. A precedent for the importance of post-translational modification is set by the proteolytic cleavage of IMC1 coinciding with a transition in filament skeleton rigidity (67). The smaller than expected bands for several IMC YFP fusion proteins in the western blots could be indicative of such proteolytic processing; however, at this point we cannot exclude the possibility that these sizes could originate in degradation during sample preparation (Fig. 2.7). In other intermediate protein filament systems assembly is controlled by post-translational modifications such as acylation and phosphorylation (84, 86). Several of the IMC proteins contain predicted palmitoylation sites (Fig. 2.3) and numerous potential phosphorylation sites (not shown).

The appearance of IMC7, 12, and 14 in the G1 phase of the cell cycle (Fig. 2.9) is surprising as by G1 the daughters are mature and independent of the mother. The need for these additional cytoskeletal components is puzzling. One possible mechanism is that the G1 phase separates two subsequent cytokinetic events and these IMC proteins serve as markers to distinguish the mother cytoskeleton from future budding daughters. This model complements one of the most remarkable features of internal budding by *Toxoplasma*: it takes place in the presence of a mature mother cytoskeleton that at some point must be disassembled concurrently with the maturation of the daughters. Most Apicomplexa divide through schizogony wherein the mother's IMC is disassembled long before new daughters are being assembled (87) and, thus, do not require features to

differentiate mother and daughter. The possibility of IMC7, 12, and14 playing the role of maturity marker is supported by the lack of orthologs in other apicomplexans (Table 2.3). The other cortical IMCs, IMC1, 3, 4, 6, and 10, which engage in the daughter budding process, are well conserved across the Apicomplexa (Table 2.3 and Fig. 2.16).

IMC7, 12, and 14 may serve another function as well since they relocate back to the cytoplasm in most parasites after egress from the host cell (Tomasz Szetanek, Brooke Anderson-White, Michael White, Jeroen Saeij, and Marc-Jan Gubbels; paper under review). Inversely, the glycolytic enzyme aldolase-1 moves from the cytoplasm to the pellicle in extracellular parasites in response to the same changes in potassium and calcium concentrations (88) that induce egress (89-91). It is possible that IMC7, 12, and 14 could be involved in the relocation of the glycolytic enzymes, involved in a signaling cascade upon egress and invasion as cytoplasmic IFs are involved in signaling (92), or these IMCs could provide a rigidity to the cytoskeleton that inhibits egress or invasion making their relocation to the cytoplasm necessary in extracellular parasites.

The timing of the shift of IMC5, 8, 9, and 13 from the small buds to the basal complex is reminiscent of the timing of the previously described assembly of TgCentrin2 on the basal complex, which marks the start of basal complex constriction to establish the tapered basal end of the cytoskeleton (Figs. 2.12A-C and 2.15A). TgCentrin2 has been suggested to provide the constrictive force (60). Daughter maturation and emergence coincides with relative localization shifts within the basal complex to generate three discernable regions that could coincide with the BIR and BIC revealed by EM (Fig. 2.12H-J and 2.15B). Moreover, the BIC appears to bend over the alveoli and connect

with the plasma membrane, providing the only visible connection between the IMC and plasma membrane. However this bend is not observed at all times and could either be transient or be a transitional architecture in development. In addition to functioning in the constriction of the forming daughters, this complicated basal structure could assist in the maintenance of cellular integrity. Host cell invasion is accompanied by significant forces on the cytoskeleton when the parasite squeezes through a narrow aperture. Where the conoid reinforces the apical end, the basal complex could reinforce the basal end. Unlike MORN1, which is conserved across division modes in the Apicomplexa (87), the basal complex IMC proteins are not conserved among apicomplexans (Table 2.3). This lack of protein conservation is further supported by a lack of structural conservation. Though a posterior cup similar to *Toxoplasma* tachyzoites (28) is present in *E. tenella* merozoites (33), *Plasmodium* sporozoites contain a branching ER with a posterior polar ring that is not a clearly defined structure at their basal end (93).

The contractile activity of these basal complex components is similar to the behavior of septins in other eukaryotes. Septins are actin and, in fission yeast, type II myosin dependent (94). However, in *Toxoplasma* actin disruption has no effect on parasite maturation (40). Myosin overexpression does have an effect on daughter bud maturation in *Toxoplasma* (41) but the myosin is highly divergent type XIV (42, 43). Furthermore, unlike in other eukaryotes, abscission is not complete in *Toxoplasma*, leaving the daughters connected by a cytoplasmic bridge until some form of mechanical stress breaks them apart (95). This suggests that a traditional septin apparatus is not

present in *Toxoplasma*. The basal IMCs could be part of an alternative mechanism that fulfills the same contractile role.

IMC15 colocalizes with the centrosomes upon division and currently is the earliest known cytoskeletal marker for the new daughter buds, appearing earlier than MORN1 (Fig. 2.13). A potential model is that the centrosomal association of IMC15 provides a cue for the start of daughter budding by recruiting MORN1 and the other IMC proteins. Regardless of the exact mechanism, IMC15 highlights a key step in the connection between the cell cycle and mitosis.

Taken together, several IMC proteins are conserved, likely playing key roles in cytoskeleton assembly. However, expansion of the IMC protein family in *Toxoplasma* appears to have created new functions for several IMC proteins potentially not shared across the Apicomplexa. Future studies of these unique proteins could further elucidate the specific mechanisms of internal daughter budding.

Table 2.1. Reciprocal BLASTp results of all IMC proteins versus ToxoDB version 4.3

Both ToxoDB version 4 and version 5 gene names and IMC numbers are shown. Results up to an e-value = 10^{-3} cut-off value were reciprocally BLASTp searched and are shown. IMC proteins were numbered consecutively, first on basis of their discovery order and secondarily based on their ToxoDB sequence name. The unnumbered sequences presented BLASTp scores with an e-value within our arbitrary cut-off, but no alveolin motifs could be identified. Therefore, these are not considered to be part of the alveolin family and these genes were not pursued further in this study.

Table 2.1. Reciprocal BLASTp results of all IMC proteins versus ToxoDB version 4.3

IMC	ToxoDB (TGME49)	Identified by BLASTP																			Total Hits
		IMC1	IMC3	IMC4	IMC5	IMC6	IMC7	IMC8	IMC9	IMC10	IMC11	IMC12	IMC13	IMC14	IMC15	360	630	580	670	890	470	
IMC1	031640				X						X				X							3
IMC3	016000	X		X	X			X	X		X		X	X	X							9
IMC4	031630	X	X		X	X		X	X	X	X	X	X	X	X							12
IMC5	024530	X	X	X				X	X		X		X	X	X	X	X	X				12
IMC6	020270	X		X					X	X	X		X									6
IMC7	022220														X							1
IMC8	024520	X	X	X	X				X		X		X	X	X							9
IMC9	026220	X	X	X	X	X		X		X	X	X	X	X	X				X	X		14
IMC10	030210	X			X	X			X		X		X									6
IMC11	039770	X	X	X	X	X		X	X	X			X	X	X						X	12
IMC12	048700			X																		1
IMC13	053470	X	X	X	X	X		X	X	X	X	X		X	X						X	13
IMC14	060540	X	X	X	X			X	X	X	X		X		X							10
IMC15	075670	X	X	X	X			X	X		X		X	X								9
--	106360																					0
--	035630																					0
--	024580																					0
--	059670																					0
--	013890																					0
--	062470			X					X		X		X	X	X							6
	Times Hit	11	8	11	10	5	0	8	11	6	12	3	11	9	11	1	1	1	1	1	2	

Table 2.2. Yeast two-hybrid results of the basal complex components

The basal IMC proteins, IMC5, 8, 9, 13 and 15, were all shown to interact with each other in yeast two-hybrid screens except IMC5 and 15. IMC9 was shown to only interact with IMC5 when used as the bait. Similarly, IMC15 was shown to only interact with IMC8 and 9 when used as the bait. These IMC interactions that produced different results when switched from bait to prey were verified in a second transformation. MORN1 and IMC3 were shown to interact with all the IMC proteins and TgCentrin2 was shown not to interact with them. Interactions were determined by growth on –Leu/-Trp/-His/-Ade (quadruple drop out or QDO) media. MORN1, IMC3, and TgCentrin2 were found to autoactivate as bait and, therefore, were only tested as prey. Abbreviations used are I+number for IMC proteins, whereas, M1 and C2 represent MORN1 and TgCentrin2, respectively.

Table. 2.2. Yeast two-hybrid results of the basal complex components

Bait	Prey							
	I5	**I8**	**I9**	**I13**	**I15**	**M1**	**I3**	**C2**
IMC5	+	+	+	+	-	+	+	-
IMC8	+	+	+	+	-	+	+	-
IMC9	-	+	+	+	-	+	+	-
IMC13	+	+	+	+	+	+	+	-
IMC15	-	+	+	+	+	+	+	-

Table 2.3. Conservation of IMC proteins across the Apicomplexa

The *T. gondii* IMC proteins were BLASTp searched against the other apicomplexans with sequenced genomes (EuPathDB 2.12): *Neospora caninum* (ToxoDB 5.3), *Eimeria tenella* (GeneDB April 2008 release), *Plasmodium falciparum* (PlasmoDB V6.3), *Plasmodium berghei* (PlasmoDB V6.3), and *Cryptosporidium parvum* (CryptoDB V4.2). E-values of the top hits are shown. Bold numbers reflect significant homology hits. Note that not all top-hits were unique, as reflected in the total number of unique hits at the bottom.

Table 2.3. Conservation of IMC proteins across the Apicomplexa

TgIMC	*N.can*	*E.ten*	*P.fal*	*P.ber*	*C.par*
1	**E-186**	**E-135**	**E-71**	**E-69**	E-35
3	**E-188**	**E-107**	**E-66**	**E-66**	E-37
4	**E-174**	**E-141**	**E-94**	**E-93**	**E-47**
5	**E-109**	**E-50**	E-28	E-28	E-09
6*	**E-159**	**E-90**	**E-73**	**E-71**	**E-42**
7	**E-149**	E-02	E-16	E-11	E-02
8	**E-70**	E-28	E-16	E-15	E-09
9	**E-188**	**E-60**	E-21	E-21	E-35
10	**E-211**	**E-107**	**E-57**	**E-54**	E-31
11	**E-64**	E-20	E-19	E-18	E-10
12	**E-87**	E-08	E-12	E-07	E-03
13	**E-120**	**E-51**	E-23	E-22	**E-44**
14	**E-134**	E-23	E-25	E-27	E-27
15	**E-130**	E-25	**E-41**	**E-41**	E-19
# unique IMCs	13	10	10	9	6

* missing in *T. gondii* VEG strain

Figure 2.1. IMC3 is enriched in daughter buds and diminished upon maturation

(A-B) Parasites at different developmental stages stained with IMC1 antibody show universal intensity distribution (A), whereas IMC3 antibody staining displays varying levels of intensity (B). (C) A merge of the red and green channel highlights the differences in IMC1 and IMC3 expression at the cortical IMC reinforcing that IMC3 is enriched in forming daughters and recently divided, newly emerged parasites. Parasite developmental stages are as indicated. (D) A merge image with DAPI staining (blue).

Figure 2.1. IMC3 is enriched in daughter buds and diminished upon maturation

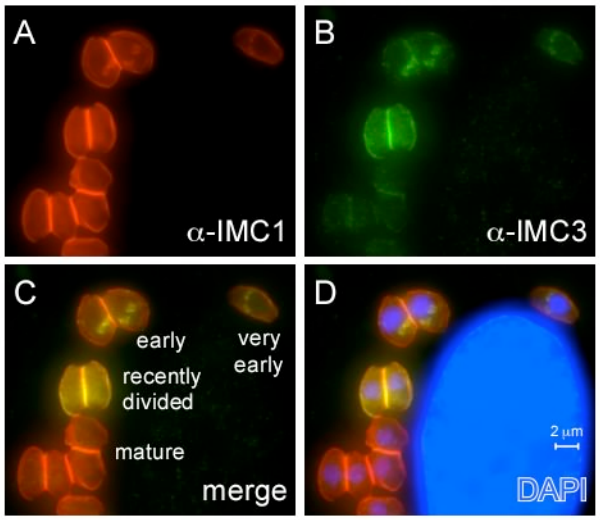

Figure 2.2. Identification of IMC14 and 15 splice variants by RACE PCR

(A) The 3'-end of the IMC14 mRNA was determined by RACE PCR using primers listed in Table 4.1. The IMC14 ORF was amplified from Prugniaud and RH strain cDNA using primers *IMC14-F-Nhe* and *IMC14-R-RV*. Three splice variants were detected in the Prugniaud strain (Pru14.1-3) and one in the RH strain. All four were different from each other and the predicted gene model (55.m04893). (B) Determination of IMC15 splicing by RACE (primers listed in Table 4.1) identifies a transcript deviating from the available gene models, in particular the 5'- and 3'-ends of the mRNA. The following IMC15 gene models, displayed in blue, were used from the top down: 64.m00327, TgTwinScan_1698, TgTigrScan_7407, TgGLEAN_0852 and TgGlmHMM_1748. Solid boxes represent the coding sequence. The models used throughout the study are marked with an asterisk (IMC14.RH and RACE validated IMC15).

Figure 2.2. Identification of IMC14 and 15 splice variants by RACE PCR

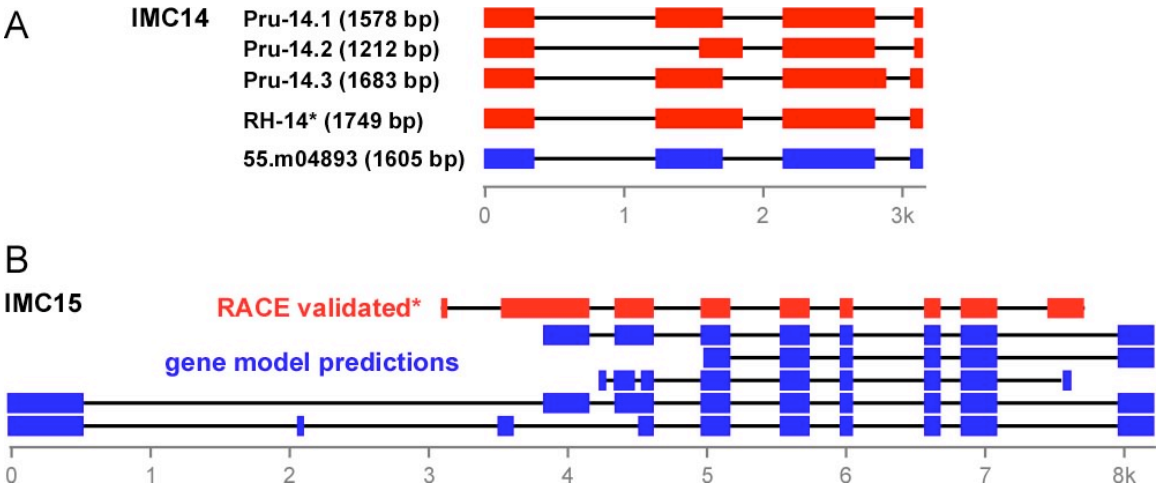

Figure 2.3. Alveolin domain-containing IMC protein family

Full-length and validated open reading frames of each IMC protein in order by IMC number and their corresponding ToxoDB gene name. The alveolin repeat regions are represented in yellow and the N- and C-termini in green. Cysteines are indicated in red and predicted palmytoylation sites marked with blue asterisks.

Figure 2.3. Alveolin domain-containing IMC protein family

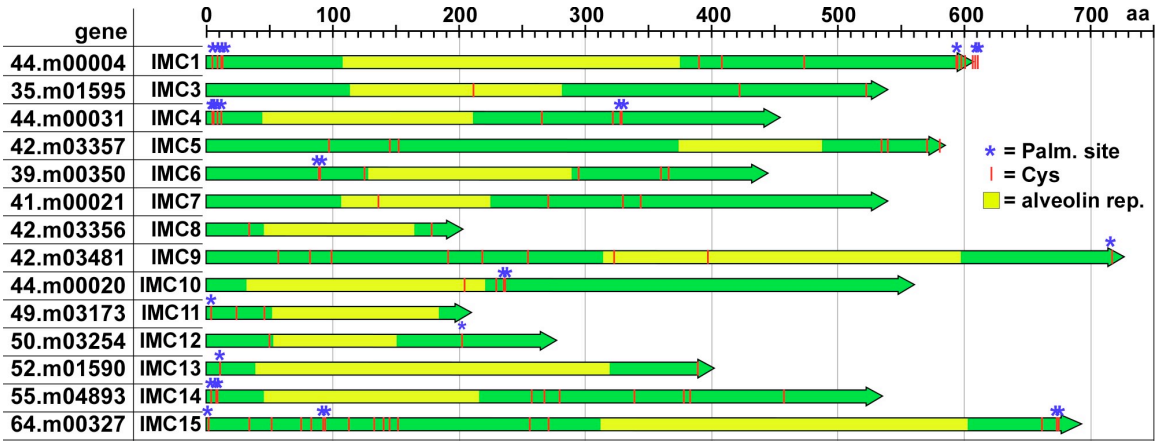

Figure 2.4. Expression of IMC proteins during tachyzoite development

(A) Affymetrix array expression pattern of the IMC mRNAs through two cycles of tachyzoite development. RH strain parasites expressing the herpes simplex thymidine kinase (TK) were synchronized by a thymidine block. Cell cycle stages and timing of budding are indicated at the top. Expression levels are normalized to internal controls on the Affymetrix array. (B) Maximum and minimum expression levels of the IMC genes in the second cycle represented in (A) (hours 6–12). Expression level is shown as the raw fluorescence hybridization data.

Figure 2.4. Expression of IMC proteins during tachyzoite development

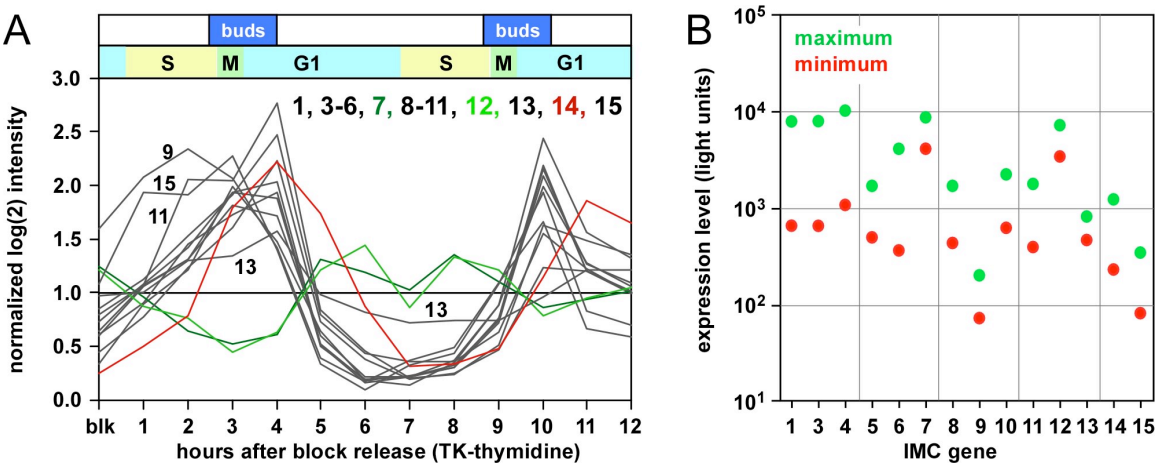

Figure 2.5. Localization of IMC1 and IMC3 throughout tachyzoite development

(A-B) Mature (A) and budding (B) parasites co-stained with antibodies against IMC1 (green) and IMC3 (red). (C) Intensity profile across the budding daughters indicated in (B) panel 3 marked by arrow "C". Relative distance is shown along the length and direction of the arrow on the x-axis and relative intensity is shown on the y-axis. Arrowheads indicate specific localization of IMC1 in the mature mother parasites not detected for IMC3. (D) Mature mother intensity profile along the arrow indicated in (C) panel 3 marked with "D". (E) IMC1-YFP expressing parasites are stained with IMC1 antibody (red) validating the interchangeable use of the fusion and antibody. The YFP tag does not appear to interfere with the localization pattern of IMC1. (F) Comparable results are obtained for YFP-IMC3 (green) and the IMC3 antibody (red). All YFP constructs are driven by the p*tub* promoter.

Figure 2.5. Localization of IMC1 and IMC3 throughout tachyzoite development

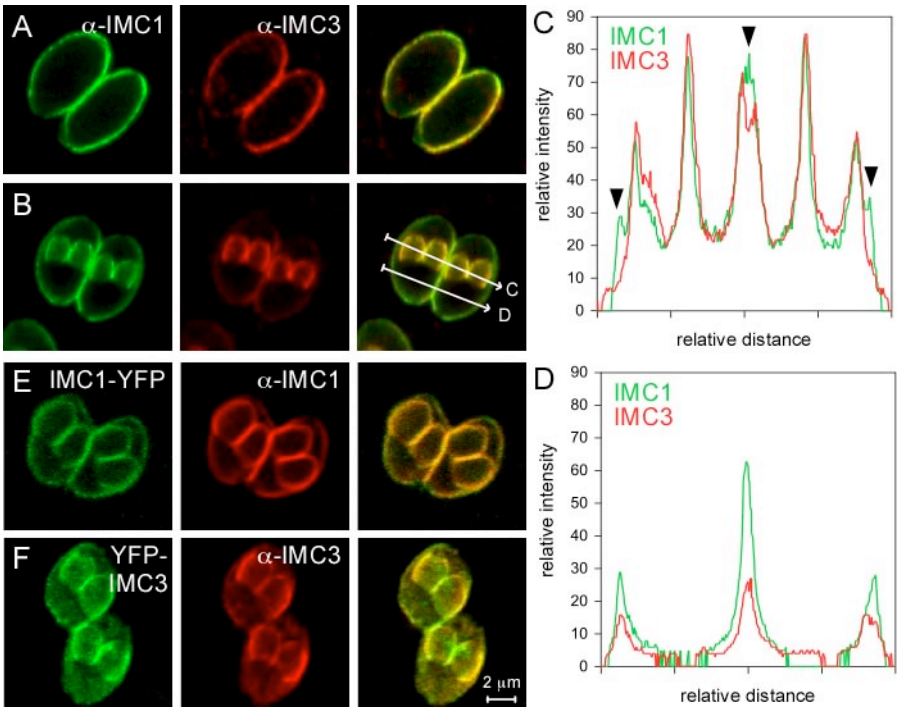

Figure 2.6. Relative localization of IMC4 throughout tachyzoite development

(A) Parasites expressing YFP-IMC4 (green) co-stained with IMC1 antibody (red) show equal intensity of IMC1 and IMC4 across development stages. (B) Parasites expressing YFP-IMC4 (green) co-stained with IMC3 antibody (red) show equal intensity of IMC4 across developmental stages, whereas IMC3 is enriched in the budding daughters. (C) Live imaging of stable parasites expressing IMC4-YFP corroborate the localization pattern observed with an N-terminal fusion. All YFP constructs are driven by the p*tub* promoter.

Figure 2.6. Relative localization of IMC4 throughout tachyzoite development

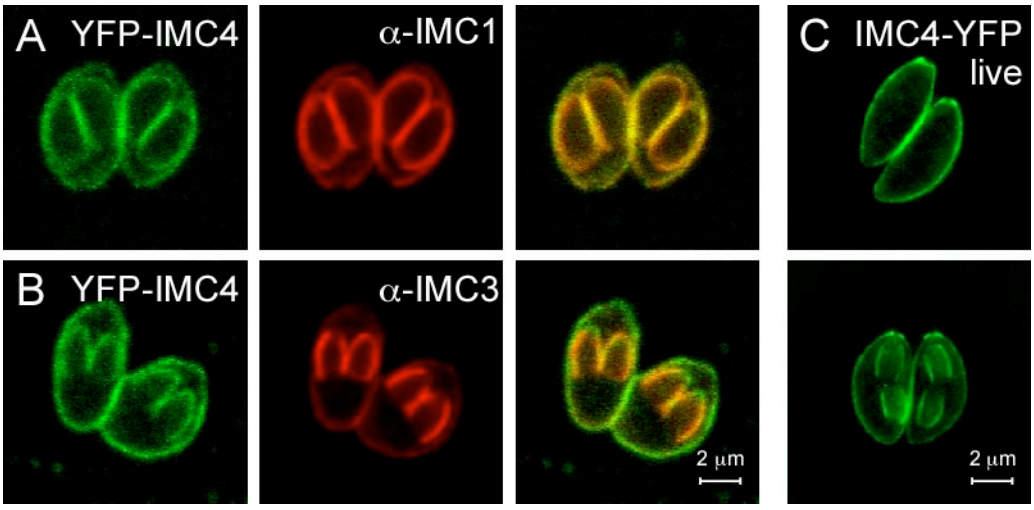

Figure 2.7. Verification of N-terminal YFP fusions with western blot

The expected masses of the IMC proteins plus the YFP tags are indicated at the bottom of each lane. Full-length fusions are marked with an asterisk (*) and smaller products of cleavage or degradation events are marked with a plus (+). The smaller product observed for IMC7 appears to be the YFP tag alone (27 kDa). For IMC14 a full-length band of the expected size is not present. Since these blots were performed using only mature parasites the data could suggest that all IMC14 is cleaved during the maturation process. IMC15 displays 2 bands slightly larger than the expected full-length fusion, which hint at potential post-translational modifications.

Figure 2.7. Verification of N-terminal YFP fusions with western blot

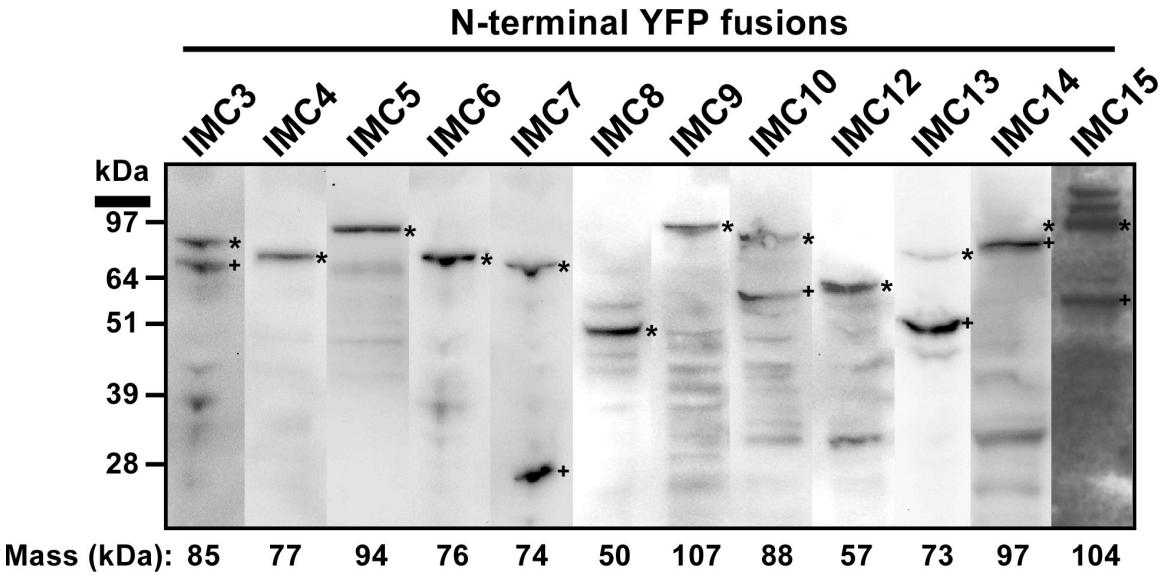

Figure 2.8. Relative localization of IMC6 and IMC10 throughout tachyzoite development

(A-B) Mature (A) and budding (B) parasites expressing YFP-IMC6 co-stained with IMC3 antibody (red). (C) Intensity profile across the budding daughters indicated in (B) panel 3 marked by arrow "C". Relative distance is shown along the length and direction of the arrow on the x-axis and relative intensity is shown on the y-axis. (D-E) Live images of YFP-IMC6 (D) and IMC6-YFP (E). (F-G) Mature (F) and budding (G) parasites expressing YFP-IMC10 co-stained with IMC3 antibody (red). (H) Intensity profile across the budding daughters indicated in (G) panel 3 marked by arrow "H". (I-J) Live images of YFP-IMC10 (I) and IMC10-YFP (J). All YFP constructs are driven by the p*tub* promoter.

Figure 2.8. Relative localization of IMC6 and IMC10 throughout tachyzoite development

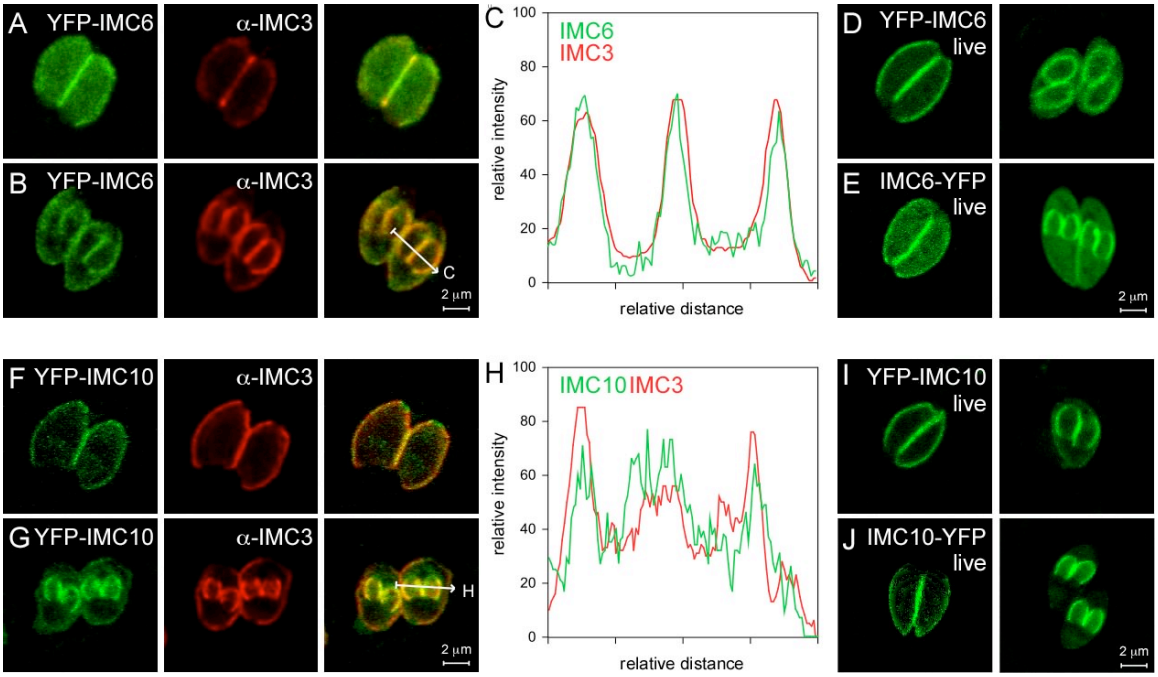

Figure 2.9. IMC7, 12, and 14 are excluded from the budding cytoskeleton

(A-C) Mature (A), mid-budding (B), and emerging (C) parasites expressing YFP-IMC7 co-stained with IMC3 antibody (red). (D) YFP-IMC7 expressing parasites co-stained with GAP45 antibody (red). (E) Intensity profile across the budding daughter indicated in (B) panel 3 marked by arrow "E". Relative distance is shown along the length and direction of the arrow on the x-axis and relative intensity is shown on the y-axis. (F) Live images of IMC7-YFP. (G-H) Mid-budding (G) and emerging (H) parasites expressing YFP-IMC12 co-stained with IMC3 antibody (red). (I) YFP-IMC12 expressing parasites co-stained with GAP45 antibody (red). (J) Live images of YFP-IMC12 driven by its native promoter. (K) Live images of IMC12-YFP driven by its native promoter. (L) Intensity profile across the budding daughter indicated in (G) panel 3 marked by arrow "L". (M) Live images of IMC12-YFP. (N-P) Mature (N), mid-budding (O), and emerging (P) parasites expressing YFP-IMC14 co-stained with IMC3 antibody (red). (Q) Intensity profile across the budding daughter indicated in (O) panel 3 marked by arrow "Q". (R) YFP-IMC14 expressing parasites co-stained with GAP45 antibody (red). All IMC7 and 14 YFP-fusion constructs are driven by their native promoters and all IMC12 YFP-fusion constructs are driven by the p*tub* promoter except for (J) and (K).

Figure 2.9. IMC7, 12, and 14 are excluded from the budding cytoskeleton

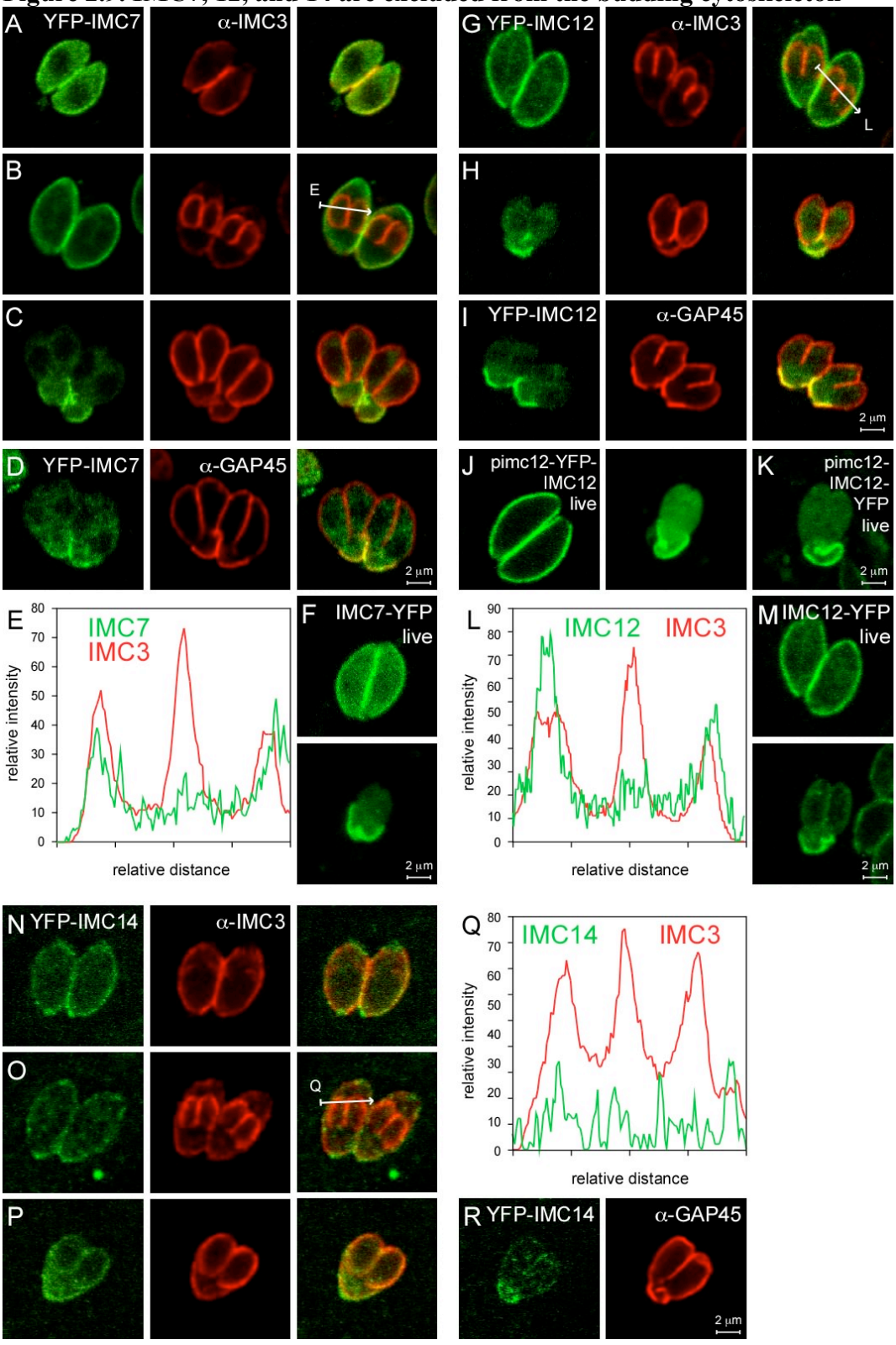

Figure 2.10. IMC7, 12, and 14 transition to the mature cytoskeleton during G1

(A) Selected frames from time-lapse images of YFP-IMC12. (B-C) CherryRFP-IMC7 (B) and CherryRFP-IMC14 (C) expressing parasites stained with cherryRFP antibodies exhibiting cortical and cytoplasmic localization. (D) FV-P6 expressing CherryRFP-IMC7 or CherryRFP-IMC14 were allowed to replicate for 18 hrs at 35°C before transition to 40°C (controls were kept at 35°C). After 16 hrs the localization of IMC7 and IMC14 was differentiated between cytoplasmic or cortical. The percentage of vacuoles with cortical signals is plotted for the conditions as indicated. (E) As in (D) except that the parasites were allowed to invade and grow at 40°C for 16 hrs (all parasites arrest before division). Results from three independent experiments and error bars denote standard deviation.

Figure 2.10. IMC7, 12, and 14 transition to the mature cytoskeleton during G1

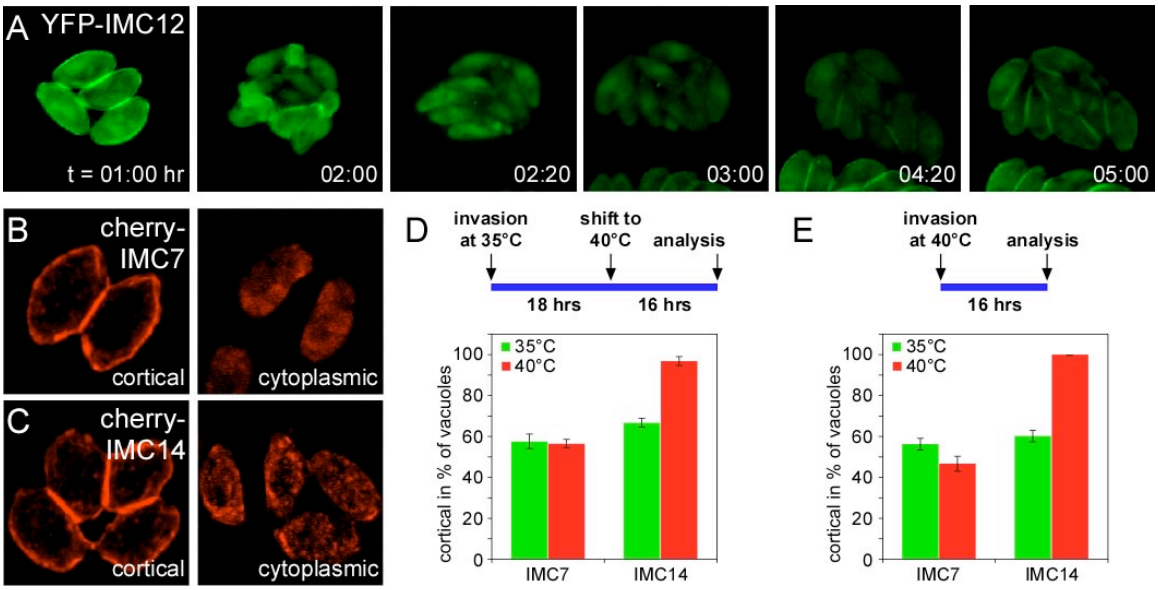

Figure 2.11. IMC11 localizes to the apical cap and colocalizes with PhIL1

(A-B) Live mature (A) and budding daughter (B) parasites expressing YFP-IMC11. The timing of the shift from full cortical IMC expression in the buds to apical cap and basal localization is unknown. Arrowheads indicate YFP localization at the basal complex. (C) Live YFP-IMC11 (green) expressing parasites co-transfected with PhIL1-CherryRFP (red). (D) YFP-IMC11 expressing parasites co-stained with MORN1 antibodies (red) and DAPI (blue). YFP-IMC11 is driven by the p*tub* promoter.

Figure 2.11. IMC11 localizes to the apical cap and colocalizes with PhIL1

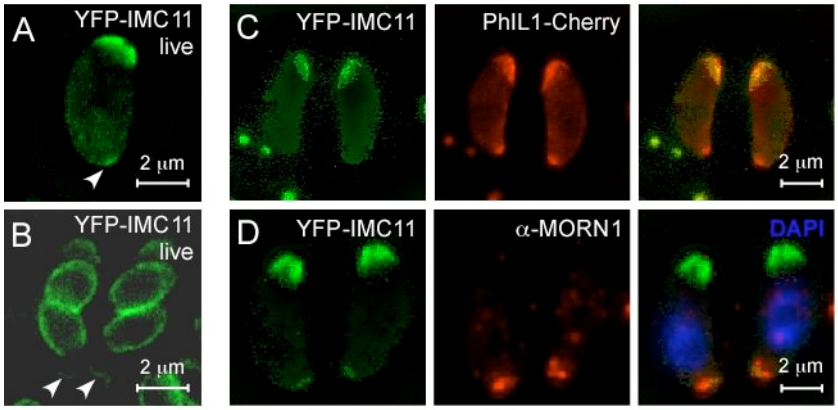

Figure 2.12. IMC5, 8, 9, and 13 localize to the budding daughters and then transition to the basal complex

(A) Live YFP-IMC8 expressing parasites at different stages of tachyzoite development (independent parasites are shown in each panel). Mother and daughter parasites are traced by dotted lines in the lower series. (B) Live images of IMC13-YFP. (C) DD-YFP-IMC5 expressing parasites are stained with IMC5 antibody (red) validating the interchangeable use of the fusion and antibody. The DD-YFP tag does not appear to interfere with the localization pattern of IMC5. (D) Wild-type parasites co-stained with anti-IMC5 serum (red), IMC1 antibodies (green), and DAPI (blue). (E) Wild-type parasites co-stained with anti-IMC5 serum (red), MORN1 antibodies (green), and DAPI (blue). (F) Pair-wise comparisons of the members of the basal complex using co-transfected YFP and CherryRFP constructs. The numbers represent the tagged IMC protein, M1 is MORN1, C2 is TgCentrin2, and the colors correspond with the fluorescent protein fusion. The asterisks in the MORN1 + IMC9 panel mark the spindle pole localization of MORN1. All YFP and DDYFP constructs are driven by the p*tub* promoter. (G-J) Electron micrographs identifying an inner collar at the basal end of the cytoskeleton. (G) Cross section through the apical complex demonstrating the absence of a comparable complex at the apical end. (H) Longitudinal section through the posterior end of a parasite displaying the basal inner collar (BIC) and the fold over the alveoli marked with arrowheads. The arrows mark the end of the alveolar vesicles. A unit membrane (UM) of unknown origin with an electron dense coating that is limited to the basal cup region is visible as a clear vesicle sitting within the very basal opening. (I) Longitudinal section through the basal complex. Arrowheads mark the BIC, which bends over the end of the alveolar membrane and

connects with the plasma membrane as indicated by the arrow. The area marked by the blue box is enlarged. (J) A transverse section through the basal complex displaying the continuity of the BIC and basal inner ring (BIR), which are visible in the enlarged area marked by the blue box. In addition, the two closely apposed UMs can be discerned. P is plasma membrane. EM images provided by Dr. David J. P. Ferguson, University of Oxford.

Figure 2.12. IMC5, 8, 9, and 13 localize to the budding daughters and then transition to the basal complex

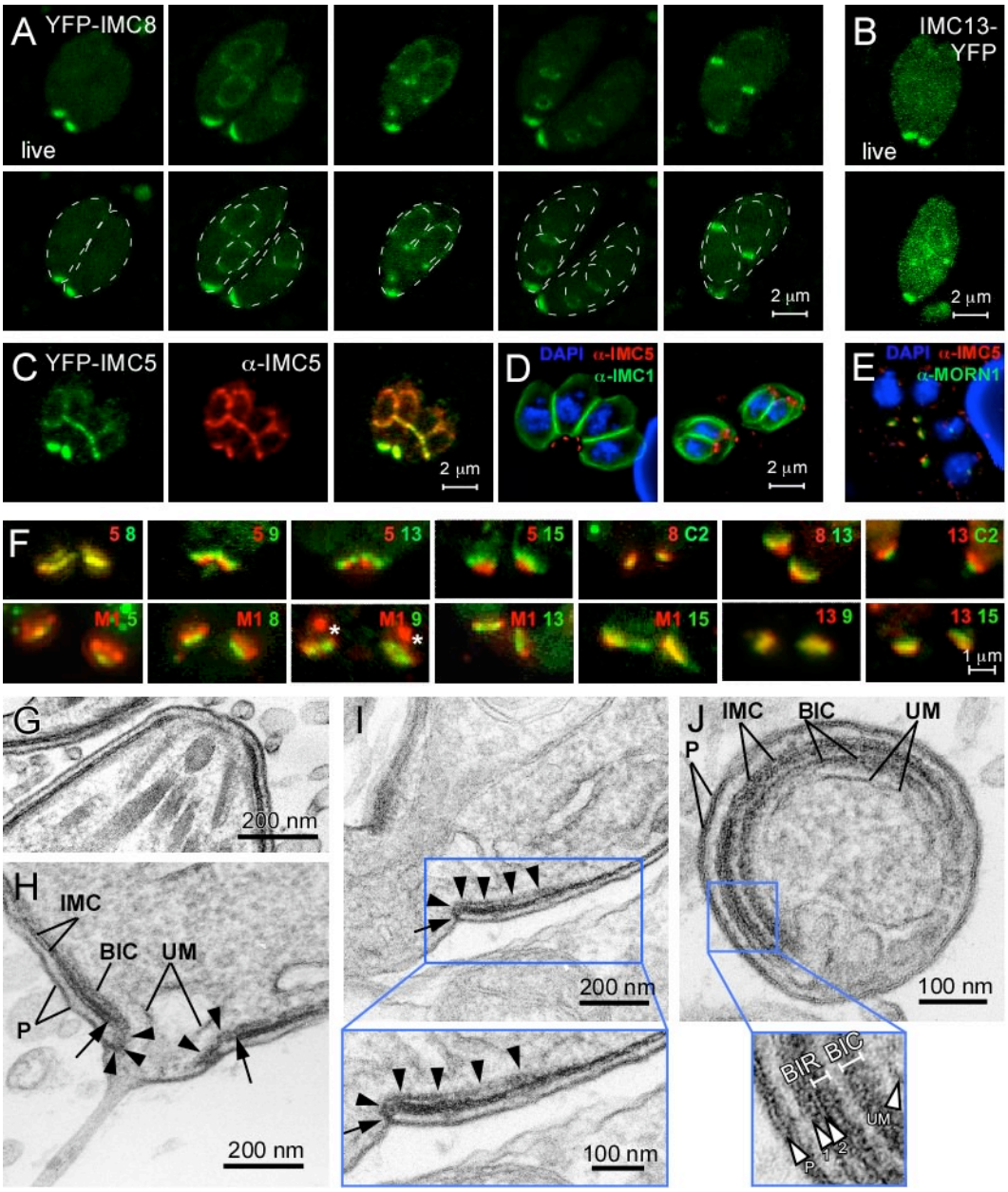

Figure 2.13. IMC15 associates with the duplicated centrosomes and transitions to the budding cytoskeleton

(A) Live mature and budding daughter parasites expressing YFP-IMC15. An arrow indicates the very basal end of the cytoskeleton, an arrowhead the very apical end, and the double arrowheads the cap region. (B) IMC15-YFP stained with anti-GFP. (C) YFP-IMC15 expressing parasites co-stained with IMC3 antibody (red) in mid-budding parasites. (D) YFP-IMC15 expressing parasites co-expressing myc_2-centrin2 and stained with myc antibody (red) in early budding parasites. Arrowheads indicate the very apical end of the parasite, double arrowheads the apical cap ringed by six TgCentrin2 foci, single arrow the very basal end, and double-headed arrows the early bud. Inset is of boxed area. (E) YFP-IMC15 expressing parasites co-stained with anti-human centrin antibody (red) in mature parasites. Arrows mark IMC15 localization to the duplicated centrosomes. Inset is of boxed area. (F) YFP-IMC15 expressing parasites co-transfected with cherryRFP-MORN1 (red) and co-stained with anti-human centrin antibody (blue) in very early budding parasites (pre-mitotic as indicated by the single, centrally located MORN1 accumulation highlighting the spindle pole). The parasite is outlined with a dotted line in the first panel. Insets are of the central region around MORN1. (G) YFP-IMC15 expressing parasites are stained with IMC15 antibody (red). The antibody recognizes only the budding aspects of the localization pattern of YFP-IMC15. (H) The same results are obtained with YFP-IMC15 under control of its native promoter. (I) S-phase wild-type parasites stained with anti-IMC15 serum (red) and co-stained with centrin antibody (green) and DAPI (blue). All insets are 2X enlargments. All YFP constructs are driven by the p*tub* promoter except (H).

Figure 2.13. IMC15 associates with the duplicated centrosomes and transitions to the budding cytoskeleton

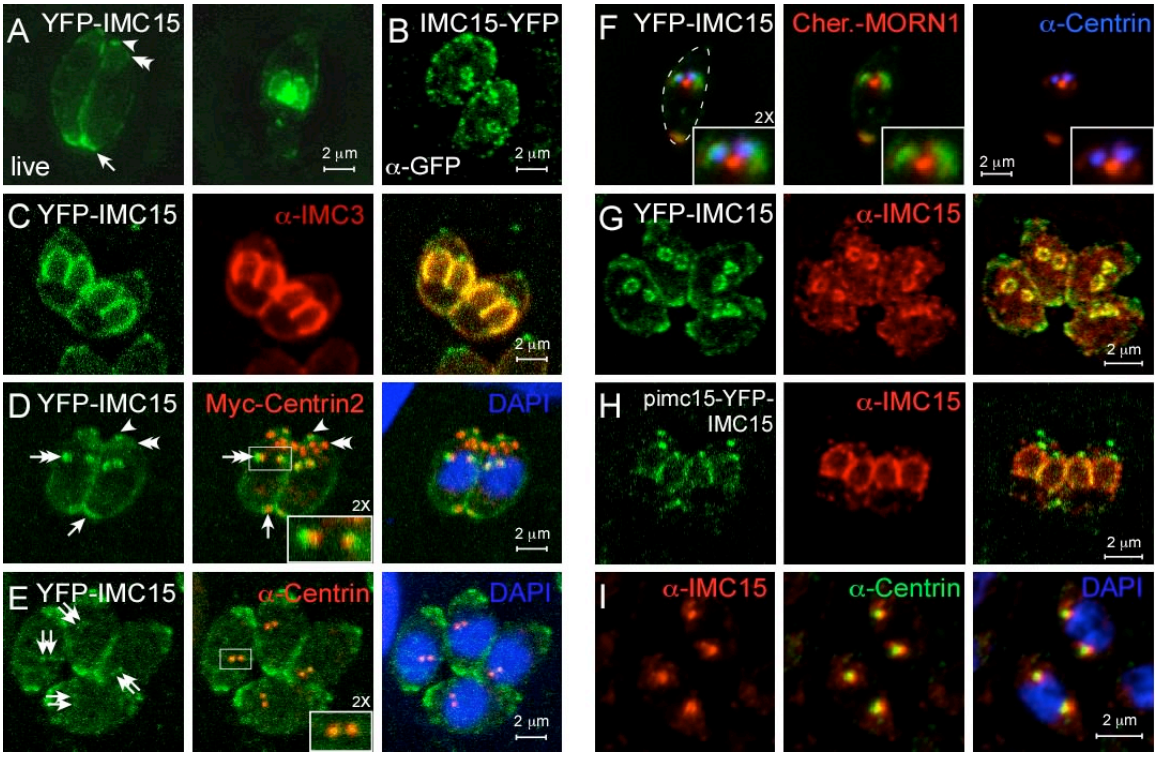

Figure 2.14. The alveolin domain contains the localization signal differentiating cortical from basal IMCs

(A-B) IMC3 (A) and IMC8 (B) are dissected to determine whether the N-terminus ("N"), alveolin domain ("A"), or C-terminus ("C") is/are responsible for their localization patterns. The domains indicated above or below each panel are fused to an N-terminal YFP and all constructs are driven by the p*tub* promoter. IMC3 domains are in blue and IMC8 domains are in green.

Figure 2.14. The alveolin domain contains the localization signal differentiating cortical from basal IMCs

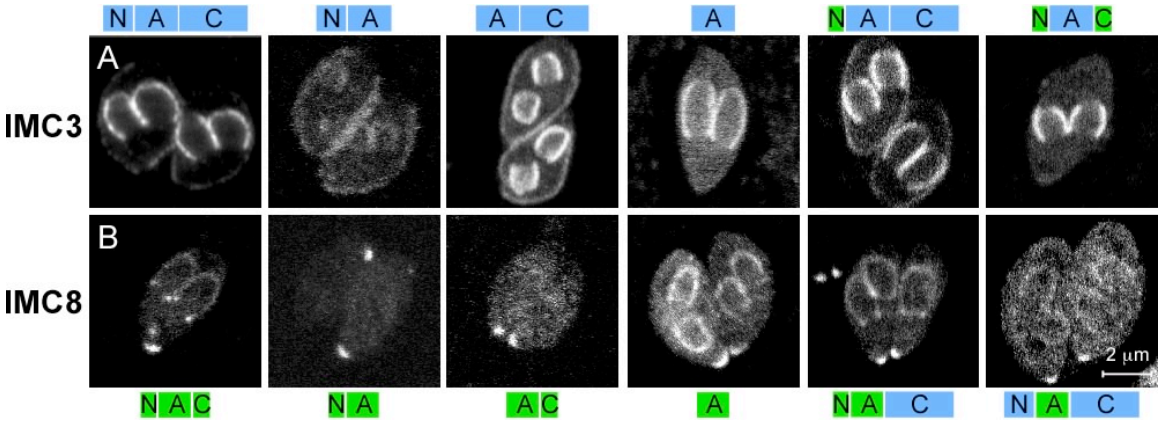

Figure 2.15. Summarizing schematics of the IMC protein dynamics throughout tachyzoite development and the structure of the basal cytoskeleton

(A) Groups of IMC proteins with a similar behavior are shown in the same color and the groups are introduced at the stage of their defining role; among the yellow, cortical IMC proteins, the ones with a preference for the immature buds are outlined (IMC3, 6, and10). IMC11 is not included. (B) The tentative structure of the basal complex in mature parasites is composed of three layers. The top layer (green) is composed of MORN1, IMC9, IMC13, and IMC15; the middle layer of IMC5 and 8; and the very basal tip contains TgCentrin2, which overlaps with the middle layer. Data in Figure 2.12F do not include clear candidates for the bend of the inner collar toward the plasma membrane seen by EM (Fig. 2.12H-J). Interpretation of the posterior cup is based on data presented in (28).

Figure 2.15. Summarizing schematics of the IMC protein dynamics throughout tachyzoite development and the structure of the basal cytoskeleton

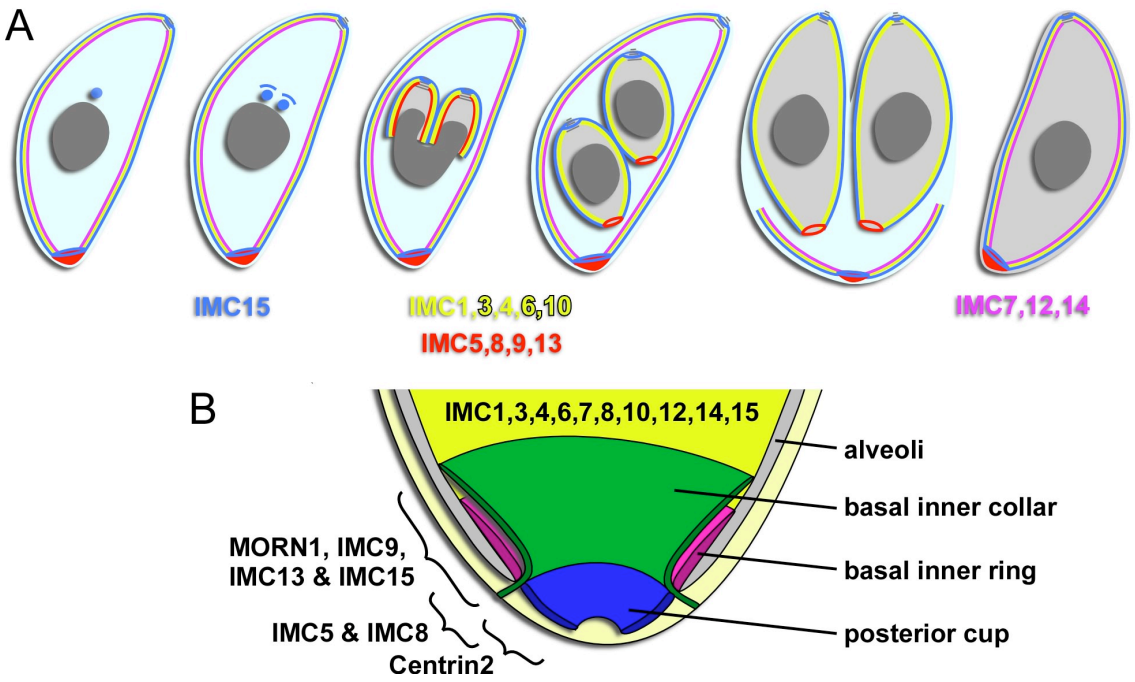

Figure 2.16. Tree of IMC proteins and their closest apicomplexan relatives

Phylogenic tree with 1000x bootstrapping of the top BLASTp results from Table 2.3. Blue circles at the nodes indicate bootstrap values of greater than or equal to 50. Red circles at the nodes indicate bootstrap values of greater than or equal to 80.

Figure 2.16. Alignment of IMC proteins and their closest apicomplexan relatives

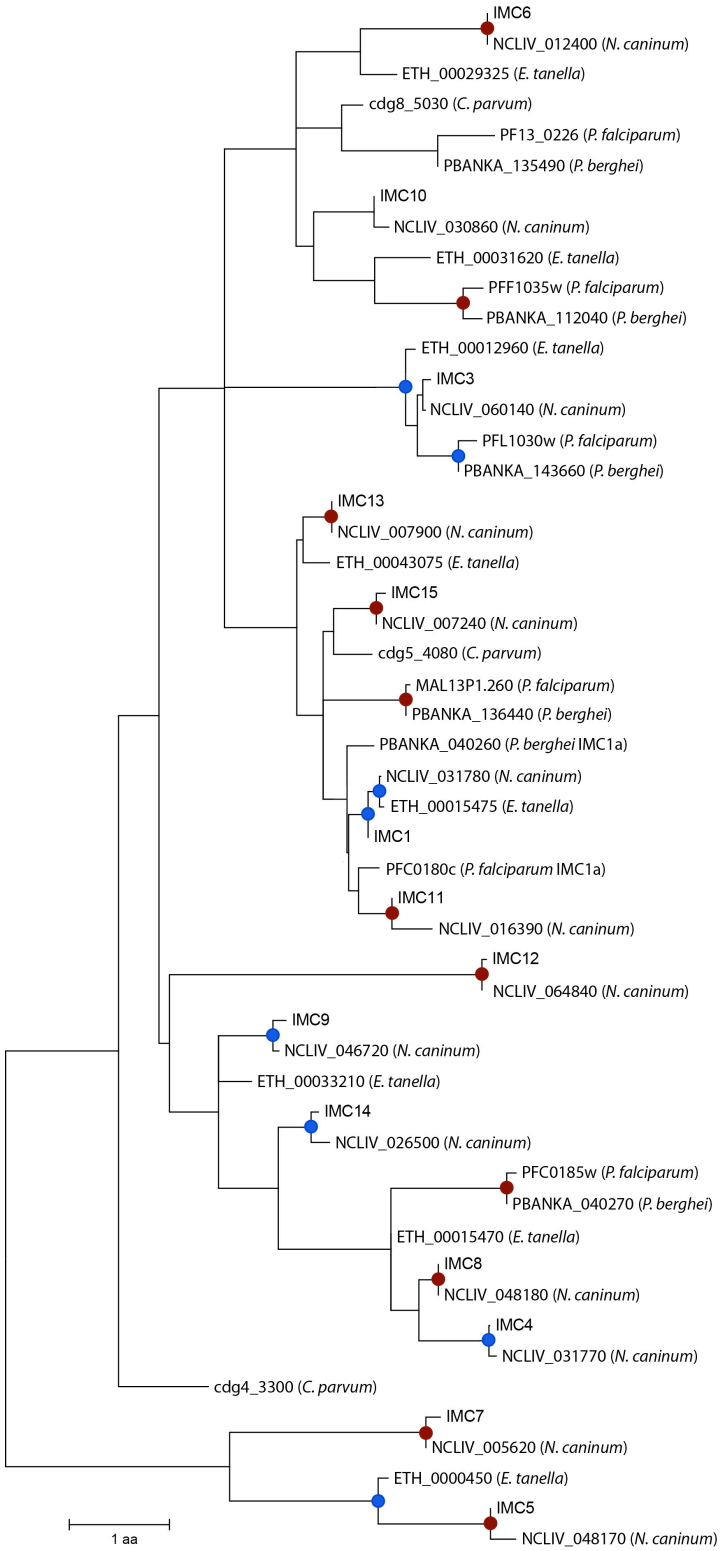

Chapter 3. Analysis of the role of IMC15 in early cytoskeletal development

3.1. Introduction

The destructive, rapid replication of *Toxoplasma* occurs by an internal budding mechanism that begins with the division of the Golgi and the duplication of the centrosome (17, 23-25, 29). Concurrent with or immediately following the duplication of the centrosome the earliest components of the cytoskeleton begin to form near the two centrosomes. The first of these components is IMC15. As the initial member of the IMC meshwork to appear in division it is possible that IMC15 nucleates the development of this IMC structure.

Precedents exist for the importance of early bud constituents in *Toxoplasma*. Another early indicator of cytoskeletal budding is Rab11B, a small GTPase that traffics the vesicles of the IMC. Conditional expression of a dominant-negative Rab11B construct blocks IMC biogenesis (13). Moreover, the absence of ISP2, a component of the central region of the IMC not imbedded in the IMC meshwork, results in a multinucleated mass containing several stunted early bud formations (14). Disrupting the proteins of the early buds does not always result in a defect early in the division process, as exemplified by MORN1. MORN1 deletion mutants develop normally until the midway point and then basal constriction and basal complex formation are abnormal (11) or cytokinesis fails to occur (10). Not only are these foremost budding factors essential for proper parasite development, but the effects of their loss are not limited to the inaugural stages of development.

In this chapter, I identified the homologs of IMC15 in other apicomplexan species and performed detergent extractions to verify that IMC15 exists within the IMC

meshwork. While delving more deeply into the function of IMC15, the inability to generate a direct knockout (KO) suggests this protein is essential. Furthermore, conditional knockouts using two different systems show that a minimal amount of IMC15 is sufficient to maintain parasite viability. Deletion constructs of IMC15 expressed in a wild-type background suggest that the localization of IMC15 is controlled by multiple factors beyond the sequence of the alveolin domain. Furthermore, the overexpression of the C-terminus appears to elicit a dominant negative effect. Constructs with palmitoylation site point mutations also suggest a prominent role for the C-terminus in proper development and support the possibility of a complex palmitoylation system in *Toxoplasma*. Characterization of IMC15 is continuing to provide novel insight into cytoskeletal development.

3.2. Results

3.2.1. Identification of IMC15 homologs in apicomplexans

Previous work with the IMC family focused on identifying all the related proteins within the *Toxoplasma* genome (96). To assess the relationship of IMC15 (TGGTI_000660) to other apicomplexans, BLASTp searches of the sequenced genomes in EuPathDB version 2.10 were performed as well as BLASTp searches in NCBI (97). Of those proteins with an EuPathDB e-value of -40 or less, 9 out of 10 appear in both result sets. These 10 hits were BLAST searched against ToxoDB and for all 10 IMC15 is the closest match (75). All BLAST results are presented in Table 3.1.

Alignment of IMC15 with the 10 homologs with the lowest e-values reveals that the N- and C-termini exhibit limited intergenus similarity (Fig. 3.1). However the alveolin repeat region (312-602 aa) shows high homology (Fig. 3.2A). As illustrated by the phylogenic tree generated from the full-length homolog sequences in Figure 3.2B, IMC15 is most closely related to its homolog in *Neospora* and closely followed by those in *Babesia* and *Theileria*. The distance of the *Plasmodium* homologs from *Toxoplasma* IMC15 could be attributed to the more conserved terminal regions amongst *Plasmodium* species (Fig. 3.1); however, a phylogenic tree comparing only the alveolin domains reveals the same relationships as the full-length sequences. Based on the alignments, the predicted palmitoylation sites discussed in Chapter 2 at cysteines 4, 92, 93, 673, and 674 (Fig. 2.3) are not conserved (Fig. 3.1). However, several potential phosphorylation sites exist within the conserved alveolin domain (Fig. 3.2A).

3.2.2. IMC15 is part of the IMC meshwork

IMC15 displays a unique spatio-temporal localization pattern during budding, appearing with the duplication of the centrosomes and then expanding to colocalize with the early MORN1 rings. IMC15 localizes to the developing IMC of the new daughters but its cortical intensity diminishes until it is undetectable as the daughters mature when visualized with our IMC15 antibody (96). Components of the mature IMC are known to be insoluble in 1% Triton X-100 (TX-100) and 1% deoxycholic acid (DOC) (28). To verify that IMC15, an alveolin repeat containing protein, is part of the IMC meshwork of

the mature cytoskeleton, detergent extractions were performed. For this we used an endogenously tagged version of IMC15, IMC15-myc$_3$ (Fig. 3.3A).

As shown in Figure 3.4, IMC15 is an insoluble component of the cytoskeleton, appearing in the pellet fractions with IMC1. These results with mature extracellular parasites verify that IMC15 is part of the mature cytoskeleton. The extremely low expression level of IMC15 (Fig. 2.4B) prohibits us from collecting enough material from the daughter buds to examine the solubility of IMC15 in the immature cytoskeleton by western blot (96). It does not appear, based on the mature-only lysate, that IMC15 undergoes a cleavage event like IMC1 upon cytoskeletal maturation (67).

3.2.3. Resistance to KO suggests IMC15 is essential

Toxoplasma exhibits a strong preference for non-homologous end-joining (NHEJ) over homologous recombination (HR) and this preference is an obstacle for the efficient generation of KOs (98-102). Ku80 is an essential element of the NHEJ machinery (103, 104) that when eliminated can shift an organism's preference to HR over NHEJ and increase the efficiency of KO generation (105-110). In order to decrease the barrier to KO creation and, thus, increase our tools to study gene function in *Toxoplasma*, a parasite strain lacking the *ku80* gene, the *Δku80* strain, was engineered (111, 112). To begin characterizing the function of IMC15 we undertook to generate a KO using the *Δku80* strain.

Multiple attempts to remove *imc15* by replacing the gene with HXGPRT were unsuccessful (Fig. 3.3B). Instead of double HR to remove the gene it provided single HR

or reinsertion of the knocked out region despite the absence of Ku80. The inability to create a KO suggests that IMC15 may be essential.

3.2.4. IMC15 strongly associates with the centrosome

The function of essential genes can be studied with a conditional knockdown (KD) so we created a conditional construct of IMC15 using the destabilization domain (DD) system (45, 113). A DDmyc-IMC15 construct under the control of p*imc15* was knocked into the uracil phosphoribosyltransferase (UPRT) locus to allow for negative selection with 5-fluorodeoxyuridine (FUDR) (Fig. 3.3C) (114-116) and subsequently the entire locus of IMC15 was knocked out using the direct KO strategy (Fig. 3.3B). The resultant transgenic strain is cultured continuously in the presence of the synthetic ligand, Shld1, which stabilizes the DD-tagged protein. When Shld1 is removed the DDmyc-IMC15 should be targeted to the proteasome and degraded.

DDmyc-IMC15 localizes normally while cultured with Shld1, appearing with the duplicated centrosomes (Fig. 3.5A) and then expanding into the early buds (Fig. 3.5B and C). When Shld1 is removed we do not observe a loss of IMC15 (Fig. 3.5D) but instead the protein remains tightly locked with the centrosomes throughout budding. Unlike wild-type, IMC15 no longer enters the buds in the absence of Shld1, at least not at a level detectable by IFA (Fig. 3.5E and F); however, these parasites are viable through several passages and exhibit no obvious phenotype. Since the DD system controls protein levels post-translationally, the tagged protein under the control of its native promoter continues to be expressed at normal levels and if it has a strong targeting signal or high affinity for

a specific cellular structure it is possible it will not be efficiently regulated by the proteasome. This could be the case for DD-controlled IMC15.

3.2.5. Minimal levels of IMC15 sufficient for parasite viability

Since conditional regulation of IMC15 post-translationally is not optimal, we tried an alternative method that employs a tetracycline (tet) repressible promoter to control protein expression at the level of transcription (117, 118). Working with a strain of *Δku80* parasites that also expresses the tetracycline transactivator, TATi*Δku80* (Drs. Lilach Sheiner and Boris Striepen; unpublished), we directly replaced the promoter of IMC15 with seven tet-operator repeats followed by one of two minimal SAG promoters, p*T7S4* (minimal SAG4 promoter) or p*T7S1* (minimal SAG1 promoter) (Fig. 3.3D) (117, 118). With the addition of anhydrous tetracycline (ATc) to either strain IMC15 expression should be reduced to minimal levels.

When different clones of the p*T7S4* promoter replacement strain were exposed to ATc and their viability assessed by plaque assay, a reduction in plaque size was observed for all clones. However, we did not not observe the complete cessation of growth we expected from minimization of an essential gene (Fig. 3.6A). The SAG4 minimal promoter does not completely abolish transcription of the gene; therefore, it is possible that the minimal amount of resultant protein expression is enough to satisfy the needs of the parasite. To further reduce the minimal expression of IMC15, the weaker SAG1 promoter was switched for the SAG4 promoter. Plaque assays were performed with three different clones of the p*T7S1* promoter KO strain. We observe a reduction in plaque

number and size that is more severe than with p*T7S4*, but again growth is not abolished (Fig. 3.6B). When the p*T7S1* controlled parasites (clone H2) are exposed to ATc for up to four days, IMC15 is still visible by IFA with anti-IMC15. These results, combined with the already low native expression level of IMC15 (Fig. 2.4B), and the DDmyc-IMC15 results suggest that extremely low levels of IMC15 are enough for parasite survival.

3.2.6. IMC15 deletions suggest importance of the C-terminus

Despite the lack of a KO background we can begin to determine what regions of IMC15 are necessary for proper protein function. We approached this in the same manner as with the IMC3 and IMC8 deletions discussed in Chapter 2. Each region of IMC15, the N-terminus, alveolin domain, and C-terminus, were expressed individually as N-terminal YFP fusions and then as pairs. In transient transfections all constructs localize like wild-type; some have more cytosplasmic localization than others and some are more faint at the apical and basal ends, but they all follow the wild-type pattern. However, the constructs that contain the C-terminus, except for full-length IMC15, cannot be supported by the parasite long-term. The inability to integrate these constructs into a stable line may suggest an important role for the C-terminus that is interrupted by overexpression.

3.2.7. IMC15 palmitoylation mutants may exert dominant negative effect

Palmitoylation has been proven necessary for the assembly of the apicomplexan glideosome (44, 65, 119) as well as the components of the *Toxoplasma* IMC (14). IMC15 has five cysteines that are strongly predicted to be palmitoylated (Fig. 2.3). Three of these

sites are in the N-terminus and two are in the C-terminus. Since the deletion constructs suggest more complex localization mechanisms for IMC15 than simply the sequence of the alveolin domain, these predicted palmitoylation sites might be important. To examine if any of these cysteines are involved in proper IMC15 localization they were each mutated individually (sequential predictions were treated as one site and mutated together): Cys 4 to Ala (C4A), Cys 92 and 93 to Ala (C92A/C93A), and Cys 673 and 674 to Ala (C673A/C674A); followed by mutated in pairs; and then finally all mutated at once. All mutants were then cloned as N-terminal YFP-fusions.

As with the deletion constructs, all of these mutants localize like wild-type in transient transfection in wild-type parasites. However, three of the constructs (C673A/C674A, C4A.C92A/C93A, and C4A.C673A/C674A) exhibit extremely low transfection efficiencies (< 10%) and the constructs did not produce stable lines despite multiple attempts (Fig. 3.7). Inclusion of the C-terminal potential palmitoylation sites in two of these constructs supports the possible importance of the C-terminus to proper IMC15 function. Most importantly these constructs could be exerting a dominant negative effect.

3.3. Discussion

IMC15, the earliest cytoskeletal component of daughter budding in *Toxoplasma*, is well conserved across apicomplexans (Table 3.1 and Fig. 3.1 and 3.2). This protein is insoluble in 1% TritonX-100 and 1% DOC verifying that it is part of the non-extractable cytoskeleton and more specifically the IMC protein meshwork (Fig. 3.4). IMC15 has thus

far proven resistant to direct KO. However, the locus is accessible and removable by the described method as it can be knocked out when IMC15 is ectopically expressed, as in the DD-IMC15 controlled KD. This suggests IMC15 is essential. The conditional KD using the DD system indicates that IMC15 may not be necessary in the early bud and its primary role could occur during the period of colocalization with the centrosomes (Fig. 3.5). Furthermore the results of a conditional KD with the tet repressible promoter indicate that the parasite requires very little IMC15 to remain viable (Fig. 3.6). Deletion constructs of and mutations at predicted palmitoylation sites in IMC15 suggest the C-terminus may be important for proper IMC15 function and overexpression. The suspected dominant negative effect of some of these potential palmitoylation and deletion mutants may be sufficient to further characterize IMC15 behavior.

The conservation of IMC15 across apicomplexans is intriguing since division modes vary throughout the Apicomplexa family as discussed in Section 2.3. MORN1 is another essential protein involved in the development of the *Toxoplasma* cytoskeleton that is conserved throughout apicomplexan species and between endodyogeny, endopolygeny, and schizogony (95). The primary role of MORN1 appears to occur later in the division process (10, 11), whereas we hypothesize the primary role of IMC15 occurs earlier, perhaps linked with the newly duplicated centrosomes. Fortunately, centrosomes in *Sarcocystis* and centriolar plaques in *Plasmodium*, though not as well studied, appear to fulfill similar important niches in endopolygeny (120) and schizogony (121) as in endodyogeny (24, 25, 29).

When IMC15 is overexpressed as a N-terminal YFP fusion we observe clear localization of IMC15 to the mature, cortical IMC (Fig. 2.13); however, when native IMC15 is visualized with antiserum the cortical localization cannot be detected (Fig. 2.13I). Detergent extractions on fully mature parasites show IMC15 to be insoluble under the conditions used to isolate the cytoskeleton and, therefore, it is part of the cortical IMC or the basal complex (28) (Fig. 3.4). The ability of the IMC15 antibody to recognize the brightest accumulations of IMC15 in the centrosomes and the early buds and the inability of the IMC15 antibody to recognize the cortical IMC15 suggests a high detection limit for the antibody. The only intense IMC15 structure seen with the YFP-fusions and not with the antibody is the small ring at the apical end (Fig. 2.13G and H). Since the IMC15 antibody was raised against the N-terminal region of the protein it is possible that this region is not accessible to the antibody when in that structure. The detergent extractions did not suggest that IMC15 undergoes a cleavage event similar to IMC1 (67), but further experiments would be necessary to verify the absence of such an event.

The inability to KO this potentially essential gene led us to develop two conditional KDs using the DD system and the tet repressible promoter. Though neither system sufficiently downregulated IMC15 to produce a useful KO-like background (Fig. 3.5 and 3.6) we were able to extract information from these conditional strains. First, IMC15 has a strong affinity for the centrosomes. Whether this affinity is the result of a targeting sequence, a post-translational modification, and/or tight protein-protein interactions remains to be determined. Since IMC15 does not transition from the centrosomes to the early buds, at least not in levels detectable with anti-IMC15, and the

parasites are viable for several passages in the DD conditional KD without Shld1, the primary function of IMC15 could be at the earliest stages of mitosis with the duplicated centrosomes (24, 25, 29). Finally, a minimal level of IMC15 transcription is sufficient for parasite survival so any other KD system will not provide a satisfactory downregulation of IMC15 for further functional studies. A conditional KO using the Cre-Lox system (122-124) or a dominant negative construct are alternative options.

Mutation of potential palmitoylation sites in three combinations, C673A/C674A, C4A.C673A/C674A, and C4A.C92A/C93A, may offer the dominant negative effect necessary to further characterize IMC15. The low transfection efficiencies of these mutants and the inability to form stable lines with them suggests they are toxic. C673 and C674 are in the C-terminus of IMC15 and their mutation alone disrupts the parasite suggesting an important role for the C-terminus in IMC15 behavior. However, the mutation of these C-terminal sites along with C92 and C93 of the N-terminus and the mutation of all of the potential palmitoylation sites at once do not exhibit any obvious deleterious effects. It is possible that the mutation of all of the predicted palmitoylation sites renders the protein in an inert-like state where it can potentially dimerize with the native IMC15 and be carried along to the proper sub-compartments of the parasite. The possibility that the sites must be palmitoylated in a specific sequence should be considered as an explanation for the other results. Furthermore, a complex system of palmitoyl acyltransferases (PATs) has been proposed in *Toxoplasma* that could affect these mutants (14). The palimitoylation of IMC15 remains to be verified to support that

the observed effects result from a lack of palmitoylation and not from misfolding due to the substitution of an Ala for a Cys.

The importance of the C-terminus suggested by the potential palmitoylation mutants is supported by the results of the deletion constructs. Only those constructs that contain the C-terminus, IMC15C, IMC15AC, and IMC15NC, did not become stable when overexpressed as YFP-fusions. Furthermore, unlike the results for IMC3 and IMC8 (Section 2.2.8), the alveolin domain was not shown to be necessary or sufficient for IMC15 localization. IMC3 and IMC8 were originally selected for the deletion and chimera project because they lack predicted palmitoylation sites; therefore it is quite reasonable that palmitoylation affects the behavior of IMC15.

In addition to palmitoylation, phosphorylation could contribute significantly to the behavior of IMC15. Phosphoylation plays a major role in the regulation of classical intermediate filaments (125) and in the development of the *Toxoplasma* cytoskeleton-associated glideosome (126). When the apicomplexan homologs of IMC15 are aligned there are five conserved sites in the alveolin domain: Thr 419, Ser 545, Ser 547, Thr 352, and Ser 386. In the N-terminus there is a potential NIMA kinase site, Ser 254, that is of interest but is not conserved (127) (Fig.3.1 and Fig. 3.2A). Mutations of these sites could produce dominant-negative effects as well.

It was proposed in Section 2.3 that the basal IMCs appear to fulfill a similar role to the septins of other eukaryotic organisms during cytokinesis. More generally septins oligermerize to create filaments that organize into membrane-associated cytoskeletal scaffolds and arrange to demarcate subcellular compartments (94). This description

suggests that the entire IMC family is septin-like. Before cytokinesis a conserved protein, anillin, nucleates the formation of septins at the contractile ring in the same way we hypothesize IMC15 nucleates the formation of the IMC cytoskeleton (128). Anillin does not remain in the cytoskeleton but relocates to the nucleus during interphase in most organisms. It does not form filaments itself and is actin dependent (128). As with the basal IMCs and septins, IMC15 is not a traditional anillin protein and no anillin homolog is present in the *Toxoplasma* genome. Even though IMC15 and the IMC family are not canonical anillin and septins, they are possibly fulfilling the analogous functions of anillin and septins in the non-actin based cytoskeleton of *Toxoplasma.*

IMC15 is the earliest component of the *Toxoplasma* cytoskeleton to indicate the initiation of daughter bud formation. The unique mechanisms of daughter bud formation are poorly understood and continued functional analysis of IMC15 is providing novel insight into the early stages of this process.

Table 3.1. IMC15 BLASTp searches identify several apicomlexan homologs

EuPathDB results for BLASTp searches with the IMC15 sequence are shown with a cut-off e-value of 10^{-20}. The next highest score is another *Toxoplasma* IMC protein. The cut-off e-value for the NCBI searches is 10^{-32} for the same reason. Those proteins identified in both searches and with an EuPathDB score less than 10^{-40} were reciprocally BLAST searched in ToxoDB and the e-value for IMC15 in their results recorded. IMC15 was the top hit for all proteins. IMC15 matches to itself with an e-value of greater than 0 in the EuPathDB and ToxoDB searches because the databases have not been updated with the correct published annotation.

Table 3.1 IMC15 BLASTp searches identify several apicomlexan homologs

ID	Organism	EuPathDB blastp	NCBI blastp	ToxoDB blastp	Annotation
TGGT1_000660	*Toxoplasma gondii*	-197	0	-198	IMC15
NCLIV_007240	*Neospora caninum*	-130	-162	-133	hypothetical
BBOV_I004150	*Babesia bovis*	-47	-42	-29	membrane skeletal protein
TA14770	*Theileria annulata*	-43	-33	-29	hypothetical
TP02_0724	*Theileria parva*	-43	-32	-21	hypothetical
PVX_083475	*Plasmodium vivax*	-42	-48	-29	hypothetical
PKH_120230	*Plasmodium knowlesi*	-41	-52	-30	conserved, unknown function
MAL13P1.260	*Plasmodium falciparum*	-41	-49	-21	alveolin
PCHAS_136900	*Plasmodium chabaudi*	-41	-43	-20	conserved, unknown function
PY03838	*Plasmodium yoelii*	-40	-52	-23	Erythrocyte membrane protein
PBANKA_136440	*Plasmodium berghei*	-40		-23	conserved, unknown function
NCLIV_031780	*Neospora caninum*	-26			hypothetical
ETH_00024620	*Eimeria tenella*	-26			erythrocyte membrane protein PFEMP3
PY00506	*Plasmodium yoelii*	-21			hypothetical
PKH_083620	*Plasmodium knowlesi*	-20			membrane skeletal protein
PFC0180c	*Plasmodium falciparum*	-20			Inner membrane complex protein 1a
PCHAS_040350	*Plasmodium chabaudi*	-20			Inner membrane complex protein 1a
PBANKA_040260	*Plasmodium berghei*	-20			Inner membrane complex protein 1a
PVX_119325	*Plasmodium vivax*	-20			membrane skeletal protein

Figure 3.1. The termini of IMC15 homologs are not conserved

The alignment of the ten strongest BLASTp results shows very little homology in the N- and C-termini to IMC15. The conserved alveolin domain is shaded green. Amino acid colors that indicate a consensus in a column as well as chemical properties are: green (>50%; hydroxyl/amine/basic/glutamine), blue (>60%; hydrophobic), cyan (>50%; histidine/tyrosine), magenta (>50%; acidic), and red (>60%; lysine/arginine). Other colors are orange (glycine), yellow (proline), and pink (cysteine). Red arrows indicate predicted IMC15 palmitoylation sites (C4, C92, C93, C673, and C674). Blue arrows indicated potential phosphorylation sites that are conserved between IMC15 and *Plasmodium* (S254, T419, S545, and S547) or between IMC15, *Neospora*, *Babesia*, and *Theileria* (T352 and S386).

Figure 3.1. The termini of IMC15 homologs are not conserved

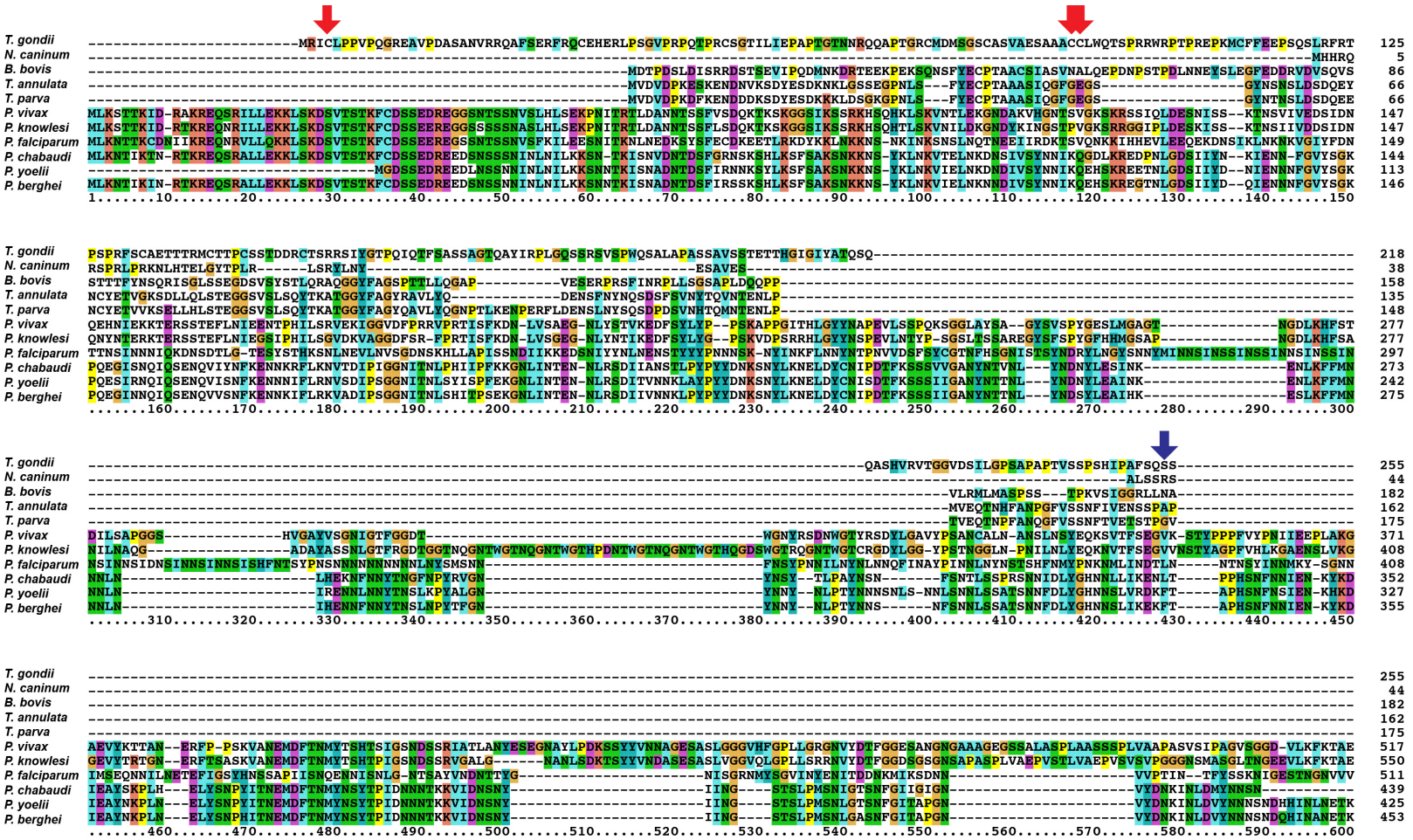

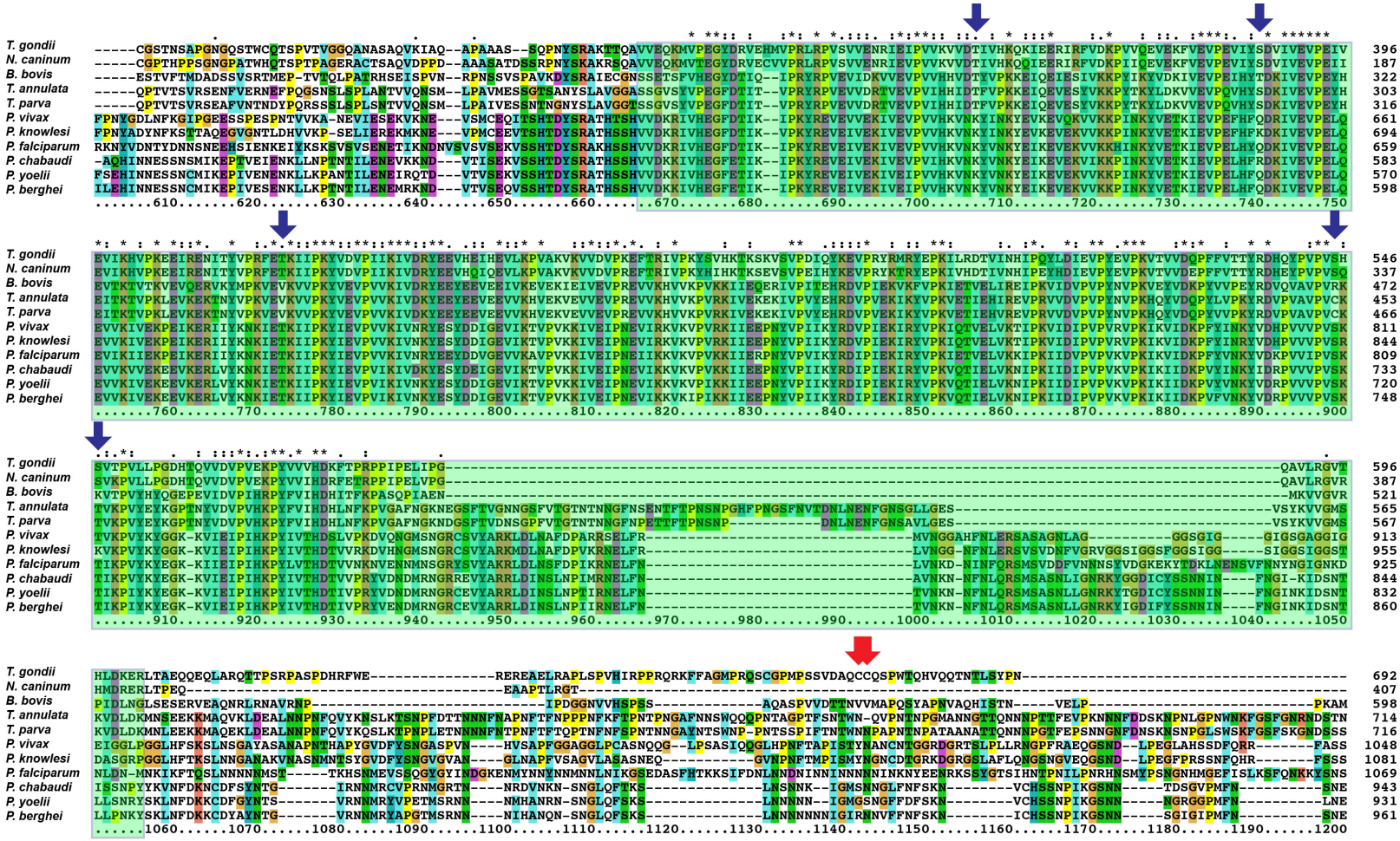
T. gondii
N. caninum
B. bovis
T. annulata
T. parva
P. vivax
P. knowlesi
P. falciparum
P. chabaudi
P. yoelii
P. berghei

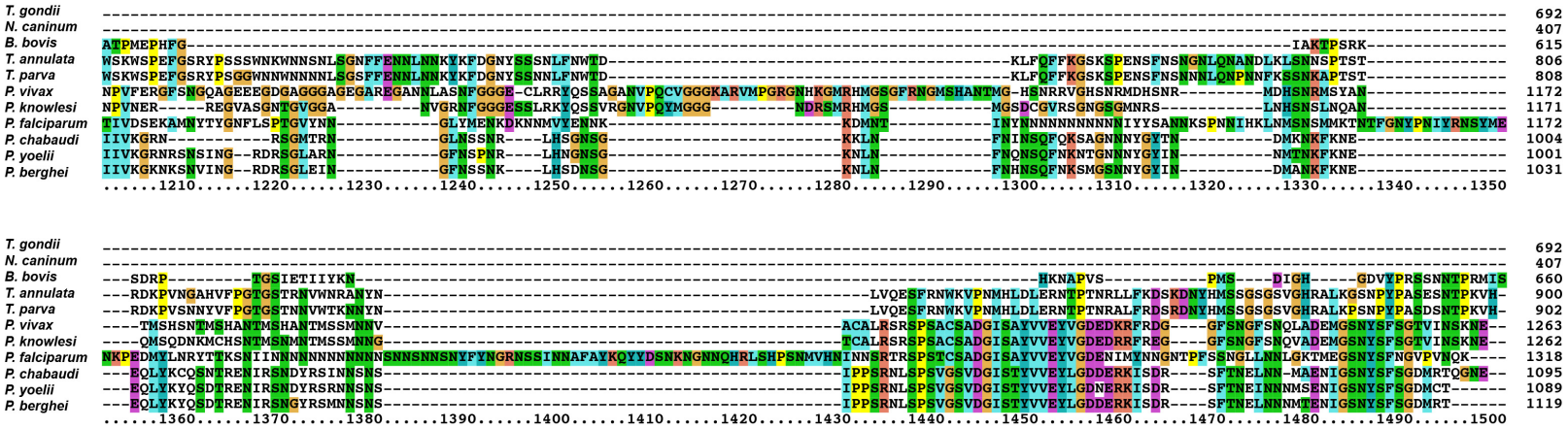
T. gondii
N. caninum
B. bovis
T. annulata
T. parva
P. vivax
P. knowlesi
P. falciparum
P. chabaudi
P. yoelii
P. berghei
692
407
615
806
808
1172
1171
1172
1004
1001
1031
660
900
902
1263
1262
1318
1095
1089
1119
1210
1220
1230
1240
1250
1260
1270
1280
1290
1300
1310
1320
1330
1340
1350
1360
1370
1380
1390
1400
1410
1420
1430
1440
1450
1460
1470
1480
1490
1500

Figure 3.2. The conserved IMC15 alveolin domain contains potential phosphorylation sites

(A) The IMC15 alveolin domain aligned with the top 10 strongest BLASTp hits (enlargement of the green shaded region in Fig. 3.1). Colors the same as above. Blue arrows indicate conserved potential phosphorylation sites between IMC15 and *Plasmodium* (S254, T419, S545, and S547) or between IMC15, *Neospora*, *Babesia*, and *Theileria* (T352 and S386). (C) Phylogenic tree of IMC15 conservation across apicomplexans. Phylogeny based on full-length sequences with 1000x bootstrapping. Values shown at nodes.

Figure 3.2. The conserved IMC15 alveolin domain contains potential phosphorylation sites

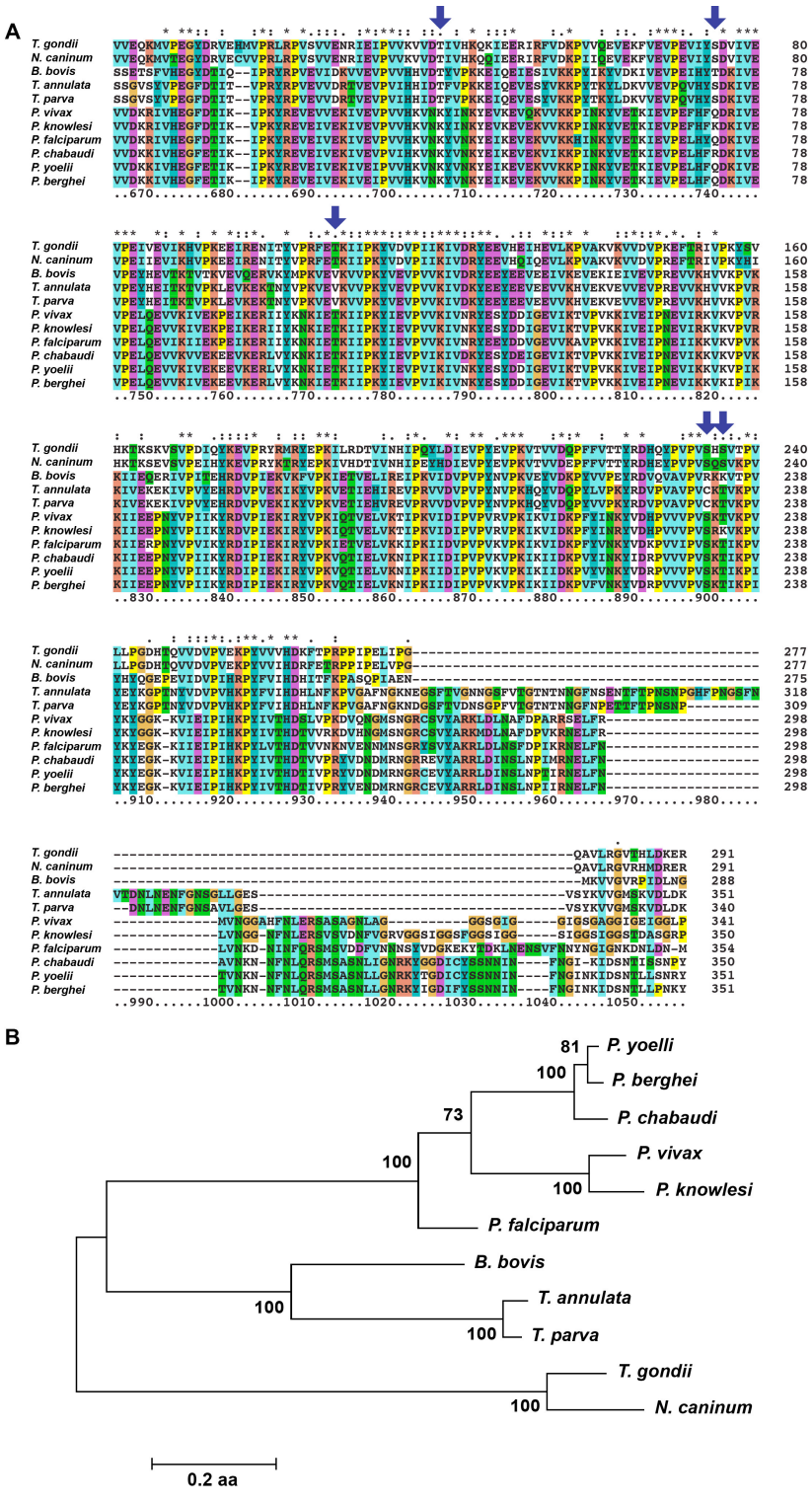

Figure 3.3. Homologous recombination strategies for IMC15

(A) Single HR strategy for endogenous cloning of IMC15-myc$_3$. 3'HR is sequence homologous to the 3' end of IMC15 (before and not including the stop codon) and 3'dhfr is the dhfr-ts 3'UTR. A single black hash mark indicates linearization of the plasmid for transfection. Single crossover results in tagging of the 3' end of IMC15. (B) Double HR strategy for direct IMC15 KO. 5'HR is sequence homologous to a genomic region upstream of the promoter and 3'HR is sequence downstream of the stop codon. Double crossover results in KO of the IMC15 locus and KI of DHFR. (C) Double HR strategy for replacement of the UPRT locus with a DDmyc tagged IMC15 construct. Similar strategy as in (B). Double crossover results in KO of the UPRT locus and KI of the tagged construct. (D) Double HR strategy for promoter replacement. p*T7SX* is seven tet operator repeats followed by a minimal promoter (p*sag1* or p*sag4*). 5'HR is sequence homologous to a genomic region upstream of the promoter and the 3'HR is from the start codon into IMC15. Double crossover results in KO of the IMC15 promoter and KI of DHFR-TS and the tet-regulated promoter.

Figure 3.3. Homologous recombination strategies for IMC15

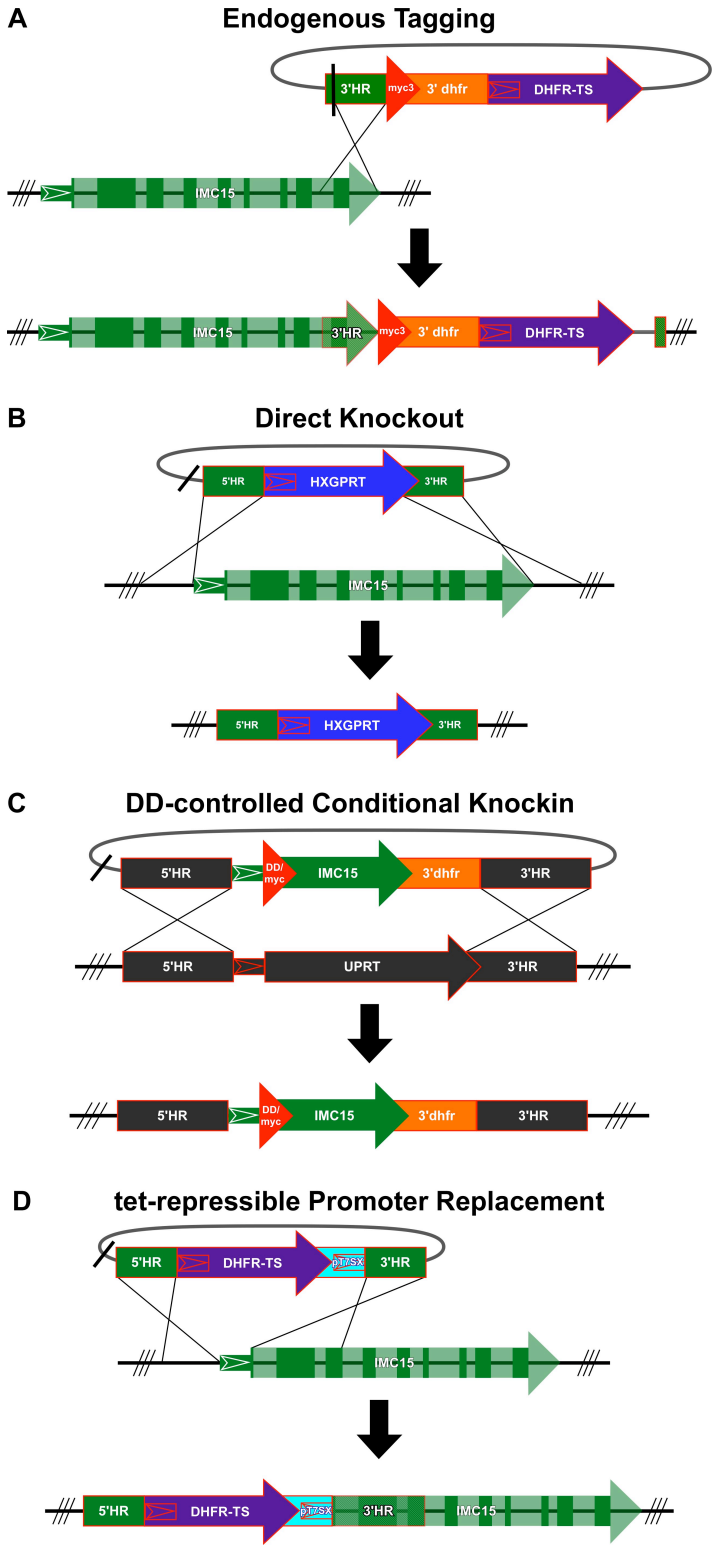

Figure 3.4. IMC15 is part of the IMC meshwork

Western blots of detergent extractions using resuspension buffer (RB), 1% Triton X-100 (TX-100), 1% deoxycholic acid (DOC), and 1% sodium dodecyl sulfate (SDS). Lanes are labeled “P” for pellet fraction and “S” for soluble fraction. The anti-myc blot was striped and re-probed with anti-IMC1 and anti-GRA1.

Figure 3.4. IMC15 is part of the IMC meshwork

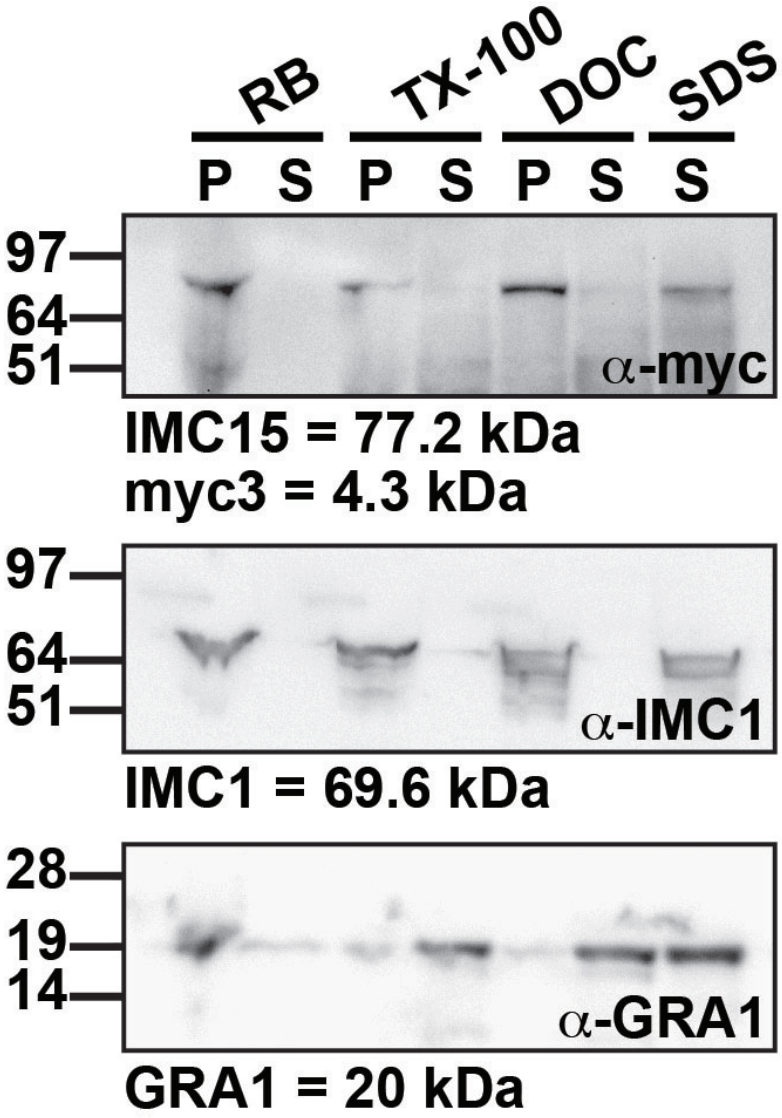

Figure 3.5. IMC15 remains in the centrosomes when regulated under the DD system

(A-C) Conditional KD parasites expressing p*imc15* driven DDmyc-IMC15 stabilized with Shld1 and stained with anti-IMC15 (red) and anti-hCentrin (green) (A-B) or anti-IMC3 (green) (C). IMC15 colocalizes with the centrosomes (A) and then expands into the early (B) and mid-buds (C). (D-F) The same parasite strain stained with the same antibodies without Shld1 shows colocalization at the centrosomes with TgCentrin1 (D), but then DDmyc-IMC15 fails to expand into the early buds (E) or the mid-buds (F) and instead remains in the centrosomes.

Figure 3.5. IMC15 remains in the centrosomes when regulated under the DD system

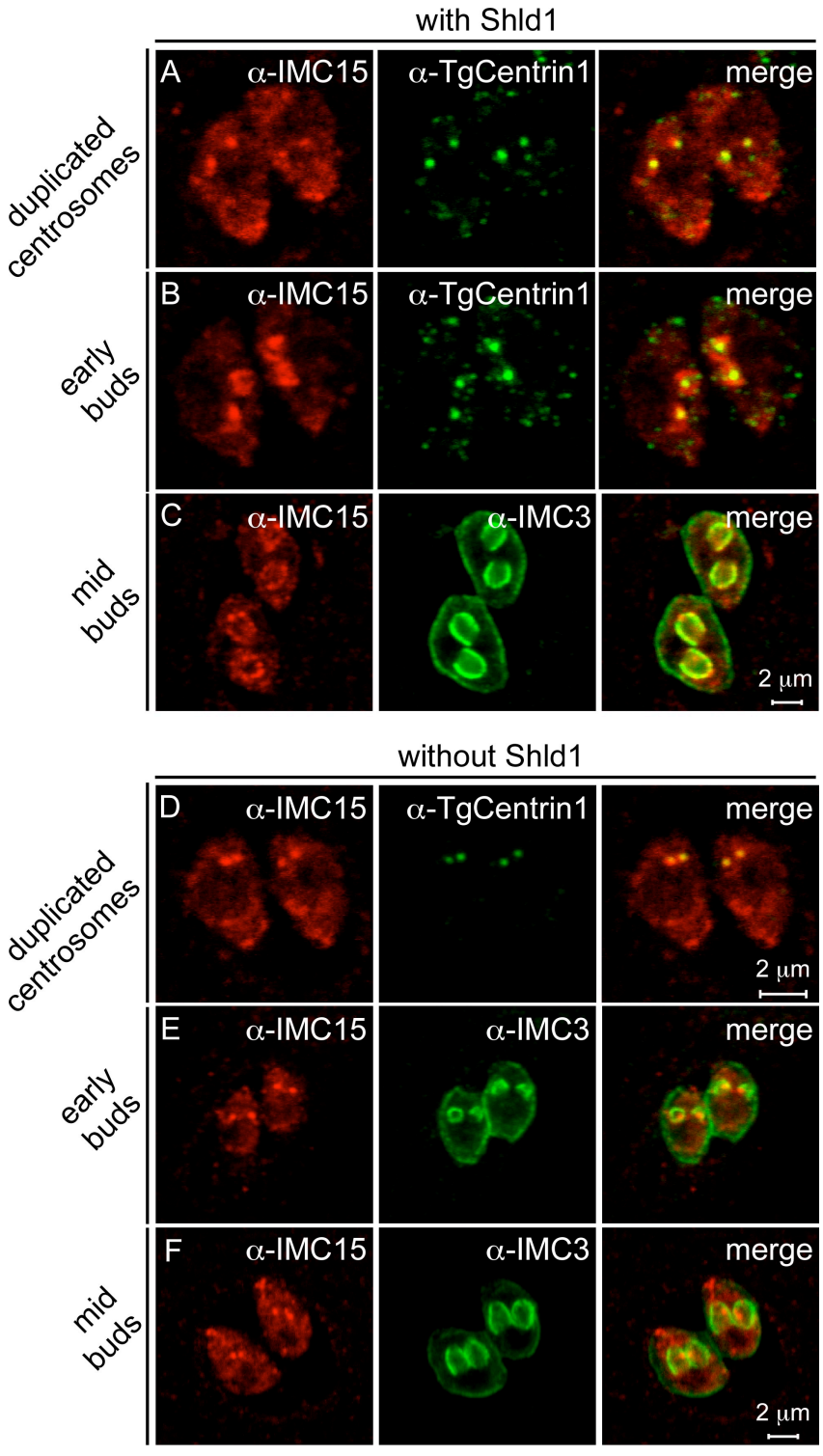

Figure 3.6. Parasites survive under tet mediated repression of IMC15 transcription

(A) Plaque assays of two different representative clones, numbers 23 and 27, of IMC15 driven by p*T7S4*. The left panel of each pair was cultured for seven days without ATc and the right panel of each pair was cultured for seven days with ATc. (B) Graph comparing the average plaque size of TATi *Δku80* parasites, MORN1 KO parasites that do not form plaques with ATc (10), and three different clones of IMC15 driven by p*T7S1* cultured for seven days without ATc (blue) and with ATc (red).

Figure 3.6. Parasites survive under tet mediated repression of IMC15 transcription

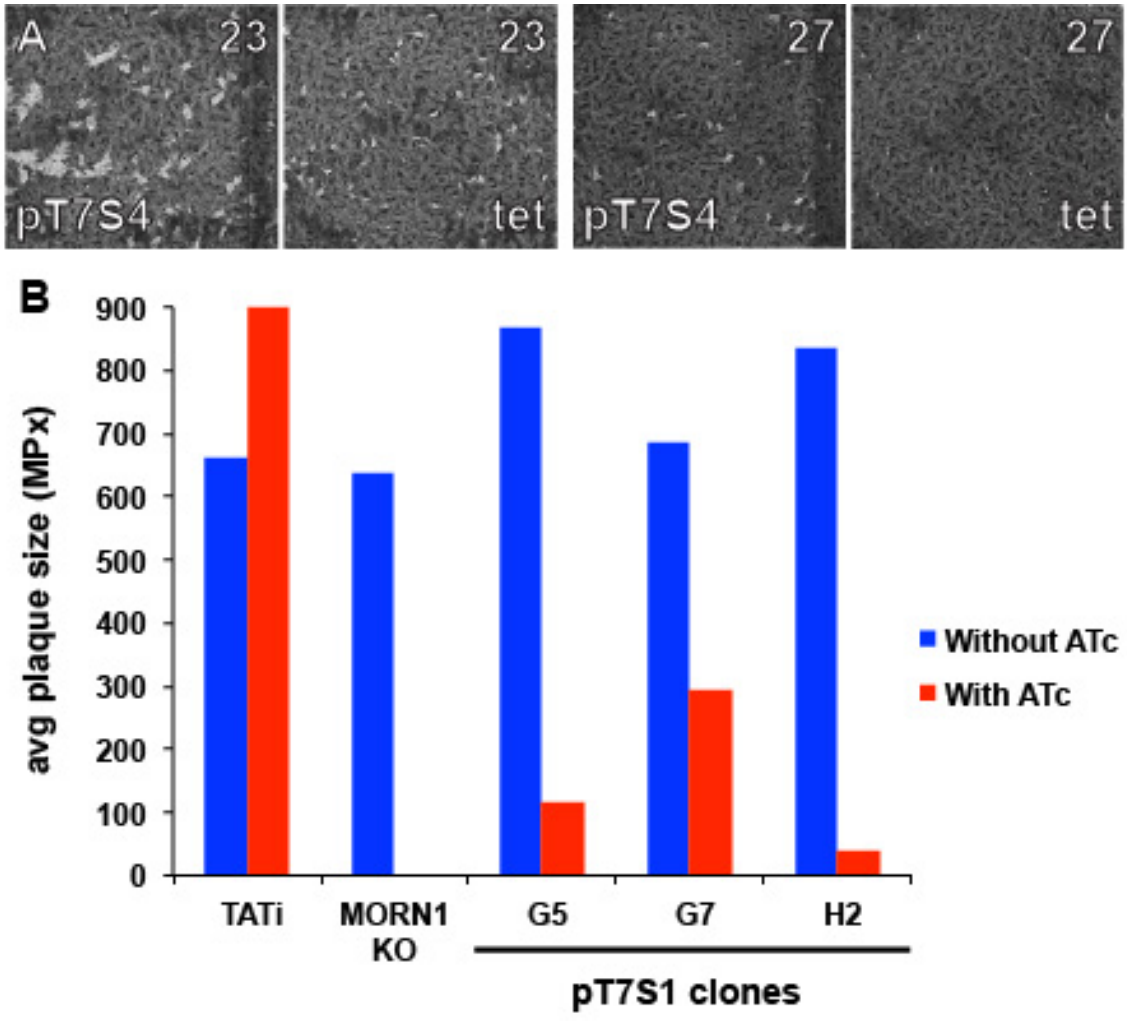

Figure 3.7. IMC15 mutants suggest complex palmitoylation scheme

On the left are the palmitoylation mutations followed by if the N-terminal YFP fusion of each resultant mutant produces a stable parasite line after transfection. On the right are diagrams of the mutants. The N- and C-termini are in green flanking the yellow alveolin domains. Predicted palmitoylation sites are marked with a blue asterisk and a red "X" indicates a mutated site.

Figure 3.7. IMC15 mutants suggest complex palmitoylation scheme

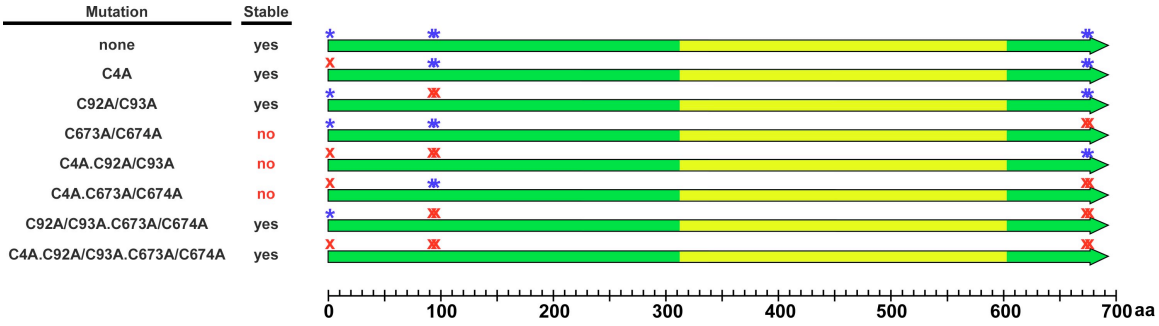

Chapter 4. Coordinated dynamics of budding in *Toxoplasma gondii*

4.1. Introduction

The visualization of cytoskeletal components in *Toxoplasma* by fluorescence microscopy has revealed daughter budding to be a highly coordinated phenomenon. The process of budding can be generalized by observation into four stages of cytoskeletal dynamics: initiation, early bud assembly, mid-budding, and late stage budding. During the initiation of budding and early bud assembly the foundations are laid for each layer of the cytoskeleton and the conoid. This seemingly chaotic stage is followed by elongation of the cytoskeleton to the midpoint of budding, at which time the components of the basal complex join MORN1 on the leading edge of the developing parasites. After the midpoint, the daughters begin to contract and move into the late stages of budding. The late stages of budding are indicated by the assembly of the glideosome and the incorporation of the mother's plasma membrane onto the daughters. The timing of incorporation of cytoskeletal elements into the daughter buds has been determined individually based on comparisons to developmental markers such as MORN1 for early bud formation (60, 61), GAP45 for late stage budding (44), and IMC1 for everything in between (19, 67). This method allows for subjectivity in the timing determinations as different authors using different markers have different definitions of budding stages. This is especially true for early budding when a large number of proteins are converging on a small subcellular area in a short amount of time (about 30 minutes) (25).

In this chapter a comprehensive timeline for cytoskeletal development is described based on co-IFAs with established cytoskeletal components. This timeline provides a clear framework for evaluating the timing of incorporation of future

cytoskeletal factors. Furthermore, these data used in conjunction with KO phenotypes will provide insight into potential protein relationships and mechanisms during the budding process.

4.2. Results

4.2.1. Initiation of budding

After division of the Golgi, at a DNA content of about 1.2N, the centrosome duplicates (19, 24, 25). The activity of the centrosomes can be monitored using the three identified centrin proteins in *Toxoplasma*, TgCentrin1, 2, and 3 (27, 72). At the point of centrosome duplication IMC15 and Rab11B colocalize apical to the centrosomes (Fig. 4.1A and B and Fig. 2.13D, E, F, and I). IMC15 is the earliest member of the IMC meshwork to appear in the initial bud. Rab11B is a small GTPase that is believed to traffic the vesicles of the alveoli to the budding daughters (13). It is reasonable that the two structures of the IMC, the protein meshwork and the membranous alveoli, would develop in tandem. In addition to Rab11B, the actin-like protein 1 (ALP1) may assist in the development of the IMC membranes. Previous work showed that ALP1 appears at the bud before other members of the IMC family, such as IMC1, but the exact timing in relation to Rab11B and IMC15 remains to be determined (129). MORN1 enters the daughter buds after Rab11B and IMC15 (Fig. 4.1C and Fig. 2.13F).

The MT structures of the cytoskeleton begin to form at this initial budding stage as well. The subpellicular MT and the unusual α-tubulin-only MT of the conoid both begin to assemble with the duplication of the centrosome (13, 27). The MT binding

protein that associates with the two intraconoid MT, TgICMAP1, appears with the two centrosomes as well (62); however, its exact timing has yet to be determined.

4.2.2. Early budding

Following MORN1, the next components to enter the new buds are the IMC-associated ISP proteins. ISP3 enters first, appearing after the spindle pole has divided and the MORN1 rings have begun forming (Fig. 4.2A and B). ISP1 and ISP2 closely follow ISP3 (Fig. 4.2C-F). It is difficult to determine if ISP1 precedes ISP2 slightly or if they enter the bud concurrently (Fig. 4.3). About 30 minutes after centrosome duplication, at a DNA content of about 1.8N, IMC3 and IMC1 follow the ISP proteins into the daughters (19, 25). Often there are a faint accumulations of IMC3 near early ISP1, but IMC3 does not begin to form recognizable buds until the intensity of the ISP1 signal increases (Fig. 4.4). It is currently assumed that the other IMC proteins that localize cortically in budding parasites, IMC4, 6, and 10, enter the daughters with the same timing as IMC1 and 3, but this has not been rigorously tested. The basal complex IMCs, IMC5, 8, 9, and 13, join the early bud as well, but it is unclear if they do so concurrently with IMC3 or slightly later (Fig. 2.11 and Fig. 2.12). The components of the glideosome begin to appear during this early stage of budding as well. GAP50 and GAP40 are the earliest glideosome elements (44, 65) but their time of arrival to the daughters compared to the ISP or IMC proteins has yet to be determined.

With all of the earliest components in place, the forming daughter cytoskeletons begin to elongate. A ring of MORN1 marks the growing posterior end of the cytoskeleton

and the early conoid indicates the apical end (27, 61). Once the advancing cytoskeleton reaches the edge of the forming apical cap, the annuli of TgCentrin2 form (27, 60) and as the cytoskeleton continues past the cap region toward the budding midpoint, ISP1 remains behind (14) (Fig. 1.3).

Based on fluorescence recovery after photobleaching (FRAP) experiments IMC1 is generated *de novo* in the growing daughters and not recycled from the mother parasite (19). On the other hand, FRAP experiments with IMC4 suggest some of the protein may be salvaged from the mother (27). These results support the idea that multiple and complex mechanisms operate even within the same family of proteins to cultivate the daughter buds.

4.2.3. Mid- to late budding

About 1.5 hr after centrosome duplication, TgCAM1, TgCAM2, and TgDLC localize to the MT region of the conoid (25, 27). This corresponds to about the midpoint of budding based on comparison of TgCAM1 and IMC3 (Fig. 4.5B). The midpoint of budding coincides with redistribution of the posterior IMC proteins, IMC5, 8, 9, and 13, from the periphery of the daughter buds to the growing ends where MORN1 is located (96) (Fig. 2.12). This transition marks the widest part of the future mature daughters. Past this point the buds begin to contract as they elongate. Soon after they begin to contract heat shock protein 20 (Hsp20), whose function is unknown, localizes in a discontinuous striped pattern to the outer membrane of the IMC (130). In addition, PhIL1 localizes to the apical cap in these later stages of daughter development (63).

During basal complex contraction, karyokinesis is completed and RNG1 appears at the apical polar ring (15). With the completion of contraction, the mature basal complex is formed. The mother cytoskeleton then begins to break down and the plasma membrane of the mother is incorporated into the pellicles of the new daughters in a Rab11A-dependent process (12, 17). The glideosome assembles between the forming plasma membrane and the IMC as GAP45 is recruited to GAP50 bringing along MLC1 and MyoA (44, 65). Overexpression of a dominant negative Rab11A construct reveals that this transport protein is required for proper completion of the glideosome as well (12).

4.2.4. Mature parasites in G1

The emergent daughter parasites are now fully mature and the mother parasite has been left behind as a residual body. For unknown reasons that are the subject of much speculation in Chapter 2, three more IMC proteins are incorporated into the cytoskeleton during G1: IMC7 and 12 in the first third of G1 and IMC14 at about the midway point of G1 (96) (Fig. 2.9 and 2.10). Throughout G1 IMC1 is continually added to the mature cytoskeleton but at a slower rate than during budding (19). It is unknown if there is active turnover and replacement of the other cytoskeletal proteins after budding is complete. It is reasonable to speculate that this is true for proteins like IMC1 and IMC4 that maintain their level of intensity in IFA between daughter development and G1 phase (Fig. 2.4-6). Proteins like IMC3, 6, and 10 that exhibit significantly weakened signals during G1 are

probably less dynamic during G1, being degraded but not being replaced (96) (Fig. 2.5 and 2.8).

4.3. Discussion

Internal daughter budding in *Toxoplasma* has four main stages: initiation, early bud formation, mid-budding, and late stage budding. Based on comparative IFAs performed for this project, I was able to develop a timeline of early through mid-budding activity. Two of the first indicators of budding are IMC15 and Rab11B representing the beginnings of the IMC meshwork and the IMC alveoli, respectively (13) (Fig. 4.1A and B and Fig. 4.6 panel 1). MORN1, a basal complex component, organizes into small rings at the nascent buds immediately following the organization of these earliest cytoskeletal components (27, 60, 61) (Fig. 4.1C, Fig. 4.2B, and Fig. 4.6 panel 2). MORN1 is followed by ISP3, ISP1, and ISP2 (Fig. 4.2, Fig. 4.3, and Fig. 4.6 panels 3-5). The cortical IMC proteins of the buds enter the daughters next either concurrent with or immediately preceding the basal IMCs (Fig. 4.4 and Fig. 4.6 panel 6). At about the midpoint of budding the TgCAM1 of the conoid is added to the daughters (27, 63)(Fig. 4.5 and Fig. 4.6 panel 7). At the midpoint the basal IMC proteins redistribute to the leading edge of the bud to join MORN1 (Fig. 4.6 panel 7).

It is important to note, especially with the early bud formation findings, that the observed dynamics reported here are all based on comparative IFAs. With the earliest stages the differences in timing are probably only minutes long since this stage lasts around 30 minutes. With such short temporal differences, variations in expression levels

become more important and could amplify differences in detection limits, skewing the results. A protein that has a low expression level may be localizing to the bud as early as IMC15 but its detection may be delayed. Furthermore, some of the constructs presented here are driven by overexpression promoters that could alter their expression timing. Those proteins visualized with epitope or fluorescence tags could have delayed entrance to their proper sub-compartment contributable to hindrance from the tag. Moreover, they may experience altered residence times due to the tag. Despite these issues all of the reported results coincide with currently available literature and the resulting timeline fulfills the goal of developing a framework for defining the specific steps of daughter budding.

The earliest stages of daughter budding are highly coordinated with the addition of proteins clearly staggered throughout a short period of time. These differences in timing suggest that complex mechanisms and relationships are involved in daughter bud initiation. The addition of PhIL1, several conoid components, and RNG1 to specific compartments of the daughters during the middle to late stages of budding shows that the daughters are not simply built from the top down, but instead it is in an iterative process that must involve several coordinated signals. Furthermore RNG1, which forms in the latest stages of budding, will continue forming rings even if bud formation and nuclear division is blocked with oryzalin (15). This presents the possibility of budding controls that are not associated with bud formation or a lack of checkpoints once mitosis is initiated. In addition, the trigger for relocalization of the posterior IMCs at the midway point of budding remains unknown.

Though the comprehensive timeline of daughter bud organization and development presented here does not provide mechanistic information, it does clearly define the steps of bud development. These definitions will eliminate much of the subjectivity currently involved in classifying components of the cytoskeleton as early, middle, and late elements and allow for more direct comparisons of timing amongst proteins. This model of developmental dynamics can be used in conjunction with future cytoskeletal KOs to identify and further define relationships and mechanisms involved in internal daughter budding.

Figure 4.1. IMC15 and Rab11B precede MORN1 into the initial daughter bud

(A-B) Parasites expressing YFP-IMC15 (green) and DDmyc-Rab11B (red) in the presence of Shld1 colocalize at the centrosomes (A) and then expand into the forming daughter buds (B). (C) DDmycRab11B (red) co-stained with anti-MORN1 (green). Arrow indicates an unduplicated spindle pole. Both constructs are driven by the p*tub* promoter.

Figure 4.1. IMC15 and Rab11B precede MORN1 into the initial daughter bud

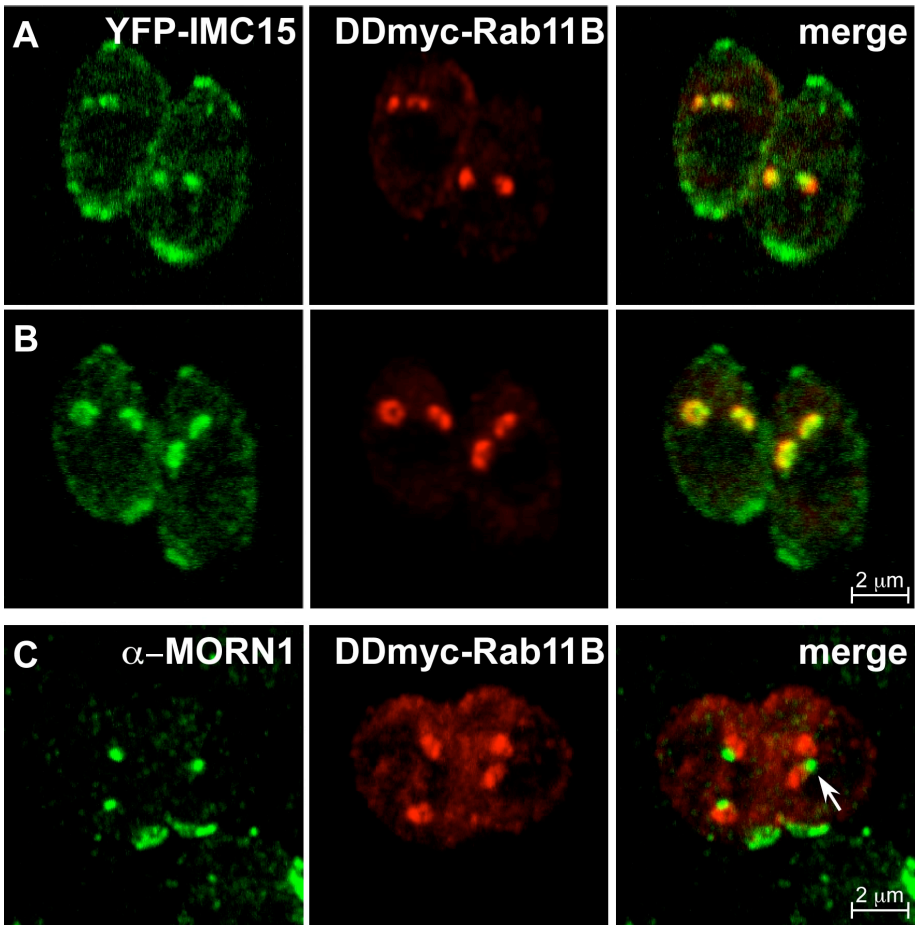

Figure 4.2. ISP3 precedes the related ISP1 and ISP2 into the forming daughter buds

(A-B) Parasites expressing ISP3-YFP (green) are co-stained with anti-MORN1 (red) showing no ISP3 at the recently divided spindle poles (A) and then colocalization of ISP3 with the early MORN1 rings (B). ISP3-YFP parasites present with numerous inclusion bodies; therefore, the arrows indicate the bud-associated ISP3. (C-D) ISP3-YFP parasites (green) co-stained with anti-ISP1 show clear rings of ISP3 without ISP1 (C) and then slightly later stage parasites with early expression of ISP1 (D). (E-F) Parasites expressing ISP3-YFP (green) and ISP2-HA (red) show no ISP2 at an early budding stage (E) and then colocalization with ISP3 (F). ISP3-YFP is driven by the p*tub* promoter and ISP2-HA is under the control of its native promoter.

Figure 4.2. ISP3 precedes the related ISP1 and ISP2 into the forming daughter buds

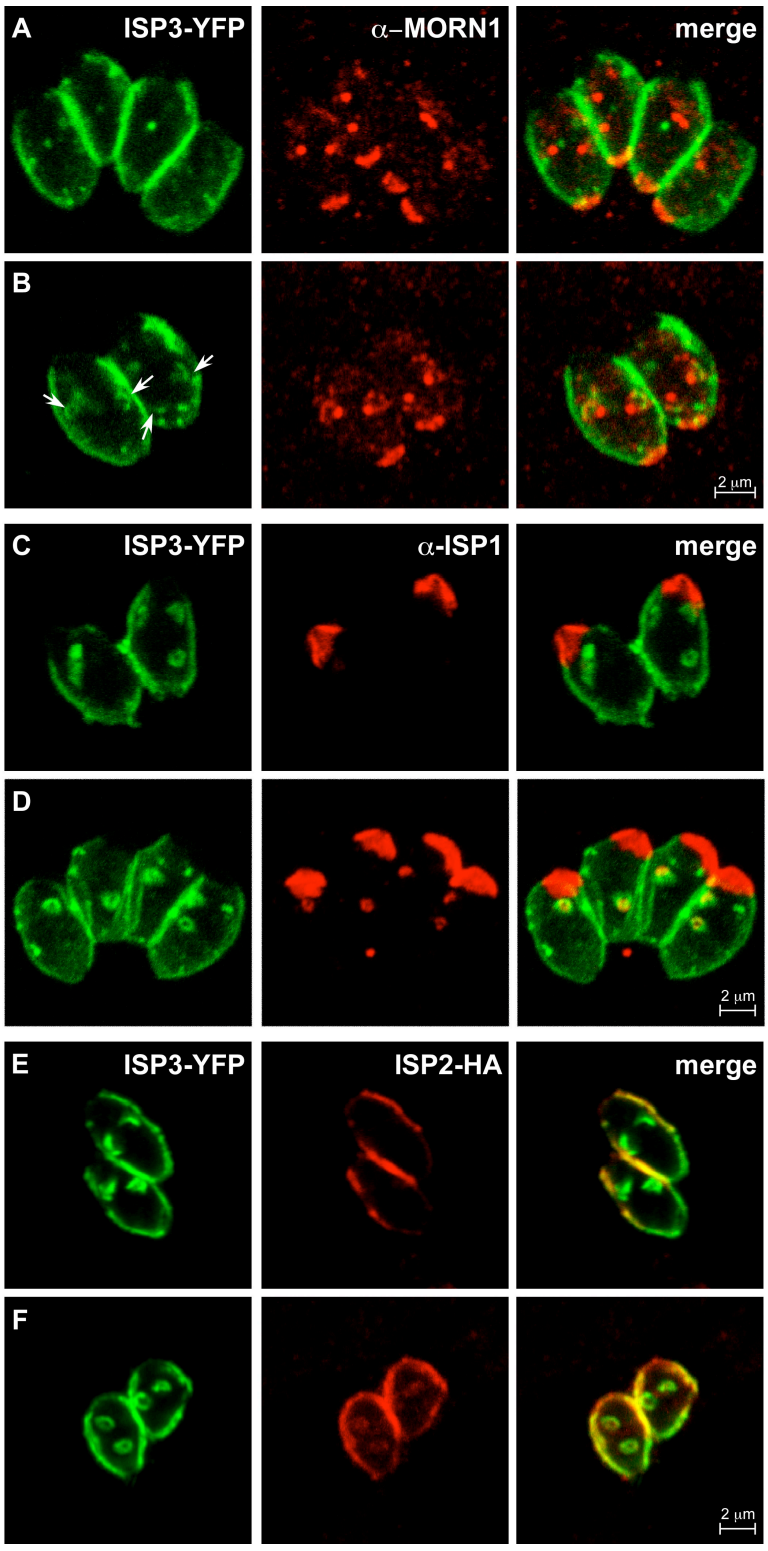

Figure 4.3. ISP1 and ISP2 may associate with the early bud concurrently

Parasites expressing ISP2-HA (red) are co-stained with anti-ISP1 (green). Arrows indicate faint ISP2 buds that colocalize with the more intense ISP1. ISP2-HA is under the control of its native promoter.

Figure 4.3. ISP1 and ISP2 may associate with the early bud concurrently

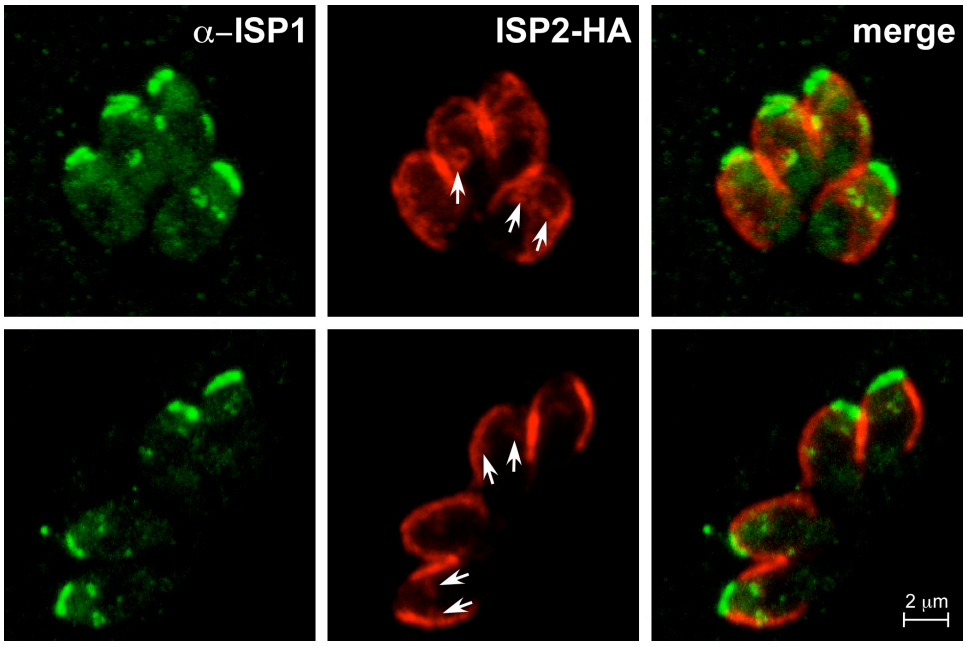

Figure 4.4. ISP1 associates with the daughter buds slightly before IMC3

(A-B) Wild-type parasites co-stained with ISP1 and IMC3. Arrows in (A) indicate amorphous accumulations of IMC3 near the buds as indicated by ISP1. The IMC3 does not fully associate with the buds until after ISP1, but both proteins are clearly established in the daughters at an early stage (B).

Figure 4.4. ISP1 associates with the daughter buds slightly before IMC3

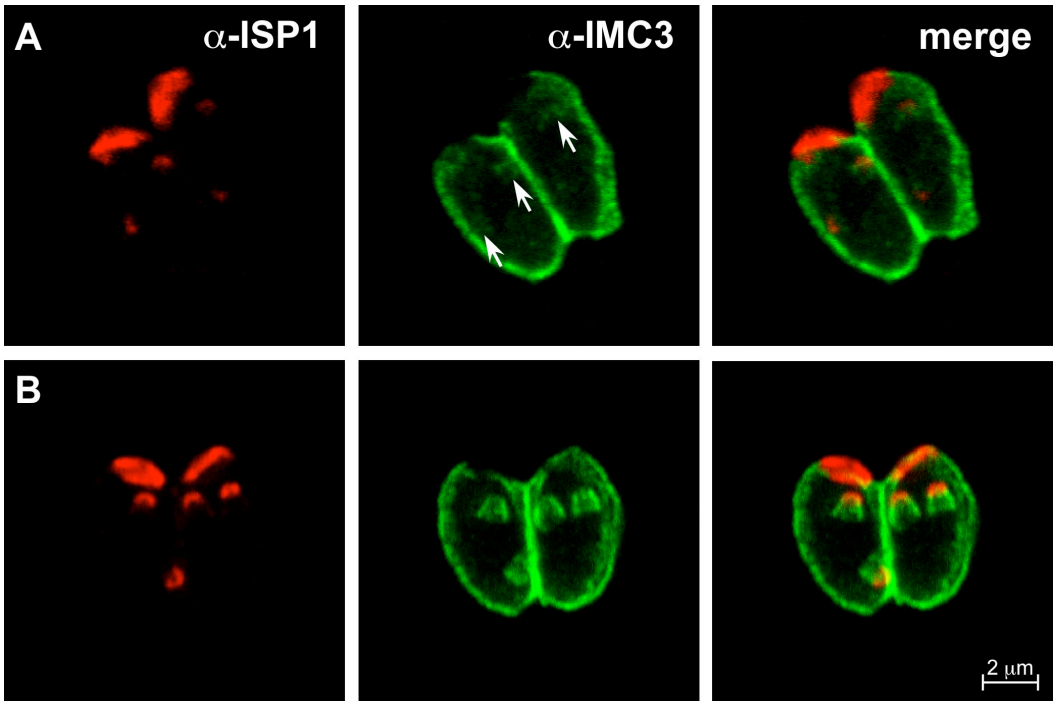

Figure 4.5. TgCAM1 enters the conoid near the midpoint of budding

(A-B) Parasites expressing TgCAM1-YFP (green) co-stained with anti-IMC3 show an absence of TgCAM1 in the early bud (A). TgCAM1 enters the conoid around the midpoint of budding as indicated by the arrows (B). TgCAM1-YFP is driven by the p*tub* promoter.

Figure 4.5. TgCAM1 enters the conoid near the midpoint of budding

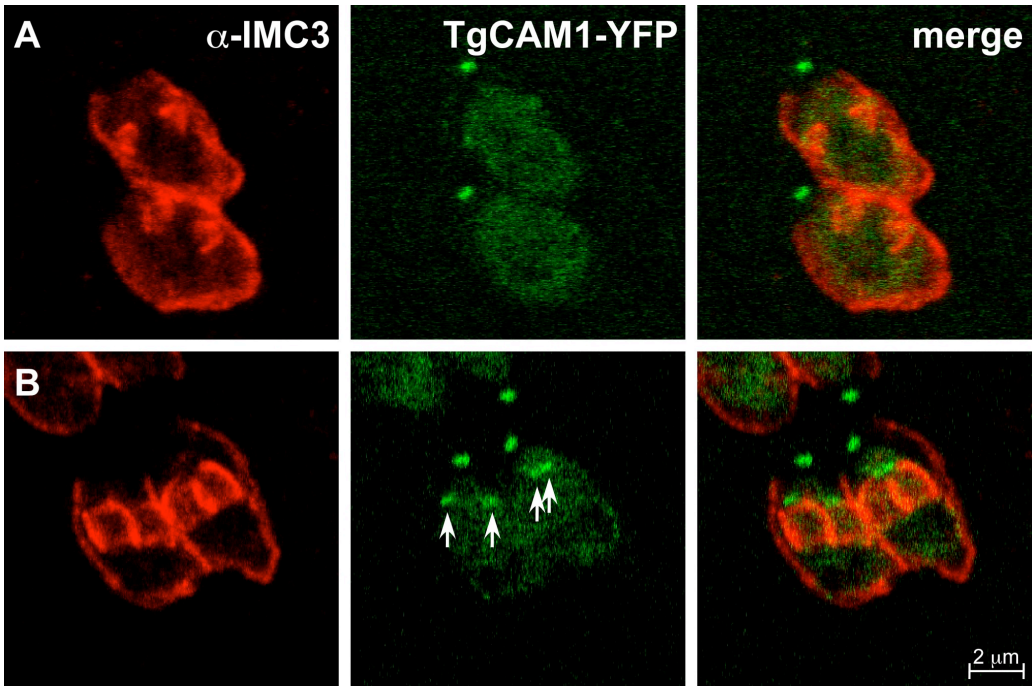

Figure 4.6. Timeline of early budding activity

Panel 1 is the initiation stage of budding, panels 2 through 6 are the early stages, and panel 7 represents the midpoint of budding. Bud components correspond to the text colors below the panels. Included components are those whose timing has been verified by comparative IFA as part of this project.

Figure 4.6. Timeline of early budding activity

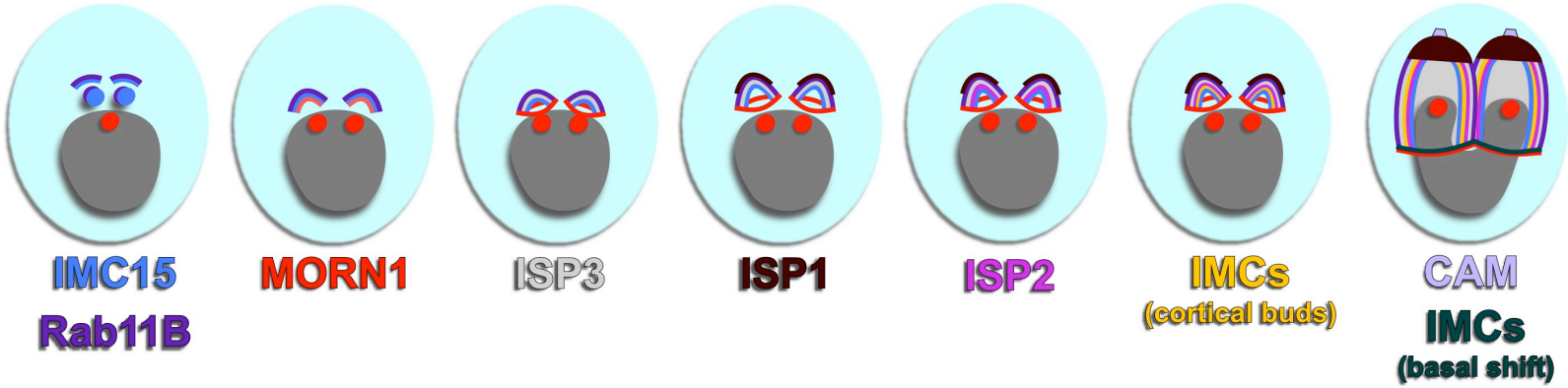

Chapter 5. Conclusions and Future directions

5.1. Conclusions

Toxoplasma replicates rapidly, destroying infected cells, and causing the tissue lesions that are responsible for the escalation of toxoplasmosis. Replication occurs by an internal budding mechanism that begins with the division of the Golgi and the duplication of the centrosome (17, 23-25, 29). Progression of budding requires the proper development of the cytoskeleton (10-16); therefore, the components of this structure are attractive potential therapeutic targets and comprise a growing area of research.

In this thesis, a new family of cytoskeletal proteins was identified. The spatial and temporal model of cytoskeletal development that evolved from documenting the subcellular localization dynamics of all 14 members of the *Toxoplasma* alveolin motif-containing intermediate filament-like protein family provided unprecedented detail into the process of IMC biogenesis and exposed phenomena not previously observed. The diverse behaviors of these related genes are controlled at three levels: expression profile, primary protein sequence, and post-translational modifications. The localization of IMC7, 12, and 14 to the cortical IMC during G1 is strongly correlated to their expression patterns (Fig. 2.4) with IMC14 expression peaking in the first third of G1 and IMC7 and 12 toward the middle of G1. The importance of the primary protein sequence is illustrated by the ability of the IMC3 and IMC8 alveolin domains to localize properly when expressed alone. The impact of post-translational modifications is expressed in the proteolytic cleavage of IMC1 (67) and the potential dominant negative effects of IMC15 predicted palmitoylation site mutants.

The intriguing localization of IMC7, 12, and 14 to the independent, seemingly fully formed cytoskeleton during G1 could serve to distinguish the mother parasite that must be degraded prior to cytokinesis from the internally budding daughters as discussed in Section 2.3. Furthermore, IMC7, 12, and 14 may serve another function since they mostly relocate back to the cytoplasm after egress from the host cell (Tomasz Szatanek, Brooke Anderson-White, Michael White, Jeroen Saeij, and Marc-Jan Gubbels; paper under review). These *Toxoplasma*-specific proteins could be tied to the relocation of the glycolytic enzymes (88), part of a signaling cascade, and/or involved in cytoskeletal stabilization and flexibility for egress and invasion.

IMC5, 8, 9, and 13 localize to the early buds and then at the midpoint of budding they shift to basal end of the growing parasite with TgCentrin2 and the daughters begin to constrict (Fig. 2.12). The trigger for this basal migration is unknown as is the role of these basal IMCs in constriction. Involvement in a septin-related mechanism is unlikely based on the minimal role of actin in daughter budding (40), the highly divergent nature of *Toxoplasma* myosins (42, 43), and the often incomplete abscission of the daughters (95). However, it is possible that these IMCs function in a divergent yet analogous mechanism in *Toxoplasma*.

Once the parasite is mature, these IMCs and TgCentrin2 along with IMC15 and MORN1 form a three-ringed structure at the posterior end of the parasite. These regions could coincide with the BIR and BIC revealed by EM (Fig. 2.12H-J and 2.15B). The BIC may bend over the alveoli to provide the only visible connection between the IMC and the plasma membrane, but this requires closer examination to verify. In addition to a role

in constriction, the members of this basal complex could be involved in maintenance of cytoskeleton integrity at the posterior end of the parasite during the mechanical stresses of invasion. A similar basal complex has only been described in *E. tenella* merozoites (33) and, like IMC7, 12, and 14; IMC5, 8, 9, and 13 are unique to *Toxoplasma*.

IMC15 is the earliest cytoskeletal indicator of daughter bud formation as it colocalizes with the duplicated centrosomes. From the centrosomes, IMC15 expands into the daughter buds (Fig. 2.13D and G) and remains cortical in the mature IMC (Fig. 2.13A-G). However, the amount of IMC15 that remains in the mature parasite is beyond the detection limit of the IMC15 antibody (Fig. 2.13H and I) so its presence was verified through detergent extractions (Fig. 3.4).

Unlike IMC7, 12, and 14 and the IMCs of the basal complex, IMC15 is conserved across the Apicomplexa despite the variations in division modes within this phylum. Though the primary role of IMC15 may be earlier in division, MORN1 is an essential protein involved in the development of the *Toxoplasma* cytoskeleton that is conserved throughout apicomplexan species and between endodyogeny, endopolygeny, and schizogony (95). Our inability to KO IMC15 suggests that it is essential as well as conserved like MORN1. To delve into the specific function of IMC15 three conditional KD strains were created using the DD-system, the T7S4 repressible promoter, and the T7S1 repressible promoter. None of the strains could sufficiently downregulate IMC15 to a KO-like background level, proving that extremely low levels of IMC15 expression are sufficient for parasite viability. Furthermore, use of the DD-system exposed a high affinity of IMC15 for the centrosomes. The basis for this affinity is yet to be determined.

Post-translational modification could factor into the behavior of IMC15. Based on the detergent extractions it does not appear that IMC15 undergoes a cleavage event similar to IMC1 (67), but further experiments would be necessary to verify the absence of such an event. Post-translational modifications could influence the localization of IMC15 since primary protein sequence alone is not sufficient as it is in IMC3. IMC15 has five sites strongly predicted to be palmitoylated. The three sites in the N-terminus appear to be redundant as no defect is observed after mutation of these sites until all three are mutated together. The quintuple mutant has no observable phenotype and, therefore, may create an inert-like protein that interacts with the native IMC15 and is carried to the proper sub-compartments. However, three mutant constructs (C673A/C674A, C4A.C92A/C93A, and C4A.C673A/C674A) could potentially exert toxic dominant negative effects on the parasite. We cannot verify at this time that this toxicity is due to an abrogation of palmitoylation or a secondary effect from changing the Cys amino acids to Ala. In addition to palmitoylation, phosphorylation state could affect the behavior of IMC15. We have identified six conserved potential phosphorylation sites, including a potential NIMA kinase site (127), that are candidates for mutation.

The IMC family was incorporated into the broader context of cytoskeletal genesis with the development of a comprehensive relative timeline of daughter budding (Chapter 4). This timeline provides a framework for identifying the precise temporal organization of all current and future cytoskeletal components. It will serve as a tool to assist in the identification of developmental mechanisms and protein relationships especially as more KOs are created.

The IMC proteins are active in cytoskeletal development from the duplication of the centrosomes through the constriction of the posterior end. The diversity of the subcellular dynamics of this group suggests complex interactions between the members of this family as well as with other cytoskeletal elements. Further elucidation of the functions of these proteins will increase the resolution of the timing and the mechanisms behind the development of the daughter buds. A greater understanding of these *Toxoplasma*-specific proteins could lead to improved therapeutics in the future.

5.2. Future directions

Based on the data presented here, the organization of the IMC proteins is varied and complex. In order to determine if this diversity in subcellular localization is reflected in their functions we will need to continue to create KOs and conditional KDs of these proteins. Specifically the mature-only IMCs, IMC7, 12, and 14, and the basal IMCs, IMC5, 8, 9, and 13, are of interest. The members of these groups are unique to *Toxoplasma* and elucidation of their functions would increase our understanding of *Toxoplasma*-specific mechanisms. The possible redundancy of the IMCs that share the same spatio-temporal patterns may necessitate the generation of multi-gene KOs to evaluate their functions.

For IMC7, 12, and 14 it would be interesting to test if their extracellular relocation to the cytoplasm is calcium and/or potassium concentration dependent. This would involve experiments similar to those described in Pomel et al., such as incubating parasites in media mimicking extracellular and intracellular potassium levels and

monitoring protein localization (88). These experiments could be repeated with KO strains to fully assess the function of IMC7, 12, and 14.

A sufficient KO background of IMC15 remains elusive. Due to the very low level of IMC15 expression sufficient for parasite survival a complete KO is required. We are currently constructing a Cre-Lox controlled conditional KO (122-124). As a secondary approach for functional studies we are developing DD-controlled dominant negative constructs based on the deletion and palmitoylation mutants. Furthermore, we are conducting competition assays with the tet-repressible conditional KDs to verify that they do exhibit slower growth than the parental TATi*Δku80* strain.

Once an IMC15 KO has been established the contributions of the individual domains (N-terminus, alveolin, and C-terminus) to IMC15 behavior can be determined. All previous experiments have taken place in a wild-type background where interactions between the constructs and the native proteins could account for the observed localization patterns. Emphasis should be placed on the C-terminus, which may have an important function. Furthermore, the contributions of post-translational modifications, specifically palmitoylation and phosphorylation, to IMC15 should be studied in the KO background. It has not been determined that changes in palmitoylation state and not a secondary change related to the Cys to Ala mutations are responsible for the potentially toxic effects of the mutants; thus palmitoylation assays will be considered.

The detergent solubility experiments with IMC15 did not suggest that IMC15 undergoes a cleavage event during maturation similar to IMC1 (67); however, further experimentation would be necessary to prove this. Pulse-chase labeling experiments

would be a possibility. It is important to keep in mind that these experiments would require large numbers of parasites for sufficient protein detection due to the low expression levels of IMC15.

An interesting experiment that would solidify a role for IMC15 in the nucleation of budding would be to attempt reactivation of rapid budding in parasites that have differentiated from tachyzoites to slow growing pseudo-cystic bradyzoites. This could be accomplished in two ways: first, a DD-controlled construct could be transfected into Prugniuad parasites (Type II strain) and then IMC15 activated with the addition of Shld1 after bradyzoite differentiation; or, alternatively, YFP-IMC15 driven by the tubulin promoter could be transfected into Prugniuad parasites to test if constitutive overexpression of IMC15 inhibits bradyzoite differentiation. It is important to bear in mind that these experiments assume IMC15 is the limiting factor in bradyzoites for budding initiation and not any enzymes that may modify IMC15 or any binding partners necessary to instigate cytoskeletal formation.

The conservation of IMC15 across apicomplexan species suggests that its function may be conserved across apicomplexan division methods. We are collaborating with a *Sarcocystis* lab to look at the role of IMC15 in endopylogeny and are establishing a collaboration with a *Plasmodium* lab to look at schizogony. There are clear homologs of IMC15 in *Plasmodium* (Fig. 3.4) and, though the *Sarcocycstis* genome sequencing efforts are in the early stages making identification of an IMC15 homolog difficult, it is the closest relative to *Toxoplasma* after *Neospora* (131).

Nanoresolution microscopy is an underutilized tool in the *Toxoplasma* field that would greatly improve our ability to resolve the fine details of cytoskeletal development. Since immunoprecipition with the *Toxoplasma* cytoskeletal proteins is difficult due to solubility issues, the identification and validation of interactions is difficult. Nanoresolution microscopy could assist in this process and would be especially useful in future studies of early budding, the apical complex, and the basal complex.

The ultimate goal of infectious disease work is to contribute to the improvement of therapeutics. Drug screening is not the intent of this work, but there are drugs that target traditional IFs currently used to treat other diseases that could be tested for their efficacy in disrupting the IF-like proteins of *Toxoplasma*. One such drug is withaferin A (WFA), which is used to treat cancer by modifying the cysteines of Type III IFs in tumors (132). Many of the IMC proteins are cysteine rich so we attempted to inhibit cytoskeletal formation by treating parasites with WFA. Unfortunately, WFA did not affect *Toxoplasma,* but identifying and testing the effects of other currently approved IF targeting drugs could be pursued in the future.

Chapter 6. Materials and Methods

6.1. Parasites

RH strain parasites, *Δku80* strain parasites (111), TATi*Δku80* (Drs. Lilach Sheiner and Boris Striepen; unpublished), and transgenic derivatives of these primary strains were used throughout this study. Parasites were maintained in human foreskin fibroblasts (HFF) as previously described (116). All parasites were grown at 37°C except for the FV-P6 temperature sensitive mutant, which was grown at 35°C (permissive) or 40°C (restrictive). Stable parasites expressing transgenes were selected under chloramphenicol, pyrimethamine, or mycophenolic acid pressure and cloned by limiting dilution.

6.2. RACE

For IMC genes 7, 9, and 12-15 we determined the 5'- and 3'-ends by RACE using the GeneRacer kit (Invitrogen) according to the manufacturer's instruction. All primer sequences are provided in Table 4.1.

6.3. Sequence analysis

The IMC gene family was identified through reciprocal BLASTp searches of the *T. gondii* genome of the ME49 strain in ToxoDB version 5.1 using a cut-off e-value of 10^{-3} (75, 133). The alveolin repeat domains of each IMC were determined by first identifying the VPV and EKIVEVP repeats as defined in (74) and then analyzing the protein sequences for novel repetitive regions with the REPRO program (76). The final determination of each alveolin domain's boundaries was done manually based on the V/E/K/Q/R/P richness of the domain. Predictions of lipid modification (myristoylation,

farnesylation, geranylgeranylation, palmitoylation) were performed using the suite available at http://mendel.imp.ac.at/mendeljsp/index.jsp, (134, 135).

IMC15 homologs were identified through BLASTp searches of the apicomplexan sequenced genomes (*Babesia, Cryptosporidium, Eimeria, Neospora, Plasmodium, Theileria,* and *Toxoplasma*) in EuPathDB (97). A cut-off e-value of -20 was selected as it is the next lowest score compared to the e-value of the first *Toxoplasma* IMC protein result. NCBI BLASTp queries with IMC15 used the non-redundant protein sequences database and a cut-off e-value of -32 as determined in the same manner as for EuPathDB. The 10 strongest hits were reciprocally BLAST searched in ToxoDB version 7.0 (75). IMC15 was aligned with these best 10 hits using ClustalW version 2.1 and analyzed using ClustalX ver 2.1 (136, 137).

The phylogenetic trees were generated with the MEGA program version 5.05 (138) using a maximum likelihood model with 1000X bootstrapping. Palmitoylation sites were predicted (medium to high likelihood) by CSS-Palm2.0 (77). Phosphorylation sites were predicted by NetPhos 2.0 with T352, T419, and S545 being greater than the threshold of 0.5 (139).

6.4. Plasmids

All PCR primer sequences are provided in Table 6.1. Plasmids p*tub-YFP-IMCx/sagCAT* and p*tub-IMCx-YFP/sagCAT* are based on the p*tub-YFP*$_2$*(MCS)/sagCAT* plasmid (140) with an extra multiple cloning site containing *EcoR*V and *Xma*I/*Sma*I introduced after the stop codon of the second YFP based on the p*tub-cherryRFP*$_2$*/sagCAT* plasmid (kindly

provided by Giel van Dooren and Boris Striepen, University of Georgia). Complete ORFs were amplified from cDNA generated from either Type I (RH strain) or Type II (Prugniaud strain; cDNA library kindly shared by Peter Bradley, UCLA) tachyzoites. Amplicons were *Bgl*II/*Avr*II cloned for C-terminal YFP fusions or *Avr*II/*Eco*RV, *Avr*II/*Xma*I, or *NheI*/*Xma*I for N-terminal YFP fusions. The same strategy was employed to generate cherryRFP fusions. 1500 bp endogenous promoters were PCR amplified from genomic DNA and cloned by *Pme*I/*Bgl*II into p*tub-YFP-IMCx/sagCAT*, p*tub-IMCx-YFP/sagCAT*, or p*tub-IMCx-cherryRFP/sagCAT*. Deletion and chimeric proteins were cloned by PCR-fusion amplification of select domain inserts flanked with *Avr*II/*Eco*RV or *Nhe*I/*Xma*I sites (141) and cloned into p*tubYFP*$_2$*(MCS)/sagCAT*.

Transfection of p*tub-YFP-IMC5*/*sagCAT* did not result in a stable parasite line. Therefore a second conditional expression system, the DD system, was employed for IMC5. p*tub-DD-YFP-IMC5*/*sagCAT* was generated by PCR amplification of *YFP-IMC5-3'dhfr* from p*tub-YFP-IMC5*/*sagCAT* with primers *Nhe-Sph-YFP-F* and *3dhfr-Not-R*, digested with *Nhe*I and *Not*I and cloned into p*tub-DDmycYFP-CAT* [kindly provided by Markus Meissner, Heidelberg University; (142)] digested with *Avr*II and *Not*I. The myc epitope tag was removed by *Sph*I digestion and religation. This resulted in plasmid p*tub-DD-YFP-IMC5*/*sagCAT*.

Plasmid p*tub-myc2-centrin2/sagCAT* was generated by *Avr*II/*Not*I swapping of the *TgCentrin2-3'dhfr* segment from plasmid p*min-RFP-Centrin2/sagCAT* [(83); kindly provided by Dr. John Murray, University of Pennsylvania] into p*tub-myc2-MORN1/sagCAT* (10).

For endogenous tagging the plasmid *LIC-3'1.5kbIMC15-myc$_3$/DHFR* was created as previously described (111). 1.5 kb of IMC15 upstream of the stop codon (stop codon omitted) was amplified from genomic RH DNA using the primers *IMC15-F-Ku80LIC* and *IMC15-R-Ku80LIC*. The PCR product was treated with T4 polymerase and dCTP for 20 min at 37°C, 2 μL of 0.5M EDTA was added to stop the reaction, and the PCR product was purified over a column. *LIC-myc$_3$/DHFR* (kindly provided by Micheal White, University of South Florida) was digested with *Pac*I and then treated with T4 polymerase and dGTP. For ligation independent cloning (LIC) 2 μL of the T4 treated PCR product, 8 μL of the T4 treated *LIC-myc$_3$/DHFR*, 2 μL of ligase buffer, and 20 μL of dH_2O were incubated at room temperature overnight. 10 μL were then transformed into chemically competent DH5α cells. The plasmid was linearized within the homologous region with *Mfe*I prior to transfection.

IMC15 direct KO vectors were created using the MultiSite Gateway Pro system (Invitrogen). Plasmid p*DONR221-5' IMC15* R1/R4 was cloned by PCR amplifying 1,035 bp upstream of the IMC15 promoter from genomic DNA using the primers *5'IMC15-F-B1* and *5'IMC15-R-B4* and then cloned by BP reaction into the plasmid p*DONR221* P1/P4 (kindly provided by Jeroen Saeij, MIT). Plasmid p*DONR221-3'IMC15* R3/R2 was cloned by PCR amplifying 1,035 bp after the IMC15 stop codon using the primers *3'IMC15-F-B3* and *3'IMC15-R-B2* and then cloned by BP reaction into the plasmid p*DONR221* P3/P2 (kindly provided by Jeroen Saeij, MIT). Plasmids p*DONR221-5' IMC15* R1/R4, p*DONR221-HXGPRT* R4r/R3r (kindly provided by Jeroen Saeij, MIT), and p*DONR221-3'IMC15* R3/R2 were combined with the destination vector p*TgKO2*

(kindly provided by Jeroen Saeij, MIT) to create the plasmid p*TgKO2-IMC15-HXGPRT* by LR reaction. Plasmids were linearized with *Mfe*I prior to transfection.

Constructs were targeted to the UPRT locus using the plasmid *5'UPRT-YFP-3'UPRT*. First the p*tub-YFP$_2$(MCS)/sagCAT* plasmid was modified by destruction of the *Not*I site through digestion, T4 polymerase overhang removal, and religation and then the p*sagCATsag* cassette was removed through *Xho*I digestion and religation. The 1,000 bp 5' UPRT sequence is 166 bp upstream of the 5'UTR and was amplified using the primers *5UPRT-F-XhoI* and *5UPRT-R-BglII*. The reverse primer also contains *Age*I and *Pme*I sites to create a new multiple cloning site. The 3' region is 1,000 bp that begins immediately after the 3'UTR of UPRT and was amplified using the primers *3UPRT-F-AvrII* and *3UPRT-R-BamHI*. The forward primer also contains *Not*I and *Hpa*I sites to create a new multiple cloning site. The 5' and 3' regions were cloned into the modified p*tub-YFP$_2$(MCS)/sagCAT* plasmid with *Xho*I/*Bgl*II and *Avr*II/*BamH*I respectively.

The DD-tagged conditional KD IMC15 construct was created by amplifying *IMC15-3'dhfr* from p*tub-YFP-IMC15/sagCAT* with *IMC15-F-Nhe*I and *3dhfr-R-Not*I and then cloning into p*tub-DDmycYFP/CAT* digested with *Avr*II and *Not*I. The promoter was added through *Pme*I/*Bgl*II swapping with p*imc15-YFP-IMC15/sagCAT* to create the p*imc15-DDmyc-IMC15/sagCAT* plasmid. *5'UPRT-pimc15-DDmyc-IMC15-3'dhfr-3'UPRT* was created by *Pme*I/*Not*I cloning. *Apa*I was used to linearize the plasmid for transfection.

The p*T7S4* promoter KO plasmid was cloned by amplifying a 5' 1 kb region immediately upstream of the promoter with the primers *5'IMC15-F-AseI* and *5'IMC15-*

R-AseI; digesting it with *Ase*I; and ligating into the plasmid p*2NdeI_DHFR_T7S4_myc3* (kindly provided by Lilach Sheiner and Boris Striepen; University of Georgia) digested with *Nde*I. The 2 kb 3' region starting with the IMC15 start codon was amplified with the primers *IMC15-F-Bgl* and *IMC15int-R-NheI* and then cloned by *Bgl*II/*Avr*II or *Nhe*I digest into the 5' sequence containing plasmid to create *Tet7Sag4*-p*imc15 KO-DHFR*. The plasmid was linearlized with *Not*I before transfection.

The plasmid *Tet7Sag1*-p*imc15 KO-DHFR* was created by digesting p*TetOSag1-A-NLS-CRE-myc-DHFR* (Marc-Jan Gubbels; unpublished) with *Not*I, blunting the end with T4 polymerase, and then digesting with *Bcl*II, and then ligating the promoter into p*2NdeI_DHFR_T7S4_myc3* using a third irrelevant enzyme site (TIES) with *Sca*I, *Spe*I, and *Bgl*II to avoid an internal *Spe*I site (143). The plasmid was linearlized with *Sca*I before transfection.

Palmitoylation and phosphorylation mutants were generated using QuickChange Site-Directed Mutagenesis (Stratagene). Mutated sequences were amplified from p*SC-A-IMC15* (Stratacloned plasmid; Stratagene) and sequenced with the T7 and T3 primers (MWG Operon). Triple, quadruple, and quintuple mutants were created through multiple rounds of PCR with different primers. Mutant sequences were cloned by *Nhe*I/*Xma*I swapping into *Avr*II/*Xma*I digested p*tubYFP*$_2$*(MCS)/sagCAT*. Mutant C4A was cloned by amplifying *IMC15* with the primers *IMC15.C4A-F-NheI* and *IMC15-R-XmaI* , digesting with *Nhe*I and *Xma*I, and ligating into *Avr*II/*Xma*I digested p*tubYFP*$_2$*(MCS)/sagCAT*.

Plasmid p*tub8-DD.myc.Rab11B_WT_HX* was kindly provided by Dr. Markus Meissner (University of Glasgow). The ISP plasmids: p*isp1-ISP1-YFP/HXGPRT*, p*isp2-*

ISP2-HA/HXGPRT, and p*tub-ISP3-YFP/HXGPRT* were kindly provided by Dr. Peter Bradley and Josh Beck (UCLA).

6.5. PCR verification of homologous recombinations

All verification PCR primer sequences are provided in Table 6.1. Endogenous tagging of IMC15 was verified with the primer pairs *IMC15-CF*/*IMC15-R-XmaI* and *myc-F1*/*3dhfr-Not-R*. Replacement of the entire IMC15 locus with HXGPRT was verified with the primer pairs *5'IMC15ver-F*/*HX-ver-R* and *HX-ver-F*/*3'IMC15ver-R*. Reinsertion of genomic IMC15 was identified with the primer pair *IMC15-NheI-F* and *IMC15int-ver-R*. Proper UPRT vector insertion was verified with the primer pairs *5'UPRT-F-ver*/*UPRT-R-ver* and *3'UPRT-R-ver*/*UPRT-F-ver*. Proper insertion of *Tet7Sag4*-p*imc15KO-DHFR* and no reinsertion of p*imc15* were verified with the primer pairs *5'IMC15ver-F*/*5'DHFRCXR*, *T7Sag4-F-PmeI*/*IMC15int-ver-R (alveolin)*, *pimc15-F-PmeI*/*pimc15-R-BglII*, and *pimc15-ver-F*/*IMC15int-ver-R (alveolin)*. Proper insertion of *Tet7Sag1*-p*imc15KO-DHFR* and no reinsertion of p*imc15* were verified with the primer pairs *5'IMC15ver-F*/*5'DHFRCXR*, *Tet7ver-F*/*IMC15int-ver-R (alveolin)*, *pimc15-F-PmeI*/*pimc15-R-BglII*, and *pimc15-ver-F*/*IMC15int-ver-R (alveolin)*.

6.6. Generation of antisera

The full length ORF of *IMC11* and the 5'-end before the alveolin repeats from *IMC3* (1-120 aa), *IMC5* (1-350 aa), and *IMC15* (1-350 aa) were amplified from cDNA and cloned into plasmid *AVA0421* (144) to generate a His_6 N-terminal fusion. Fusion proteins were expressed in BL21 Star (DE3) pLysS *E. coli* (Invitrogen) and purified over TALON

Resin (Clontech). Polyclonal antisera were generated by rat immunizations (Covance). Antibodies were affinity purified against corresponding recombinant protein cross-linked to cyanogen bromide Sepharose 4B (Sigma) (145).

6.7. Immunofluorescence assays

IFAs were performed as described (82). The following primary antibodies were used: MAb 45:36 IMC1 (kindly provided by Gary Ward, Univ. Vermont), rat anti-IMC3, rabbit anti-IMC3 (68), rat anti-IMC5, rat anti-IMC15, rabbit anti-MORN1 (82), rabbit anti-human centrin (kindly provided by Iain Cheeseman, Whitehead Institute), rabbit anti-cherryRFP (kindly provided by Iain Cheeseman, Whitehead Institute), rabbit anti-GAP45 (44), rabbit anti-TgCentrin1, mouse anti-ISP1 (kindly provided by Peter Bradley and Josh Beck, UCLA) and rabbit anti-FKBP12$_{N12}$ (Thermo Scientific). Secondary antibodies conjugated to Alexa350, 488 or 594 were used (Invitrogen). Nuclear material was co-stained with 4',6-diamidino-2-phenylindole (DAPI).

6.8. Fluorescence microscopy

A Zeiss Axiovert 200M wide-field fluorescence microscope equipped with a α-Plan-Fluar 100x/1.45 NA oil objective, and a Hamamatsu C4742-95 CCD camera was used. In addition, a Leica TCS SP5 inverted confocal microscope with a 100x/1.4 NA oil objective was used. Time-lapse microscopy was performed on the Zeiss microscope. Images were analyzed and processed using Openlab and Volocity (Improvision).

6.9. Electron microscopy

Intracellular parasites were fixed in 4% glutaraldehyde in 0.1 M phosphate buffer pH 7.4 and processed for routine electron microscopy (146). In summary, cells were post-fixed in OsO_4 and treated with uranyl acetate prior to dehydration in ethanol, treatment with

propylene oxide, and embedding in Spurr's epoxy resin. Thin sections were stained with uranyl acetate and lead citrate and examined with a JEOL 1200EX electron microscope.

6.10. Detergent extractions

Parasites were allowed to be extracellular for 24 hr before they were filtered and resuspended in resuspension buffer (50 mM Tris pH 8.0 and 150 mM NaCl) to a concentration of $4x10^6$ parasites/μL. Triton-X100, DOC, and SDS were added to individual aliquots at a concentration of 1%. A protease inhibitor cocktail (Sigma) was added in a 1:100 ratio. SDS extraction was performed for 10 min at 98°C and then the samples were spun at room temperature for 20 min at 13,000 rpm. All other extractions were performed on ice for 45 min and then spun at 4°C for 20 min at 13,000 rpm. Supernatants were removed as the soluble fraction and the pellets were resuspended in a volume of resuspension buffer equivalent to the supernatant.

6.11. Western blots

Western blots were performed as previously described (82). For the anti-GFP blots, lysate equivalent to $20x10^6$ to $40x10^6$ parasites was loaded on a 12% NuPAGE Bis-Tris gel (Invitrogen). Proteins were transferred to PVDF membrane (Bio-Rad) and then blocked overnight in 5% ImmunoPure Normal Goat Serum (Thermo Scientific). YFP fusion proteins were detected with mouse anti-GFP (1:1,000 or 1:2,000; Abgent) in 5% goat serum and then washed 3 times for 10 min each with TBS containing 0.1% Tween (TBST). Subsequently the membrane was incubated with horse radish peroxidase (HRP)

conjugated anti-mouse antibody (1:10,000; DakoCytomation), washed again with TBST, and finally washed for 5 min with TBS alone. Signals were visualized using Immobilon chemiluminescent HRP substrate (Millipore) and captured on a Syngene G:BOX ChemiHR16 running GeneSnap software (v7.07) for 2 to 20 min.

For the detergent extraction blots, lysate equivalent to $80x10^6$ parasites was loaded and 5% milk was used to block. Endogenous IMC15-myc_3 was detected with mouse anti-c-myc(9E10)-horseradish peroxidase (HRP) conjugated (1:2000, Santa Cruz Biotech), IMC1 was detected with mouse anti-IMC1 (1:2000, Gary Ward, University of Vermont), and GRA1 was detected with mouse anti-GRA1 [1:15,000 of stock, Marie-France Cesbron-Delauw, Institut Pasteur de Lille, (147)]. For IMC1 and GRA1 the blot was incubated with HRP conjugated anti-mouse antibody (1:10,000; DakoCytomation). All dilutions were in 5% milk. Signal visualization on the Syngene G:BOX was 80 min for anti-c-myc and 2 min for anti-IMC1 and anti-GRA1 . The blot was stripped between labelings by washing with 1X PBS for 10 min at room temperature, then incubating with stripping buffer (62.5 mM Tris-HCl pH 6.7, 2% SDS, 100 mM β-mercaptoethanol, and dH_2O) for 30 min at 50°C, and finally washing the blot with 1X PBS twice for 10 min each at room temperature. The blot was blocked again with 5% milk for at least 1 hr after stripping.

6.12. Yeast two-hybrid

Protein interactions were mapped using the yeast two-hybrid system with the DNA binding plasmid p*DEST-GBKT7-BD-AttR1_2* and the activation domain plasmid p*DEST-*

GADT7-AD-AttR1_2 [kindly provided by Michael White, University of Southern Florida (Invitrogen)] in the AH109 yeast-two hybrid reporter strain (Invitrogen). Genes were cloned into the plasmids by Gateway recombination cloning. Primer sequences are provided in Table 4.1 (148). A matrix of plasmid combinations were co-transformed into the AH109 strain using a modified version of the TRAFO high efficiency transformation protocol (149) and plated on -Leu/-Trp media (dropout powders and SD minimal agar media from Clontech). Plates were grown at 30°C for four days and then replica plated to plates lacking histidine, adenine, leucine, and tryptophan (quadruple drop-out or QDO) and grown under the same conditions. The strengths of self-interactions were assessed by replica plating from QDO to 5 mM, 10 mM, 25 mM, and 50 mM 3-aminotriazole (3-AT). The empty p*GBK* and p*GAD* plasmids were used for negative controls and Snf4 and Snf1 encoding plasmids p*SE1112* and p*SE1111*, respectively, were used as positive controls (150).

6.13. Plaque assays

Confluent T-12.5 flasks of hTERT HFF cells were infected with 200 parasites in ED-1 or ED-1 with 1μg/mL ATc (Invitrogen) and incubated undisturbed at 37°C for 7 days. The monolayers were stained with crystal violet and the plaques counted. Total plaque area was quantified in Improvision Openlab (version 5.5.0) and average plaque size calculated by dividing total plaque area by the number of plaques.

Table 6.1. Primer Sequences

Overview of all primer names and sequences used to generate plasmids for this study. Restriction enzyme sites are underlined. LIC extensions are in italics and bold font. AttB Gateway recombination sites are in bold font.

Table 5.1. Primer Sequences

Primer name	sequence
RACE primers	
RACE-IMC7-5′	GGCGTTGAACTGGTTGAGCGCCTCGAGG
RACE-IMC7-5′nest	CGCCGTTCGTCGTGCCGCAGTACCAAG
RACE-IMC7-3′	CGGAAATCGCGCGCTTTGTACCCTCCGTC
RACE-IMC9-5′	CGGACTTCAACAATCTTGTCGACAGGAACG
RACE-IMC9-5′nest	CGAATTTCTCAGCGACGACGCACTGCG
RACE-IMC9-3′	GCCTCAGGTGATGGTTCGAGAACGCG
RACE-IMC9-3′nest	CGTCCGAAAGGAGAAGGTCGTCACAATTC
RACE-IMC12-5′	CCTCGACGTATCGGGGCACATAAATCGGC
RACE-IMC12-5′nest	GACGTCGTAGTACTTGGGCTGAATCCGGG
RACE-IMC12-3′	GCCAGTCGAAGTCACCAAGGTTGCTGTG
RACE-IMC12-3′nest	GCCGCGTGAAGTCAACGTCATCCAGGC
RACE-IMC13-5′	GCTTTTCAATGATGCGTTCCTGAGGGACG
RACE-IMC13-5′nest	CGGACCGGGAACATGGCGAATCTTCTCG
RACE-IMC13-3′	GTGCCACGAACTGACATTCAGTGGGTGG
RACE-IMC13-3′nest	GGAGAAGTACGTGGAGGTTCCACAGATC
RACE-IMC14-3′	ATGGAGCTCTGCGAGAGCCCCTGCTGCG
RACE-IMC14-3′nest	CGGTACTCCCACTCGCCACCGTTGGAG
RACE-IMC15-5′	GTGAATTTGTCGTGCACGACCACATATGGC
RACE-IMC15-5′nest	CGGTATGTGGTTAATGACAGTGTCGCGGAG
RACE-IMC15-3′	CACATGGTCCCGCGGTTACGCCCAGTG
RACE-IMC15-3′nest	GAGGTCGAGAAGTTTGTCGAGGTTCCAG
YFP/RFP fusion primers	
3dhfr-Not-R	GGTGGCGGCCGCTCTAGAAC
YFPIMC3-F	cagCCTAGGATGTCGGACGCCGGGACCCCG
YFPIMC3-R	cagGATATCtcaCTGCTCGTAGACGACTTCGCGCTC
IMC3-BamHI-F	cagGGATCCATGTCGGACGCCGGGACCCCG
IMC3-AvrII-R	cagCCTAGGCTGCTCGTAGACGACTTCGCGCTC
IMC4-F-AvrII	cagCCTAGGatgttttctgagtgctgccagc
IMC4-R-RV	cagGATATCctagttgatattgacttgggtctg
IMC4-F-Bgl	cagAGATCTaaaATGTTTTCTGAGTGCTGCCAG
IMC4-R-Avr	cagCCTAGGGTTGATATTGACTTGGGTC
IMC5-F-AvrII	CCTAGGatggttcagttcgcgcacggcc
IMC5-R-XmaI	CCCGGGctattcccctccatttcgacagtc
IMC6anno-F-Avr	cagCCTAGGATGGCTCAGACAGCCCCGAAC
IMC6anno-R-RV	cagGATATCTCAGTGCACCTCGCCTTCGGAG
IMC6-F-Bgl	cagAGATCTaaaATGGCTCAGACAGCCCCGAAC
IMC6-R-Avr	cagCCTAGGGTGCACCTCGCCTTCGGAG
IMC7-F-Avr	cagCCTAGGATGGAGTTCACTGCTGACAAC
IMC7-R-RV	cagGATATCCTACGCAGCGATTGGGAC
IMC7-F-Bgl	cagAGATCTATGGAGTTCACTGCTGACAAC
IMC7-R-Avr	cagCCTAGGCGCAGCGATTGGGACAGCGGTG
pIMC7-F-PmeI	cagGTTTAAACGTGGGCTCGTCTGGTTTTCTCCG
pIMC7-R-BglII	cagAGATCTTGCGAAGAAGGCGTGAAAAAGCAAG
IMC8anno-F-Avr	cagCCTAGGATGTATTCCAGCAGACCGTATCCTG

IMC8twin-F-Avr	cagCCTAGGATGTCGTCGCAGTATGCTACCTC
IMC8-R-RV	cagGATATCTTACATCGGAGTCGGTGGAAAGGGC
IMC9-F-TgG-AvrII	cagCCTAGGATGGCTTCGTCCTCAGCCCCG
IMC9-R-RV	cagGATATCCTAGTTGACGGCCTGTGAGAG
IMC10-F-AvrII	cagCCTAGGATGTCTCAGTTTCAACAGCCAC
IMC10-R-RV	cagGATATCTTAGGCGCTGATCTGTGCCTC
IMC10-F-Bgl	cagAGATCTaaaATGTCTCAGTTTCAACAGCC
IMC10-R-Avr	cagCCTAGGGGCGCTGATCTGTGCCTCTTC
IMC11-F-Avr	cagCCTAGGATGAGCGGCTGCCAGCAAAACGAC
IMC11anno-R-NruI	cagTCGCGATCACCTGACGCGGTATTGGTCATC
IMC11-F-Bgl	cagAGATCTaaaATGAGCGGCTGCCAGCAAAAC
IMC11(TwSc)-R-Avr	cagCCTAGGCCTGACGCGGTATTGGTC
pimc11-F-Pme	cagGTTTAAACGAGTGGGAGACGGCAAGCTTG
IMC11(ME49)-R-Nhe	cagGCTAGCACCCTCTAACCAGGCACAGGC
IMC11-F-XmaI	cagCCCGGGATGAGCGGCTGCCAGCAAAACGAC
YFPIMC12-F	cagCCTAGGATGGCAACCGAGTTCGTCGTTC
YFPIMC12-R	cagGATATCtcaCTGGGGCATGGAGTCGACG
IMC12-F-Bgl	cagAGATCTATGGCAACCGAGTTCGTCGTTC
IMC12-R-Avr	cagCCTAGGCTGGGGCATGGAGTCGACGGAC
pIMC12-F-PmeI	cagGTTTAAACCACCAACAAATCCAACAACTTCCG
pIMC12-R-BglII	cagAGATCTCTGCAAATTCACAGAGCGAAGTAGC
IMC12-F-NruI	cagTCGCGAATGGCAACCGAGTTCGTCGTTC
IMC13-F-Avr	cagCCTAGGATGGAAACGATGGCTCAGCAG
IMC13-R-RV	cagGATATCTTACTTCTCGAAGCCAGGCG
IMC13-F-Bgl	cagAGATCTATGGAAACGATGGCTCAGCAG
IMC13-R-Avr	cagCCTAGGCTTCTCGAAGCCAGGCGAAGAG
IMC14-F-Nhe	cagGCTAGCATGGAGCTCTGCGAGAGCCCCTG
IMC14-R-RV	cagGATATCTCACCTTTTCATAAAGTCTTCGTTG
IMC14-F-Bgl	cagAGATCTATGGAGCTCTGCGAGAGCCCCTG
IMC14-R-Nhe	cagGCTAGCCCTTTTCATAAAGTCTTCGTTGTTCAG
pIMC14-F-PmeI	cagGTTTAAACTCGCATGCTGAGGAACCAACC
pIMC14-R-BglII	cagAGATCTCGTGTCCACTATTGGTAACGGAT
IMC15-F-NheI	cagGCTAGCATGCGGATCTGCTTGCCACCAG
IMC15-R-XmaI	cagCCCGGGTCAGTTCGGATAAGACAACGTGTTG
IMC15-F-Bgl	cagagatctaaaatgcggatctgct
IMC15-R-Nhe	caggctagcgttcggataagacaacgtg
pIMC15-F-PmeI	cagGTTTAAACCGCCAATAACAGCACTGACCACAG
pIMC15-R-BglII	cagAGATCTTTTAGAAAAATTCTCTCCTATGCTGCTG
TgCAM1-BglII-F	ccgAGATCTATGCCGCCTCGGGGCAG
TgCAM1-AvrII-R	ggcCCTAGGTTTATTCGCGGAAGGC

DD system primers

Nhe-Sph-YFP-F	cagGCTAGCaGCATGCcagtgagcaagggcgaggagctg
3dhfr-Not-R	GGTGGCGGCCGCTCTAGAAC

Recombinant protein expression / LIC primers

IMC5-LIC-F	***gggtcctggttcg***ATGGTTCAGTTCGCGCACGCC
IMC5-LIC-R	***cttgttcgtgctgttta***CTACGGGCC TTGCGGCGGTAAC
IMC11-F-LIC	***gggtcctggttcg***ATGAGCGGCTGCCAGCAAAACGAC
IMC11-R-LIC	***cttgttcgtgctgttta***TTACCTGACGCGGTATTGGTCATC
IMC15-LIC-F	***gggtcctggttcg***ATGCGGATCTGCTTGCCACC

IMC15-LIC-R	***cttgttcgtgctgttta***CTAGACTACTTTGACTACAGG

Deletion and Chimera construct primers

IMC3-AR-RV	cagGATATCttaTGGCGGCTGGTACGGGATTTC
IMC3-AF-Avr	cagCCTAGGCCTCCAGAGGTCCGACAGAAG
IMC8-AR-RV	cagGATATCttaATCCTCGTCCACGTAGACGAC
IMC8-AF-Avr	cagCCTAGGGACCCTGTACTCGAGGAACGG
IMC8-CF-3AR	GAAATCCCGTACCAGCCGCCAGGTAGCCAAACGCGCGTTCCG
IMC3-NR-8AF	CCGTTCCTCGAGTACAGGGTCCAGCGGCATCGGGCCGAG
IMC3-CF-8AR	GTCGTCTACGTGGACGAGGATGACGCGGCGACCCTCCCGCCC
IMC8-NR-3AF	CTTCTGTCGGACCTCTGGAGGAAGAAGGGTTGCACCTTCGGG
IMC3-CF-Avr	cagCCTAGGGACGCGGCGACCCTCCCGCCCTTG
IMC15-CF	caggctagcagtgttcacaaaacaaaaagcaaagtttc
IMC15-NRnew	cagCCCGGGtcaTGCCTGAGTGGTCTTCGCTCTG
IMC15-ARnew	cagCCCGGGtcaCCGTTCTTTATCTAGGTGAGTGAC
IMC15-AFnew	cagGCTAGCGTTGTTGAACAGAAGATGGTCCCG
IMC15-CFnew	cagGCTAGCCTAACAGCCGAGCAACAGGAAC
IMC15-CF-NRnew	CAGAGCGAAGACCACTCAGGCACTAACAGCCGAGCAACAGGAAC

Yeast two hybrid primers

Att-B1-adapt	**GGGGACAAGTTTGTACAAAAAAGCAGGCT**
Att-B2-adapt	**GGGGACCACTTTGTACAAGAAAGCTG**
AttB1-F-IMC3	**AAAAAGCAGGCT**ccATGTCGGACGCCGGGACC
AttB2-R-IMC3	**AGAAAGCTGGGT**gtcaCTGCTCGTAGACGACTTCG
AttB1-F-IMC5	**AAAAAGCAGGCT**ccatggttcagttcgcgcacggcc
AttB2-R-IMC5	**AGAAAGCTGGGT**gctattcccctccatttcgacagtc
AttB1-F-IMC8	**AAAAAGCAGGCT**ccATGTATTCCAGCAGACCGTATC
AttB2-R-IMC8	**AGAAAGCTGGGT**gTTACATCGGAGTCGGTGGAAAG
AttB1-F-IMC9.GL	**AAAAAGCAGGCT**ccATGGCTTCGTCCTCAGCCCCG
AttB2-R-IMC9.GL	**AGAAAGCTGGGT**gCTAGTTGACGGCCTGTGAGAG
AttB1-F-IMC13	**AAAAAGCAGGCT**ccATGGAAACGATGGCTCAGCAG
AttB2-R-IMC13	**AGAAAGCTGGGT**gTTACTTCTCGAAGCCAGGCG
AttB1-F-IMC15	**AAAAAGCAGGCT**ccATGCGGATCTGCTTGCCACCAG
AttB2-R-IMC15	**AGAAAGCTGGGT**gTCAGTTCGGATAAGACAACGTGTTG
AttB1-F-Centrin2	**AAAAAGCAGGCT**cccagcgaggagcactgcg
AttB2-R-Centrin2	**AGAAAGCTGGGT**gtcacgggaaagtcttcttggtc
AttB1-F-MORN1	**AAAAAGCAGGCT**AATGGAGAGCTGCCACGCG
AttB2-R-MORN1	**AGAAAGCTGGGT**GCAAGTCGACATTGAGCCATG
AttB2-R-MORN1.1-6	**AGAAAGCTGGGT**GTCAACCTTTGGCACTGA
AttB1-F-MORN1.13-AG	**AAAAAGCAGGCT**ccTACGAAGGCGAATGGACAGAC
AttB2-R-MORN1.13-AG	**AGAAAGCTGGGT**gtcaCAAGTCGACATTGAGCCATGG

Endogenous tagging and KO primers

IMC15-F-Ku80LIC	***TACTTCCAATCCAATTTAATG***GCCCGCTCTAGGTTACATAGTC
IMC15-R-Ku80LIC	***TCCTCCACTTCCAATTTTAGC***GTTCGGATAAGACAACGTGTTG
5'IMC15-F-B1	GGGG**ACAAGTTTGTACAAAAAAGCAGGCT**gcCGGTGGGCTGTTCTAAAGAAAGAC
5'IMC15-R-B4	GGGG**ACAACTTTGTATAGAAAAGTTGGGT**GCTAACGGCAACACGAAACTGGC
3'IMC15-F-B3	GGGG**ACAACTTTGTATAATAAAGTTG**cgCTCCTCCTTGAGGAGACGGATTG

3’IMC15-R-B2	GGGG**ACCACTTTGTACAAGAAAGCTGGGT**ACTGAGAGGACAAACTGGCCG
5UPRT-F-XhoI	cagCTCGAGGGAATCTACACACCGGAAGGTTC
5UPRT-R-BglII	cagAGATCTGTTTAAACACCGGTCAGCGGAGGCTCAGCGTTTCCTG
3UPRT-F-AvrII	cagCCTAGGGCGGCCGCGTTAACGTGAGGCTGCCTGGTGCGCGACAAG
3UPRT-R-BamHI	cagGGATCCGGAATCAGACCCTCGTCTCCGGTGG
5’IMC15-F-AseI	cagATTAATCGGTGGGCTGTTCTAAAGAAAGAC
5’IMC15-R-AseI	cagATTAATCTAACGGCAACACGAAACTGGC
IMC15int-R-NheI	caggctagcATTTTCGACGACGCTCACTGGGC

KO verification primers

myc-F1	gatctaaaatggaacaaaagctaatctccgaggaagacttgaacg
5’IMC15ver-F	GTGTACTGGTGTTCGAGGCTATG
3’IMC15ver-R	CAAACCAAATGATGCGGTCCCTG
HX-ver-F	gccgctcgcaaaaagttcgagaag
HX-ver-R	gtagtcttcaatgggtttggacgc
IMC15int-ver-R	GATGTAGGCACGACTTCGGCG
5’UPRT-F-ver	CGGTGTGGTTCCTGTTGACTTAG
3’UPRT-R-ver	GTGCAGGGAGGTTTGTTATCTTG
UPRT-F-ver	CGTTTCTTACTGGCATCGAATG
UPRT-R-ver	GTTGTTTCGTCTCTCTGGATG
5’DHFRCXR	ACTGCGAACAGCAGCAAGATCG
T7Sag4-F-PmeI	caggtttaaaccactagttctagaaggaccCGGTAC
IMC15int-ver-R(alveolin)	GACTACAGGAATCTCGATGCG
pimc15-ver-F	CGTCACAGCAGCATAGGAGAG
Tet7ver-F	GAGGTCGACGGTATCGATAAGC

Mutagenesis primers (mutation is lowercase)

IMC15.C4A-F-NheI	cagGCTAGCATGCGGATCgcgTTGCCACCAGTGCCTCAG
IMC15.C92/3A-F	CGCAGAATCCGCAGCAGCTgcggcgCTTTGGCAAACAAGCCCACG
IMC15.C92/3A-R	CGTGGGCTTGTTTGCCAAAGcgccgcAGCTGCTGCGGATTCTGCG
IMC15.C673/4A-F	GCCCAGTTCTGTTGATGCACAGgcggcgCAGTCACCGTGGACACAACATG
IMC15.C673/4A-R	CATGTTGTGTCCACGGTGACTGcgccgcCTGTGCATCAACAGAACTGGGC

References

1. Montoya JG & Liesenfeld O (2004) Toxoplasmosis. (Translated from eng) *Lancet* 363(9425):1965-1976 (in eng).
2. Haldar K & Mohandas N (2009) Malaria, erythrocytic infection, and anemia. (Translated from eng) *Hematology Am Soc Hematol Educ Program*:87-93 (in eng).
3. Tzipori S & Ward H (2002) Cryptosporidiosis: biology, pathogenesis and disease. (Translated from eng) *Microbes Infect* 4(10):1047-1058 (in eng).
4. Shirley MW, Smith AL, & Tomley FM (2005) The biology of avian Eimeria with an emphasis on their control by vaccination. (Translated from eng) *Adv Parasitol* 60:285-330 (in eng).
5. Bock R, Jackson L, de Vos A, & Jorgensen W (2004) Babesiosis of cattle. (Translated from eng) *Parasitology* 129 Suppl:S247-269 (in eng).
6. Bishop R, Musoke A, Morzaria S, Gardner M, & Nene V (2004) Theileria: intracellular protozoan parasites of wild and domestic ruminants transmitted by ixodid ticks. (Translated from eng) *Parasitology* 129 Suppl:S271-283 (in eng).
7. Reilly HB, Wang H, Steuter JA, Marx AM, & Ferdig MT (2007) Quantitative dissection of clone-specific growth rates in cultured malaria parasites. (Translated from eng) *Int J Parasitol* 37(14):1599-1607 (in eng).
8. Gubbels MJ, White M, & Szatanek T (2008) The cell cycle and Toxoplasma gondii cell division: tightly knit or loosely stitched? (Translated from eng) *Int J Parasitol* 38(12):1343-1358 (in eng).
9. Radke JR*, et al.* (2001) Defining the cell cycle for the tachyzoite stage of Toxoplasma gondii. (Translated from eng) *Molecular and biochemical parasitology* 115(2):165-175 (in eng).
10. Lorestani A*, et al.* (2010) A Toxoplasma MORN1 null mutant undergoes repeated divisions but is defective in basal assembly, apicoplast division and cytokinesis. (Translated from eng) *PLoS One* 5(8):e12302 (in eng).
11. Heaslip AT, Dzierszinski F, Stein B, & Hu K (2010) TgMORN1 is a key organizer for the basal complex of Toxoplasma gondii. (Translated from eng) *PLoS pathogens* 6(2):e1000754 (in eng).
12. Agop-Nersesian C*, et al.* (2009) Rab11A-controlled assembly of the inner membrane complex is required for completion of apicomplexan cytokinesis. (Translated from eng) *PLoS Pathog* 5(1):e1000270 (in eng).
13. Agop-Nersesian C*, et al.* (2010) Biogenesis of the inner membrane complex is dependent on vesicular transport by the alveolate specific GTPase Rab11B. (Translated from eng) *PLoS Pathog* 6(7):e1001029 (in eng).
14. Beck JR*, et al.* (2010) A novel family of Toxoplasma IMC proteins displays a hierarchical organization and functions in coordinating parasite division. (Translated from eng) *PLoS Pathog* 6(9) (in eng).
15. Tran JQ*, et al.* (2010) RNG1 is a late marker of the apical polar ring in Toxoplasma gondii. (Translated from eng) *Cytoskeleton (Hoboken)* 67(9):586-598 (in eng).

16. Stokkermans TJ, *et al.* (1996) Inhibition of Toxoplasma gondii replication by dinitroaniline herbicides. (Translated from eng) *Experimental parasitology* 84(3):355-370 (in eng).
17. Sheffield HG & Melton ML (1968) The fine structure and reproduction of Toxoplasma gondii. (Translated from eng) *J Parasitol* 54(2):209-226 (in eng).
18. Striepen B, Jordan CN, Reiff S, & van Dooren GG (2007) Building the perfect parasite: cell division in apicomplexa. (Translated from eng) *PLoS pathogens* 3(6):e78 (in eng).
19. Hu K, *et al.* (2002) Daughter cell assembly in the protozoan parasite Toxoplasma gondii. (Translated from eng) *Mol Biol Cell* 13(2):593-606 (in eng).
20. White MW, Radke J, Conde de Felipe M, & Lehmann M (2007) Cell Cycle Control/Parasite Division. *Toxoplasma: Molecular and Cellular Biology*, eds Ajioka JW & Soldati-Favre D (Horizon Scientific Press, Norwich, UK).
21. Gavin MA, Wanko T, & Jacobs L (1962) Electron microscope studies of reproducing and interkinetic Toxoplasma. (Translated from eng) *J Protozool* 9:222-234 (in eng).
22. Ogino N & Yoneda C (1966) The fine structure and mode of division of Toxoplasma gondii. (Translated from eng) *Arch Ophthalmol* 75(2):218-227 (in eng).
23. Pelletier L, *et al.* (2002) Golgi biogenesis in Toxoplasma gondii. (Translated from eng) *Nature* 418(6897):548-552 (in eng).
24. Hartmann J, *et al.* (2006) Golgi and centrosome cycles in Toxoplasma gondii. (Translated from eng) *Mol Biochem Parasitol* 145(1):125-127 (in eng).
25. Nishi M, Hu K, Murray JM, & Roos DS (2008) Organellar dynamics during the cell cycle of Toxoplasma gondii. (Translated from eng) *J Cell Sci* 121(Pt 9):1559-1568 (in eng).
26. Tilney LG & Tilney MS (1996) The cytoskeleton of protozoan parasites. (Translated from eng) *Curr Opin Cell Biol* 8(1):43-48 (in eng).
27. Hu K, *et al.* (2006) Cytoskeletal components of an invasion machine--the apical complex of Toxoplasma gondii. (Translated from eng) *PLoS Pathog* 2(2):e13 (in eng).
28. Mann T & Beckers C (2001) Characterization of the subpellicular network, a filamentous membrane skeletal component in the parasite Toxoplasma gondii. (Translated from eng) *Mol Biochem Parasitol* 115(2):257-268 (in eng).
29. White MW, *et al.* (2005) Genetic rescue of a Toxoplasma gondii conditional cell cycle mutant. (Translated from eng) *Mol Microbiol* 55(4):1060-1071 (in eng).
30. Striepen B, *et al.* (2000) The plastid of Toxoplasma gondii is divided by association with the centrosomes. (Translated from eng) *The Journal of cell biology* 151(7):1423-1434 (in eng).
31. Hager KM, Striepen B, Tilney LG, & Roos DS (1999) The nuclear envelope serves as an intermediary between the ER and Golgi complex in the intracellular parasite Toxoplasma gondii. (Translated from eng) *Journal of cell science* 112 (Pt 16):2631-2638 (in eng).

32. Nichols BA & Chiappino ML (1987) Cytoskeleton of Toxoplasma gondii. (Translated from eng) *J Protozool* 34(2):217-226 (in eng).
33. Russell DG & Burns RG (1984) The polar ring of coccidian sporozoites: a unique microtubule-organizing centre. (Translated from eng) *J Cell Sci* 65:193-207 (in eng).
34. Morrissette NS, Murray JM, & Roos DS (1997) Subpellicular microtubules associate with an intramembranous particle lattice in the protozoan parasite Toxoplasma gondii. (Translated from eng) *Journal of cell science* 110 (Pt 1):35-42 (in eng).
35. Morrissette NS & Sibley LD (2002) Cytoskeleton of apicomplexan parasites. (Translated from eng) *Microbiol Mol Biol Rev* 66(1):21-38; table of contents (in eng).
36. Dobrowolski JM, Niesman IR, & Sibley LD (1997) Actin in the parasite Toxoplasma gondii is encoded by a single copy gene, ACT1 and exists primarily in a globular form. (Translated from eng) *Cell Motil Cytoskeleton* 37(3):253-262 (in eng).
37. Shaw MK & Tilney LG (1999) Induction of an acrosomal process in Toxoplasma gondii: visualization of actin filaments in a protozoan parasite. (Translated from eng) *Proceedings of the National Academy of Sciences of the United States of America* 96(16):9095-9099 (in eng).
38. Dobrowolski JM & Sibley LD (1996) Toxoplasma invasion of mammalian cells is powered by the actin cytoskeleton of the parasite. (Translated from eng) *Cell* 84(6):933-939 (in eng).
39. Poupel O & Tardieux I (1999) Toxoplasma gondii motility and host cell invasiveness are drastically impaired by jasplakinolide, a cyclic peptide stabilizing F-actin. (Translated from eng) *Microbes Infect* 1(9):653-662 (in eng).
40. Shaw MK, Compton HL, Roos DS, & Tilney LG (2000) Microtubules, but not actin filaments, drive daughter cell budding and cell division in Toxoplasma gondii. (Translated from eng) *Journal of cell science* 113 (Pt 7):1241-1254 (in eng).
41. Delbac F*, et al.* (2001) Toxoplasma gondii myosins B/C: one gene, two tails, two localizations, and a role in parasite division. (Translated from eng) *The Journal of cell biology* 155(4):613-623 (in eng).
42. Heintzelman MB & Schwartzman JD (1997) A novel class of unconventional myosins from Toxoplasma gondii. (Translated from eng) *Journal of molecular biology* 271(1):139-146 (in eng).
43. Heintzelman MB & Schwartzman JD (2001) Myosin diversity in Apicomplexa. (Translated from eng) *J Parasitol* 87(2):429-432 (in eng).
44. Gaskins E*, et al.* (2004) Identification of the membrane receptor of a class XIV myosin in Toxoplasma gondii. (Translated from eng) *J Cell Biol* 165(3):383-393 (in eng).
45. Herm-Gotz A*, et al.* (2007) Rapid control of protein level in the apicomplexan Toxoplasma gondii. (Translated from eng) *Nat Methods* 4(12):1003-1005 (in eng).

46. Johnson TM, Rajfur Z, Jacobson K, & Beckers CJ (2007) Immobilization of the type XIV myosin complex in Toxoplasma gondii. (Translated from eng) *Molecular biology of the cell* 18(8):3039-3046 (in eng).
47. Dobrowolski JM, Carruthers VB, & Sibley LD (1997) Participation of myosin in gliding motility and host cell invasion by Toxoplasma gondii. (Translated from eng) *Mol Microbiol* 26(1):163-173 (in eng).
48. Morrissette NS & Sibley LD (2002) Disruption of microtubules uncouples budding and nuclear division in Toxoplasma gondii. (Translated from eng) *Journal of cell science* 115(Pt 5):1017-1025 (in eng).
49. Porchet E & Torpier G (1977) [Freeze fracture study of Toxoplasma and Sarcocystis infective stages (author's transl)]. (Translated from fre) *Z Parasitenkd* 54(2):101-124 (in fre).
50. Vivier E & Petitprez A (1969) [The outer membrane complex and its development at the time of the formation of daughter cells in Toxoplasma gondii]. (Translated from fre) *The Journal of cell biology* 43(2):329-342 (in fre).
51. Dubremetz JF & Torpier G (1978) Freeze fracture study of the pellicle of an eimerian sporozoite (Protozoa, Coccidia). (Translated from eng) *J Ultrastruct Res* 62(2):94-109 (in eng).
52. Scholtyseck E (1973) Ultrastructure. *The coccidia: Eimeria, Isospora, Toxoplasma, and related genera*, eds Hammond DM & Long PL (University Park Press, Baltimore, MD), pp 81-144.
53. Mondragon R & Frixione E (1996) Ca(2+)-dependence of conoid extrusion in Toxoplasma gondii tachyzoites. (Translated from eng) *J Eukaryot Microbiol* 43(2):120-127 (in eng).
54. Del Carmen MG, Mondragon M, Gonzalez S, & Mondragon R (2009) Induction and regulation of conoid extrusion in Toxoplasma gondii. (Translated from eng) *Cellular microbiology* 11(6):967-982 (in eng).
55. Bommer W, Hofling KH, & Heunert HH (1968) [In vivo observations on the penetration of toxoplasma into the host cell]. (Translated from eng) *Dtsch Med Wochenschr* 93(49):2365-2367 passim (in eng).
56. Scholtyseck E (1970) [Fine structure of the zoites from mature cysts of the so-called M-body (Frenkelia spec.)]. (Translated from ger) *Z Parasitenkd* 33(3):252-261 (in ger).
57. Swedlow JR, Hu K, Andrews PD, Roos DS, & Murray JM (2002) Measuring tubulin content in Toxoplasma gondii: a comparison of laser-scanning confocal and wide-field fluorescence microscopy. (Translated from eng) *Proceedings of the National Academy of Sciences of the United States of America* 99(4):2014-2019 (in eng).
58. Hu K, Roos DS, & Murray JM (2002) A novel polymer of tubulin forms the conoid of Toxoplasma gondii. (Translated from eng) *The Journal of cell biology* 156(6):1039-1050 (in eng).
59. Carruthers VB & Sibley LD (1997) Sequential protein secretion from three distinct organelles of Toxoplasma gondii accompanies invasion of human fibroblasts. (Translated from eng) *Eur J Cell Biol* 73(2):114-123 (in eng).

60. Hu K (2008) Organizational changes of the daughter basal complex during the parasite replication of Toxoplasma gondii. (Translated from eng) *PLoS Pathog* 4(1):e10 (in eng).
61. Gubbels MJ, Vaishnava S, Boot N, Dubremetz JF, & Striepen B (2006) A MORN-repeat protein is a dynamic component of the Toxoplasma gondii cell division apparatus. (Translated from eng) *J Cell Sci* 119(Pt 11):2236-2245 (in eng).
62. Heaslip AT, Ems-McClung SC, & Hu K (2009) TgICMAP1 is a novel microtubule binding protein in Toxoplasma gondii. (Translated from eng) *PLoS One* 4(10):e7406 (in eng).
63. Gilk SD*, et al.* (2006) Identification of PhIL1, a novel cytoskeletal protein of the Toxoplasma gondii pellicle, through photosensitized labeling with 5-[125I]iodonaphthalene-1-azide. (Translated from eng) *Eukaryot Cell* 5(10):1622-1634 (in eng).
64. Barkhuff WD*, et al.* (2011) Targeted Disruption of TgPhIL1 in Toxoplasma gondii Results in Altered Parasite Morphology and Fitness. (Translated from eng) *PLoS One* 6(8):e23977 (in eng).
65. Frenal K*, et al.* (2010) Functional dissection of the apicomplexan glideosome molecular architecture. (Translated from eng) *Cell Host Microbe* 8(4):343-357 (in eng).
66. Herm-Gotz A*, et al.* (2002) Toxoplasma gondii myosin A and its light chain: a fast, single-headed, plus-end-directed motor. (Translated from eng) *Embo J* 21(9):2149-2158 (in eng).
67. Mann T, Gaskins E, & Beckers C (2002) Proteolytic processing of TgIMC1 during maturation of the membrane skeleton of Toxoplasma gondii. (Translated from eng) *J Biol Chem* 277(43):41240-41246 (in eng).
68. Gubbels MJ, Wieffer M, & Striepen B (2004) Fluorescent protein tagging in Toxoplasma gondii: identification of a novel inner membrane complex component conserved among Apicomplexa. (Translated from eng) *Mol Biochem Parasitol* 137(1):99-110 (in eng).
69. Nishi M, Hu K, Murray JM, & Roos DS (2008) Organellar dynamics during the cell cycle of Toxoplasma gondii. (Translated from Eng) *J Cell Sci* (in Eng).
70. Khater EI, Sinden RE, & Dessens JT (2004) A malaria membrane skeletal protein is essential for normal morphogenesis, motility, and infectivity of sporozoites. (Translated from eng) *J Cell Biol* 167(3):425-432 (in eng).
71. Tremp AZ, Khater EI, & Dessens JT (2008) IMC1b is a putative membrane skeleton protein involved in cell shape, mechanical strength, motility, and infectivity of malaria ookinetes. (Translated from eng) *J Biol Chem* 283(41):27604-27611 (in eng).
72. Hu K (2002) Building a parasite: The study of the cell division and cytoskeleton of *Toxoplasma gondii*. (University of Pennsylvania, Philadelphia).
73. Leander BS & Keeling PJ (2003) Morphostasis in alveolate evolution. *trends in Ecology and Evolution* 18(8):395-402.

74. Gould SB, Tham WH, Cowman AF, McFadden GI, & Waller RF (2008) Alveolins, a new family of cortical proteins that define the protist infrakingdom Alveolata. (Translated from eng) *Mol Biol Evol* 25(6):1219-1230 (in eng).
75. Gajria B*, et al.* (2008) ToxoDB: an integrated Toxoplasma gondii database resource. (Translated from eng) *Nucleic Acids Res* 36(Database issue):D553-556 (in eng).
76. George RA & Heringa J (2000) The REPRO server: finding protein internal sequence repeats through the Web. (Translated from eng) *Trends Biochem Sci* 25(10):515-517 (in eng).
77. Ren J*, et al.* (2008) CSS-Palm 2.0: an updated software for palmitoylation sites prediction. (Translated from eng) *Protein engineering, design & selection : PEDS* 21(11):639-644 (in eng).
78. Bozdech Z*, et al.* (2003) The transcriptome of the intraerythrocytic developmental cycle of Plasmodium falciparum. (Translated from eng) *PLoS Biol* 1(1):E5 (in eng).
79. Le Roch KG*, et al.* (2003) Discovery of gene function by expression profiling of the malaria parasite life cycle. (Translated from eng) *Science* 301(5639):1503-1508 (in eng).
80. Behnke MS*, et al.* (2010) Coordinated progression through two subtranscriptomes underlies the tachyzoite cycle of Toxoplasma gondii. (Translated from eng) *PLoS One* 5(8):e12354 (in eng).
81. Szatanek T, Anderson-White BR, White MW, Saeij J, & Gubbels MJ (In preparation) Cactin is essential for G1 progression in *Toxoplasma gondii*.
82. Gubbels MJ, Vaishnava S, Boot N, Dubremetz JF, & Striepen B (2006) A MORN-repeat protein is a dynamic component of the *Toxoplasma gondii* cell division apparatus. *J Cell Sci* 119:2236-2245.
83. Hu K*, et al.* (2006) Cytoskeletal components of an invasion machine - the apical complex of Toxoplasma gondii. *PLoS Pathog* 2(2):121-138.
84. Herrmann H & Aebi U (2004) Intermediate filaments: molecular structure, assembly mechanism, and integration into functionally distinct intracellular Scaffolds. (Translated from eng) *Annu Rev Biochem* 73:749-789 (in eng).
85. Parry DA, Strelkov SV, Burkhard P, Aebi U, & Herrmann H (2007) Towards a molecular description of intermediate filament structure and assembly. (Translated from eng) *Exp Cell Res* 313(10):2204-2216 (in eng).
86. Gruenbaum Y, Margalit A, Goldman RD, Shumaker DK, & Wilson KL (2005) The nuclear lamina comes of age. (Translated from eng) *Nat Rev Mol Cell Biol* 6(1):21-31 (in eng).
87. Ferguson DJ*, et al.* (2008) MORN1 has a conserved role in asexual and sexual development across the Apicomplexa. (Translated from Eng) *Eukaryot Cell* (in Eng).
88. Pomel S, Luk FC, & Beckers CJ (2008) Host cell egress and invasion induce marked relocations of glycolytic enzymes in Toxoplasma gondii tachyzoites. (Translated from eng) *PLoS pathogens* 4(10):e1000188 (in eng).

89. Nagamune K, Xiong L, Chini E, & Sibley LD (2008) Plants, endosymbionts and parasites: Abscisic acid and calcium signaling. (Translated from eng) *Commun Integr Biol* 1(1):62-65 (in eng).
90. Moudy R, Manning TJ, & Beckers CJ (2001) The loss of cytoplasmic potassium upon host cell breakdown triggers egress of Toxoplasma gondii. (Translated from eng) *The Journal of biological chemistry* 276(44):41492-41501 (in eng).
91. Black MW, Arrizabalaga G, & Boothroyd JC (2000) Ionophore-resistant mutants of Toxoplasma gondii reveal host cell permeabilization as an early event in egress. (Translated from eng) *Mol Cell Biol* 20(24):9399-9408 (in eng).
92. Godsel LM, Hobbs RP, & Green KJ (2008) Intermediate filament assembly: dynamics to disease. (Translated from eng) *Trends Cell Biol* 18(1):28-37 (in eng).
93. Kudryashev M*, et al.* (2010) Positioning of large organelles by a membrane-associated cytoskeleton in Plasmodium sporozoites. (Translated from eng) *Cell Microbiol* 12(3):362-371 (in eng).
94. Versele M & Thorner J (2005) Some assembly required: yeast septins provide the instruction manual. (Translated from eng) *Trends Cell Biol* 15(8):414-424 (in eng).
95. Ferguson DJ*, et al.* (2008) MORN1 has a conserved role in asexual and sexual development across the apicomplexa. (Translated from eng) *Eukaryot Cell* 7(4):698-711 (in eng).
96. Anderson-White BR*, et al.* (2011) A family of intermediate filament-like proteins is sequentially assembled into the cytoskeleton of Toxoplasma gondii. (Translated from eng) *Cell Microbiol* 13(1):18-31 (in eng).
97. Aurrecoechea C*, et al.* (2007) ApiDB: integrated resources for the apicomplexan bioinformatics resource center. (Translated from eng) *Nucleic acids research* 35(Database issue):D427-430 (in eng).
98. Donald RG & Roos DS (1993) Stable molecular transformation of Toxoplasma gondii: a selectable dihydrofolate reductase-thymidylate synthase marker based on drug-resistance mutations in malaria. (Translated from eng) *Proceedings of the National Academy of Sciences of the United States of America* 90(24):11703-11707 (in eng).
99. Donald RG & Roos DS (1994) Homologous recombination and gene replacement at the dihydrofolate reductase-thymidylate synthase locus in Toxoplasma gondii. (Translated from eng) *Molecular and biochemical parasitology* 63(2):243-253 (in eng).
100. Fox BA & Bzik DJ (2002) De novo pyrimidine biosynthesis is required for virulence of Toxoplasma gondii. (Translated from eng) *Nature* 415(6874):926-929 (in eng).
101. Gubbels MJ*, et al.* (2008) Forward genetic analysis of the apicomplexan cell division cycle in Toxoplasma gondii. (Translated from eng) *PLoS pathogens* 4(2):e36 (in eng).
102. Roos DS, Sullivan WJ, Striepen B, Bohne W, & Donald RG (1997) Tagging genes and trapping promoters in Toxoplasma gondii by insertional mutagenesis. (Translated from eng) *Methods* 13(2):112-122 (in eng).

103. Wu D, Topper LM, & Wilson TE (2008) Recruitment and dissociation of nonhomologous end joining proteins at a DNA double-strand break in Saccharomyces cerevisiae. (Translated from eng) *Genetics* 178(3):1237-1249 (in eng).
104. Walker JR, Corpina RA, & Goldberg J (2001) Structure of the Ku heterodimer bound to DNA and its implications for double-strand break repair. (Translated from eng) *Nature* 412(6847):607-614 (in eng).
105. Ninomiya Y, Suzuki K, Ishii C, & Inoue H (2004) Highly efficient gene replacements in Neurospora strains deficient for nonhomologous end-joining. (Translated from eng) *Proceedings of the National Academy of Sciences of the United States of America* 101(33):12248-12253 (in eng).
106. Meyer V*, et al.* (2007) Highly efficient gene targeting in the Aspergillus niger kusA mutant. (Translated from eng) *J Biotechnol* 128(4):770-775 (in eng).
107. Kooistra R, Hooykaas PJ, & Steensma HY (2004) Efficient gene targeting in Kluyveromyces lactis. (Translated from eng) *Yeast* 21(9):781-792 (in eng).
108. Colot HV*, et al.* (2006) A high-throughput gene knockout procedure for Neurospora reveals functions for multiple transcription factors. (Translated from eng) *Proceedings of the National Academy of Sciences of the United States of America* 103(27):10352-10357 (in eng).
109. Goins CL, Gerik KJ, & Lodge JK (2006) Improvements to gene deletion in the fungal pathogen Cryptococcus neoformans: absence of Ku proteins increases homologous recombination, and co-transformation of independent DNA molecules allows rapid complementation of deletion phenotypes. (Translated from eng) *Fungal Genet Biol* 43(8):531-544 (in eng).
110. Ishibashi K, Suzuki K, Ando Y, Takakura C, & Inoue H (2006) Nonhomologous chromosomal integration of foreign DNA is completely dependent on MUS-53 (human Lig4 homolog) in Neurospora. (Translated from eng) *Proceedings of the National Academy of Sciences of the United States of America* 103(40):14871-14876 (in eng).
111. Huynh MH & Carruthers VB (2009) Tagging of endogenous genes in a Toxoplasma gondii strain lacking Ku80. (Translated from eng) *Eukaryotic cell* 8(4):530-539 (in eng).
112. Fox BA, Ristuccia JG, Gigley JP, & Bzik DJ (2009) Efficient gene replacements in Toxoplasma gondii strains deficient for nonhomologous end joining. (Translated from eng) *Eukaryotic cell* 8(4):520-529 (in eng).
113. Banaszynski LA, Chen LC, Maynard-Smith LA, Ooi AG, & Wandless TJ (2006) A rapid, reversible, and tunable method to regulate protein function in living cells using synthetic small molecules. (Translated from eng) *Cell* 126(5):995-1004 (in eng).
114. Pfefferkorn ER (1978) Toxoplasma gondii: the enzymic defect of a mutant resistant to 5-fluorodeoxyuridine. (Translated from eng) *Experimental parasitology* 44(1):26-35 (in eng).

115. Pfefferkorn ER & Pfefferkorn LC (1977) Toxoplasma gondii: characterization of a mutant resistant to 5-fluorodeoxyuridine. (Translated from eng) *Experimental parasitology* 42(1):44-55 (in eng).
116. Roos DS, Donald RG, Morrissette NS, & Moulton AL (1994) Molecular tools for genetic dissection of the protozoan parasite Toxoplasma gondii. (Translated from eng) *Methods Cell Biol* 45:27-63 (in eng).
117. Meissner M, Schluter D, & Soldati D (2002) Role of Toxoplasma gondii myosin A in powering parasite gliding and host cell invasion. (Translated from eng) *Science* 298(5594):837-840 (in eng).
118. Meissner M, Brecht S, Bujard H, & Soldati D (2001) Modulation of myosin A expression by a newly established tetracycline repressor-based inducible system in Toxoplasma gondii. (Translated from eng) *Nucleic acids research* 29(22):E115 (in eng).
119. Rees-Channer RR*, et al.* (2006) Dual acylation of the 45 kDa gliding-associated protein (GAP45) in Plasmodium falciparum merozoites. (Translated from eng) *Molecular and biochemical parasitology* 149(1):113-116 (in eng).
120. Vaishnava S*, et al.* (2005) Plastid segregation and cell division in the apicomplexan parasite Sarcocystis neurona. (Translated from eng) *Journal of cell science* 118(Pt 15):3397-3407 (in eng).
121. Arnot DE, Ronander E, & Bengtsson DC (2011) The progression of the intra-erythrocytic cell cycle of Plasmodium falciparum and the role of the centriolar plaques in asynchronous mitotic division during schizogony. (Translated from eng) *Int J Parasitol* 41(1):71-80 (in eng).
122. Sauer B (1987) Functional expression of the cre-lox site-specific recombination system in the yeast Saccharomyces cerevisiae. (Translated from eng) *Mol Cell Biol* 7(6):2087-2096 (in eng).
123. Sternberg N & Hamilton D (1981) Bacteriophage P1 site-specific recombination. I. Recombination between loxP sites. (Translated from eng) *Journal of molecular biology* 150(4):467-486 (in eng).
124. Brecht S, Erdhart H, Soete M, & Soldati D (1999) Genome engineering of Toxoplasma gondii using the site-specific recombinase Cre. (Translated from eng) *Gene* 234(2):239-247 (in eng).
125. Omary MB, Ku NO, Tao GZ, Toivola DM, & Liao J (2006) "Heads and tails" of intermediate filament phosphorylation: multiple sites and functional insights. (Translated from eng) *Trends in biochemical sciences* 31(7):383-394 (in eng).
126. Gilk SD, Gaskins E, Ward GE, & Beckers CJ (2009) GAP45 phosphorylation controls assembly of the Toxoplasma myosin XIV complex. (Translated from eng) *Eukaryotic cell* 8(2):190-196 (in eng).
127. Lu KP, Kemp BE, & Means AR (1994) Identification of substrate specificity determinants for the cell cycle-regulated NIMA protein kinase. (Translated from eng) *The Journal of biological chemistry* 269(9):6603-6607 (in eng).
128. Piekny AJ & Maddox AS (2010) The myriad roles of Anillin during cytokinesis. (Translated from eng) *Semin Cell Dev Biol* 21(9):881-891 (in eng).

129. Gordon JL, Beatty WL, & Sibley LD (2008) A novel actin-related protein is associated with daughter cell formation in Toxoplasma gondii. (Translated from eng) *Eukaryotic cell* 7(9):1500-1512 (in eng).
130. de Miguel N*, et al.* (2008) Toxoplasma gondii Hsp20 is a stripe-arranged chaperone-like protein associated with the outer leaflet of the inner membrane complex. (Translated from eng) *Biology of the cell / under the auspices of the European Cell Biology Organization* 100(8):479-489 (in eng).
131. Leander BS, Clopton RE, & Keeling PJ (2003) Phylogeny of gregarines (Apicomplexa) as inferred from small-subunit rDNA and beta-tubulin. (Translated from eng) *Int J Syst Evol Microbiol* 53(Pt 1):345-354 (in eng).
132. Bargagna-Mohan P*, et al.* (2007) The tumor inhibitor and antiangiogenic agent withaferin A targets the intermediate filament protein vimentin. (Translated from eng) *Chem Biol* 14(6):623-634 (in eng).
133. Kissinger JC, Gajria B, Li L, Paulsen IT, & Roos DS (2003) ToxoDB: accessing the Toxoplasma gondii genome. (Translated from eng) *Nucleic Acids Res* 31(1):234-236 (in eng).
134. Maurer-Stroh S & Eisenhaber F (2005) Refinement and prediction of protein prenylation motifs. (Translated from eng) *Genome Biol* 6(6):R55 (in eng).
135. Ren J*, et al.* (2008) CSS-Palm 2.0: an updated software for palmitoylation sites prediction. (Translated from eng) *Protein Eng Des Sel* 21(11):639-644 (in eng).
136. Goujon M*, et al.* (2010) A new bioinformatics analysis tools framework at EMBL-EBI. (Translated from eng) *Nucleic acids research* 38(Web Server issue):W695-699 (in eng).
137. Larkin MA*, et al.* (2007) Clustal W and Clustal X version 2.0. (Translated from eng) *Bioinformatics* 23(21):2947-2948 (in eng).
138. Tamura K*, et al.* (2011) MEGA5: molecular evolutionary genetics analysis using maximum likelihood, evolutionary distance, and maximum parsimony methods. (Translated from eng) *Molecular biology and evolution* 28(10):2731-2739 (in eng).
139. Blom N, Gammeltoft S, & Brunak S (1999) Sequence and structure-based prediction of eukaryotic protein phosphorylation sites. (Translated from eng) *Journal of molecular biology* 294(5):1351-1362 (in eng).
140. Gubbels MJ, Li C, & Striepen B (2003) High-throughput growth assay for Toxoplasma gondii using yellow fluorescent protein. (Translated from eng) *Antimicrob Agents Chemother* 47(1):309-316 (in eng).
141. Szewczyk E*, et al.* (2006) Fusion PCR and gene targeting in Aspergillus nidulans. (Translated from eng) *Nat Protoc* 1(6):3111-3120 (in eng).
142. Herm-Gotz A*, et al.* (2007) Rapid control of protein level in the apicomplexan Toxoplasma gondii. (Translated from eng) *Nat Methods* 4(12):1003-1005 (in eng).
143. Zeng M, Huang BR, & Lapeyre JN (1996) Cloning strategies using a third irrelevant enzyme site (TIES) to overcome certain cloning problems. (Translated from eng) *Biotechniques* 20(1):68-72, 74, 76 passim (in eng).

144. Alexandrov A*, et al.* (2004) A facile method for high-throughput co-expression of protein pairs. (Translated from eng) *Mol Cell Proteomics* 3(9):934-938 (in eng).
145. Harlow E & Lane D (1988) *Antibodies: a laboratory manual* (Cold Spring Harbor Laboratory, Cold Spring Harbor).
146. Ferguson DJ*, et al.* (1999) The expression and distribution of dense granule proteins in the enteric (Coccidian) forms of Toxoplasma gondii in the small intestine of the cat. (Translated from eng) *Exp Parasitol* 91(3):203-211 (in eng).
147. Charif H, Darcy F, Torpier G, Cesbron-Delauw MF, & Capron A (1990) Toxoplasma gondii: characterization and localization of antigens secreted from tachyzoites. (Translated from eng) *Experimental parasitology* 71(1):114-124 (in eng).
148. Kvaal CA, Radke JR, Guerini MN, & White MW (2002) Isolation of a Toxoplasma gondii cyclin by yeast two-hybrid interactive screen. *Mol Biochem Parasitol* 120(2):187-194.
149. Gietz RD & Woods RA (2002) Transformation of yeast by lithium acetate/single-stranded carrier DNA/polyethylene glycol method. (Translated from eng) *Methods Enzymol* 350:87-96 (in eng).
150. Durfee T*, et al.* (1993) The retinoblastoma protein associates with the protein phosphatase type 1 catalytic subunit. (Translated from eng) *Genes & development* 7(4):555-569 (in eng).